Louisiana State University

EVALUATION OF THE ENERGY TRANSFER IN THE CHAR ZONE DURING ABLATION

PART I: Theoretical and Experimental Results for Heat Shield Surface Temperatures up to 3000°F.

A Condensed Version of the Final Report on NASA Grant NGR 19-001-016

by

Ralph W. Pike, Associate Professor
Principal Investigator

Gary C. April, Research Associate

Eduardo G. del Valle, Research Associate

Department of Chemical Engineering

December 1, 1969

PREFACE

This is a condensed version of Part I of a two part final report on NASA Grant NGR 19-001-016, Evaluation of the Energy Transfer in the Char Zone during Ablation. This part describes the theoretical and experimental results obtained for the energy absorbed by the nonequilibrium, equilibrium and frozen flow of pyrolysis gases in the char zone for heat shield surface temperatures up to 3000°F. In Part II of this report results will be presented for the analysis of the energy absorbed in the char zone and the decomposition zone during ablation for heat shield surface temperatures up to 6000°F.

Part I of the final report also serves as the Ph.D. dissertation of Gary C. April. Reference to the unabridged version of the report is suggested for detailed discussion on all phases of the research conducted.

ACKNOWLEDGMENTS

This research was performed under the direction of Dr. Ralph W. Pike. His encouragement and guidance is gratefully acknowledged.

Appreciation is also expressed to the National Aeronautics and Space Administration's Langley Research Center which sponsored the research and, especially, to Robert T. Swann, Grant Monitor, whose interest and consultation gave an added sense of achievement to the research.

The author would also like to acknowledge the E. I. DuPont DeNemours Company for making possible, through an educational leave of absence, the opportunity to return to the university for an advanced degree; the Charles E. Coates Memorial Fund of the L.S.U. Foundation for funds to pay a portion of the typing cost of the dissertation, and, the L.S.U. Computer Research Center for the use of their facilities during the course of the study.

Special thanks are also given to Eduardo del Valle, co-worker during the research, John Balhoff, a very conscientious and adept Chemical Engineering student who assisted with much of the experimental program, Marty Love who typed the manuscript, and many friends who contributed to the successful completion of this research.

ABSTRACT

The energy transfer associated with the reacting flow of pyrolysis products through the char layer of a low density nylon-phenolic resin charring ablator was studied experimentally and theoretically. It was found that a non-equilibrium flow model, employing finite reaction rate data for the important reactions among the pyrolysis products, was necessary to accurately describe the energy transport within the char. The important reactions and kinetic data for a temperature range of 500°(533°K) to 3000°F (1925°K), with experimental simulation to 2300°F (1535°K), were determined and incorporated into the mathematical model, called the TEMPRE System. This model, in conjunction with experimental results obtained in a Char Zone Thermal Environment Simulator, were used to clearly show the shortcomings of the limiting cases of frozen and equilibrium flow in predicting the true behavior within the char layer.

A comparison of the experimental data obtained using low density, nylon-phenolic resin chars was made with the results obtained using graphite as a simulated char. The non-equilibrium flow model accurately predicted energy transport in the graphite medium using the same important reactions and kinetic data developed for flow through chars. This conclusion was needed to justify the use of graphite for the measurement of carbon deposition from methane and phenol, and, in the catalyst evaluation studies.

Carbon deposition and decomposition product distributions were determined for methane and phenol using carbon-14 tracers. The product distributions were helpful in providing additional evidence that the chemical reactions included in the model were correct. The identified products of methane and phenol thermal decomposition were carbon monoxide, carbon dioxide, methane, ethylene, acetylene and phenol. Carbon deposition measurements within the char layer were used to locate the temperature where chemical reactions among the pyrolysis products became significant. In general, deposition was greatest near the front surface where the temperature varied between 1800 - 2300°F (1252 - 1535°K).

The above results were also used in the catalyst evaluation studies. The introduction of a catalyst into the pyrolysis product stream (homogeneous) or as a coating on the graphite (heterogeneous) was made to accelerate chemical reactions by making them occur at lower temperatures. This resulted in higher energy absorption by the pyrolysis products. Bromine (homogeneous) had an excellent activity for this by lowering the temperature at which reactions start from 1900°F (1312°K) to 1500°F (1084°K). This effect was also measured by comparing the experimental exit gas compositions with the compositions calculated by the non-equilibrium flow model using conventional

non-catalytic, kinetic data. The relative difference in these values was a good measure of the extent of chemical reaction resulting from the addition of the catalyst into the system.

Molybdenum and tungsten co-catalysts (heterogeneous) had essentially no effect in accelerating chemical reactions within the char. The slightly different carbon deposition profiles obtained were not within experimental accuracy to conclusively indicate a beneficial increase in the rate of chemical reactions. Platinum catalyst was tested in earlier experiments with no success in accelerating the chemical reactions.

In addition, the air oxidation of nylon-phenolic resin chars was studied to determine the rate of oxidation of the char with distance from the front surface. The maximum rate was obtained with air flowing from the heated front surface through the char and leaving the rear surface. There was no flow of pyrolysis products. With a front surface temperature of 2047°F (1395°K) and an air mass flux of 0.035 lb/ft^2-sec (0.15 kg/m^2-sec), an 81% conversion of oxygen was obtained. The gas leaving the back surface contained 4.0% oxygen. This indicated that oxidation was taking place at all depths within the char, and this was confirmed with a non-equilibrium flow calculation.

Table of Contents

Table of Contents (Continued)

INTRODUCTION

The Nature of Aerodynamic Heating During Planetary Reentry

One of the most serious problems encountered when space vehicles reenter a planetary atmosphere is aerodynamic heating. Typical reentry velocities for various Earth orbital missions are listed in Table 1. Before a manned spacecraft can land safely, these speeds must be reduced to conventional aircraft speeds. This can be accomplished by applying a reverse thrust or by taking advantage of the frictional resistance of the atmosphere. Since the return velocity is of the same order of magnitude as the launch velocity, the reverse thrust method requires the same quantity of fuel for the reentry phase. This doubles the fuel requirement for the mission and makes the added weight to the system prohibitive. Hence it is more efficient to use the aerodynamic braking method to reduce the vehicle speed to a safe level (1,2,3).

Table 1. Initial Reentry Velocity and Kinetic Energy for Space Vehicles at Various Altitudes Above the Earth (1,2)

Orbital Altitude Nautical Miles	Velocity Ft/Sec	(m/Sec)	Kinetic Energy BTU/Lb	J/kg
300	26,000	(7910)	13,500	(31.5)
1000	27,000	(8210)	14,600	(34.1)
20000	33,800	(10350)	22,800	(53.2)
Circumlunar	36,000	(11000)	26,000	(60.6)
Venus or Mars	37,200	(11390)	27,600	(64.2)

A high speed orbiting vehicle possesses a large amount of kinetic energy (K.E. = $1/2\ mV^2$). In aerodynamic braking, this energy is converted to heat as the body descends through the resisting atmosphere. In Table 1 the kinetic energy (per unit weight) possessed by a vehicle at various orbital altitudes above the Earth is also listed. For example, a 5000 pound (2270kg) vehicle having an initial reentry velocity of 26,000 feet per second (7910 m/sec) must convert 67,500,000 BTU (71,500 J) of kinetic energy to heat. Consider a vehicle that is constructed of structural steel having a specific heat of 0.117 BTUper pound per degree Fahrenheit (4.2×10^{-4} J/kg-°K). If a temperature

increase of 1150°F (900°K) is attained, the maximum amount of heat that is absorbed is 675,000 BTU (715 J), or one percent of the total heat generated. It is evident from this example that only a small fraction of the thermal energy can be permitted to reach the vehicle without causing destructive effects. The remaining large fraction (ninety-nine percent) must be transferred to the surroundings by the proper selection of the vehicle shape and materials of construction (1,3).

There are two general classifications of body configuration used in ballistic reentry design (3,4,5,6): the slender body and blunt body configurations. The slender body shape causes a minimum aerodynamic drag condition with only slight disturbance of the air flow. This shape produces a weak, attached shock wave with a large percentage of the heat generated being absorbed by the body. The use of slender body configuration is best suited to ballistic missile and supersonic flow applications where heating loads are experienced for short periods of time.

Since reentry of space vehicles requires a maximum amount of energy transfer to the atmosphere, the blunt or high drag configuration is more applicable. A major portion of the energy is absorbed by the air flowing between the strong detached shock wave and the vehicle surface and is carried away in the wake behind the craft. The shock layer becomes progressively hotter during the course of reentry causing dissociation and ionization of the air. This results in heat transfer by conduction, convection and radiation to the surface of the vehicle. Although the heat absorbed is a small portion of the heat generated, the relative amount is sufficient to produce surface temperatures in excess of 6000°F (3590°K). Therefore, a thermal protection system must be employed to protect the vehicle from these high temperatures and heat fluxes.

One possible solution is to provide enough structural mass to safely absorb the heat (3,7). However since most metals are poor heat sinks, this method would result in extreme weight penalties.

Transpiration cooling is a second method (8). This technique protects the vehicle by injecting a fluid through openings at the body surface into the boundary layer. The injected fluid blocks heat transfer into the material and maintains a safe temperature at the space cabin wall. This method likewise requires additional weight such as equipment to pump and regulate the flow of coolant; and as a result, it is prohibitive in manned reentry applications.

Other methods of heat protection exist, i.e. convective, film and radiation cooling, but the most successful technique has been ablative cooling (7,9).

Ablative Thermal Protection of Planetary Reentry Vehicles

Ablative cooling is similar to heat sink and transpiration cooling in method, but it is drastically different in the mechanisms used to achieve the desired results. Ablation sacrifices structural stability to preserve thermal resistivity by melting, vaporizing and/or subliming relatively thin layers of the material at the surface. Although absorption of heat by phase change is the distinguishing feature of the process, energy dissipation by radiation, conduction, convection, transpiration and chemical reaction is likewise achieved (7,10).

Ideally, an ablative material must possess a low thermal conductivity, high heat capacity and large heat of degradation to effectively restrict the extreme temperatures to the surface of the vehicle. Success has been achieved employing compositions of nylon, phenolic resin, silicon elastomers and epoxy resins (5,9,14).

There are two kinds of ablative protection systems. One is non-charring, and the other is charring. A non-charring ablator is one in which the material vaporizes into gases and enters the boundary layer counter to the heat flow. This counter flow of mass effectively blocks heat transfer into the material and protects the vehicle. Teflon (polytetrafluoroethylene) is one such non-charring compound which undergoes chain shortening steps to form small polymer units that eventually vaporize. Extensive research with Teflon and other non-charring ablative meterials have been reported over a wide range of applications.

The charring ablator, on the otherhand, has proven to be one of the most successful heat shields for reentry heat protection. Being a combination of plastics that decompose to a char of porous carbon and low molecular weight gases, it protects the vehicle by conduction, convection, plastic decomposition, transpiration, endothermic chemical reactions of the pyrolysis gases, reradiation from the char surface, and thickening of the boundary layer. The charring ablator is conveniently divided into three separate zones which include the plastic decomposition zone, the char zone or layer, and the boundary layer as shown in Figure 1.

In the decomposition zone the virgin plastic degrades to char and low molecular weight gases. These gases flow through the char zone and undergo chemical reactions such as cracking, free radical formation and ionization. A very large quantity of heat is absorbed by these predominantly endothermic reactions as the gas temperature increases from the decomposition zone to the char surface. These hot gases are then injected into the boundary layer with additional absorption of heat due to expansion and further chemical reactions.

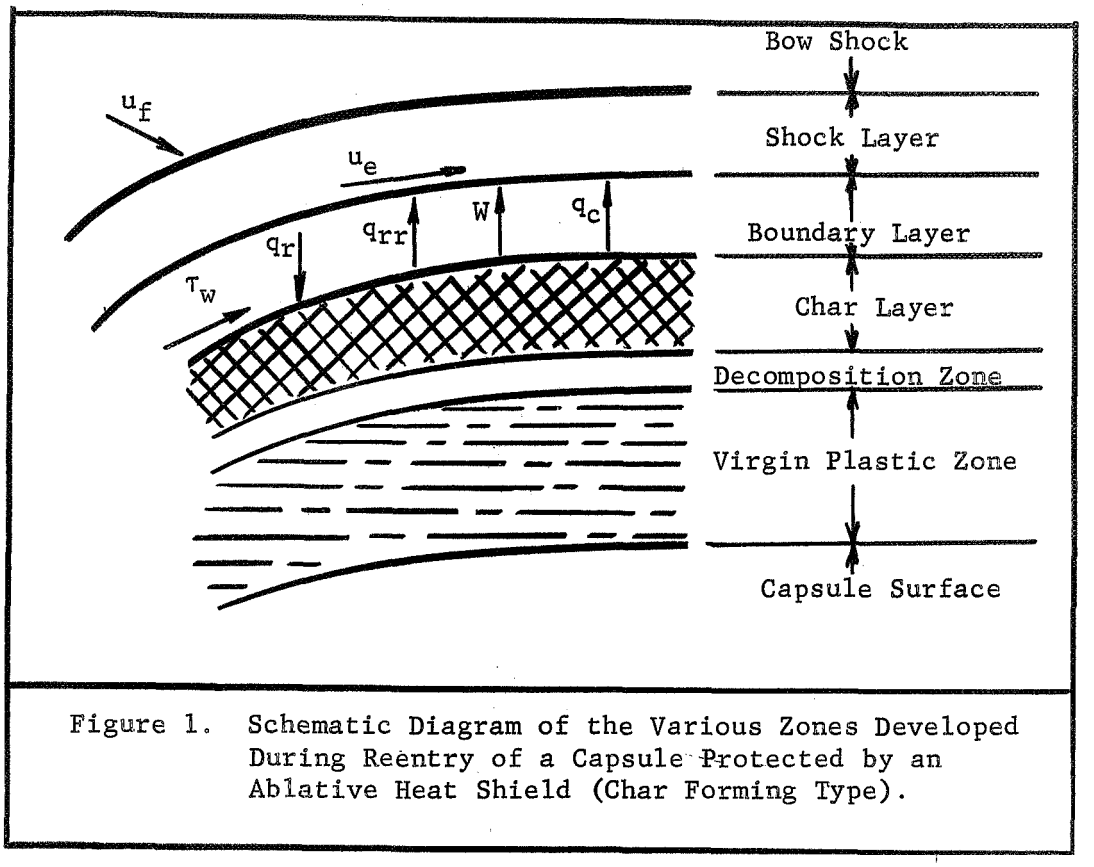

Figure 1. Schematic Diagram of the Various Zones Developed During Reentry of a Capsule Protected by an Ablative Heat Shield (Char Forming Type).

Energy Transfer in the Char Zone of a Charring Ablator

Each of the above regions has been the subject of a sizeable research effort, and various types of matematical models to describe the charring ablator process have been developed. These include the transient ablation analyses of Kratsch, et al (16), Kendall, et al (17) and Swann, et al (18) and in more related areas, transpiration cooling studies by Koh and del Casal (19,20,21), flow of methane through porous graphite by Clark (22), and carbon deposition studies by Weger, et al (23,24). In this research a better description of the phenomena taking place in the char zone is presented. An accurate description is needed of the energy transfer in the char layer and the species compositions and fluxes entering the boundary layer. At present these variables are evaluated by considering the flow to be either frozen (no reaction) or in chemical equilibrium.

For frozen flow the lower limit on the energy transfer is computed since the energy absorbed by the pyrolysis products is just the change in sensible heat as these gases flow through the porous char. This is the simplest case to evaluate mathematically, and the classical transpiration cooling solution to the energy equation is applicable (25).

For equilibrium flow in the char zone the upper limit on the energy transfer is obtained since chemical reaction rates are infinitely fast, and the composition of the pyrolysis products only vary with the temperature as predicted by thermodynamic equilibrium. This approximation gives the maximum amount of heat that can be absorbed since the reactions occurring are predominantly endothermic. The mathematical description of this case is more detailed than for frozen flow since an additional term for heat absorption by chemical reaction must be included in the energy equation. Many investigators feel this model would more accurately describe the actual behavior in the char zone since the reaction rates should be very fast at the high temperatures encountered.

For a more accurate description of the reacting flow in the char zone the kinetics of the chemical reactions must be included in solving the energy equation. The solution is more complex than the limiting cases because compositions of the pyrolysis products must be calculated from the reaction rate expressions which are differential equations. Of all the possible reactions that could occur in the char zone within the temperature range encountered, the ones that actually occur must be selected and included in the analysis.

In addition, experiments must be conducted to assure the theoretical model accurately predicts the energy transfer in the char zone. This can be accomplished by flowing a mixture of compounds typical of the actual pyrolysis gases through chars formed in arc-jet heaters. The chars can be radiantly heated to simulate the surface heating during reentry. Gases entering and leaving the char zone can be analyzed to determine the extent of the reactions taking place in the char. Thus the accuracy of the mathematical computations can be assessed.

Furthermore, the results of the analysis, referred to as the non-equilibrium model, can be compared with the limiting cases. In this way the limitations incurred by assuming equilibrium or frozen flow are evaluated. A detailed investigation into the types of reactions occurring, the amount of carbon deposition taking place in the char layer, and ways to make the ablation of char forming materials more efficient is determined.

MATHEMATICAL ANALYSIS FOR REACTING FLOW IN THE CHAR ZONE OF A CHARRING ABLATOR

General Description

The momentum, energy and mass transfer associated with the flow of pyrolysis products through the char layer of a char-forming ablative plastic is considered. The pyrolysis products, formed by the thermal degradation of the plastic heat shield, enter the char layer at the decomposition temperature of the plastic. The products experience a temperature increase as they flow through the char and undergo thermal cracking to lower molecular weight species which react with each other and with the carbonaceous char layer. These predominantly endothermic reactions are important modes of energy absorption and must be included in any realistic analysis of the energy transfer in the char layer.

The mathematical model describing the transport phenomena taking place has the form of a one dimensional and steady flow. A schematic diagram showing the pyrolysis gas flowing through the porous char layer is depicted in Figure 2. As indicated, the pyrolysis products enter the char at the decomposition temperature, T_o, and exit at a higher front surface temperature, T_L. Changes in the mass flux of the various species within the char occur as a result of chemical reactions at finite reaction rates, R_i. A pressure gradient (P_o-P_L) across the char is also experienced.

Restrictions and Assumptions

The particular restrictions and assumptions used to simplify the equations of change are listed in Table 2. Justification of these statements is presented in detail in the original work (26).

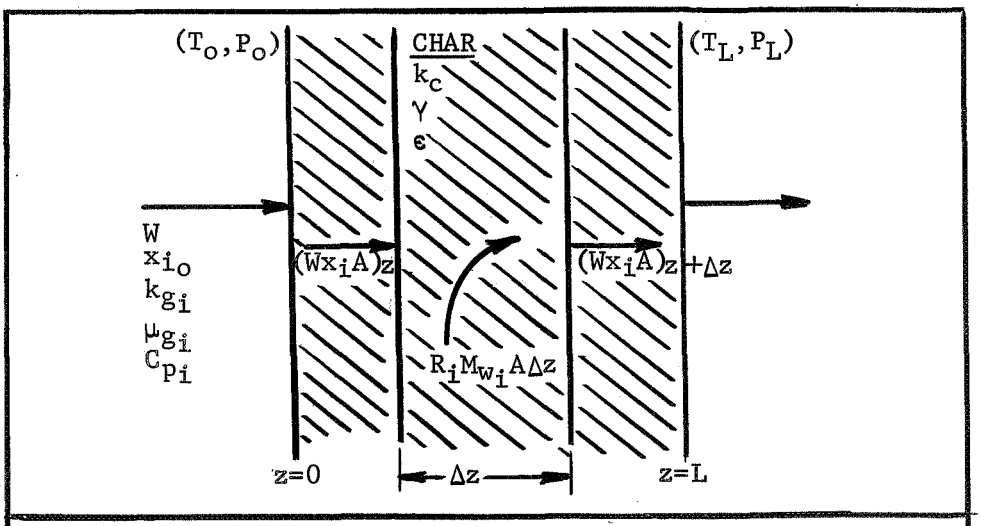

Figure 2. Schematic Diagram of the Char Layer.

Table 2. Restrictions and Assumptions Used to Simplify the Equations of Change for Reacting Gas Flow in the Char Zone

	Restriction - Assumption	Justification
1.	One dimensional flow normal to the front surface	Radius of curuature of capsules large compared with thickness
2.	Steady flow	Char thickness remains constant after short, initial transient period
3.	Ideal pyrolysis gas mixtures	High temperature, low pressure
4.	Variable gas properties	Large temperature range (500-3000°F)
5.	Constant char properties (except char conductivity)	Carbon deposition small therefore, porosity and permeability constant. Char thermal conductivity varies with temperature.
6.	Thermal equilibrium between char and pyrolysis gases	Generally small, especially in ablative applications where the char back surface temperature is nearly equal to the decomposition temperature.
7.	Momentum transfer by modified Darcy's Law	Inertial effects important because of high mass flux values
8.	PV work negligible	Small in comparison to convective and conductive transport
9.	Negligible viscous dissapation	Velocity and viscosity of the gas mixture are small
10.	Diffusional transport omitted	Small in comparison with bulk fluid transport.
11.	Work against gravity omitted	Non existent for horizontal flow

Equations of Change

The application of the above simplifications to the general equations of change result in the important differential equations for describing the flow of pyrolysis products in the char layer. These, shown in Table 3, are the species continuity equation, the momentum equation, the energy equation and the surface heat flux equation.

Table 3. Summary of the Important Equations Related to the Flow of Pyrolysis Products in the Char Zone.

Species Continuity Equation:	$\frac{d}{dz}(\rho_i v) = R_i$ (1)
Momentum Equation (Darcy's Law):	$P = \{P^2_L + 2R\left[\int_z^L (\frac{\mu}{\gamma})(W)(\frac{T}{M_w})\,dz + \int_z^L \beta(\frac{T}{M_w})(W)^2\,dz\right]^{1/2}$ (2)
Energy Equation:	$\epsilon\bar{C}_p W_p \frac{dT}{dz} = \frac{d}{dz}[k_e\frac{dT}{dz}] - [\bar{H}_c R_c + \sum_{i=1}^{K} H_i R_i]$ (3)
Heat Flux Equation:	$q_{cz} = (q_L - q_o) = \sum_{i=1}^{K}\int_{T_o}^{T_L} \epsilon W_p C_{pi} x_i\,dT + \sum_{i=1}^{K+1}\int_o^L H_i \bar{R}_i\,dz$ (4)

A detailed derivation of these equations from the general equations is presented in reference (26).

Boundary Conditions

There are two important sets of boundary conditions that can be used to solve the equations of change for flow of reacting gases in the char zone. These are shown in Table 4. The first set specifies the pressure and temperature at the front surface, and, the temperature and pyrolysis gas composition entering the back surface of the char. These conditions for mass flux, W, as a parameter make the solution of the energy equation a two point boundary value problem.

Table 4. Boundary Conditions for the Solution of the Char Zone Equation of Change.

Location	Iterative Solution Boundary Conditions	Non-iterative Solution Boundary Conditions
Back Surface (z=o)	$T = T_o$ $x_i = x_{io}$	$T = T_o$ $q_p = -(k_e \frac{dT}{dz})_o$ (5)
Front Surface (z=L)	$T = T_L$ $P = P_L$	$P = P_L$ (6)

This requires an iterative solution. Because PV work is negligible in the energy equation, the momentum equation (Modified Darcy's Law) can be solved for the pressure distribution after a solution of the energy equation is obtained using an average pressure in the char. The heat flux at the char front surface is also calculated using equation (4). The computer program used for these solutions is called the Iterative TEMPRE System (IT).

The second set of boundary conditions specifies the temperature, initial pyrolysis gas composition and the sum of the heat of pyrolysis and the heat conducted in the virgin plastic at the back surface of the char, q_p. For mass flux, W, and q_p as parameters, the solution of the energy equation as an initial value problem can be obtained. This does not require an iterative solution as did the first case. To be useful, however, a parametric study of W and q_p is needed over the range of values expected during reentry.

In order to calculate the pressure distribution within the char, the front surface pressure is again specified. The heat flux and pressure distribution calculations are the same as those made in the Iterative TEMPRE System. The computer program for this method of solution is called the Non-Iterative TEMPRE System (NIT).

Both systems are discussed in detail in reference (26) where a complete block flow diagram and program listing are presented. The particular application of the equations of change and the above boundary conditions to frozen, equilibrium and nonequilibrium flow of pyrolysis gases within the char layer will be developed in the following sections.

Application of the Transport Equations to Frozen, Equilibrium and Non-Equilibrium Flow in the Char

As mentioned in the Introduction, there are two limiting cases currently used to simplify the analysis of the flow of pyrolysis gases through the char zone. These are to consider the flow to be either frozen or in thermodynamic equilibrium. This research deals with the development of a third model, one for non-equilibrium flow, which will predict more accurately the actual behavior within the char layer. In this section the equations of continuity, momentum, energy and surface heat transfer will be applied to develop each of the three flow models. In a subsequent section, the solutions of the particular equations for each model will be compared with each other and with experimental data. In this way the the accuracy of the analysis for non-equilibrium flow in the char zone can be evaluated and the extent to which the two limiting cases predict the behavior can be determined.

Frozen flow.-The frozen flow model is an idealization in which the pyrolysis products entering the char zone do not change in composition as they pass through the medium. Therefore, any benefit from the energy absorbed by the predominently endothermic chemical reactions which occur between the gases and char is not obtained. It specifies a lower limit on the amount of energy absorbed in the char zone. Of the three cases it is the simplest because the chemical reaction terms in the energy and heat flux equations are zero:

$$\sum_{i=1}^{K+1} H_i \bar{R}_i = 0 \qquad (7)$$

Applying this to the equations of change developed previously results in the following simplifications for frozen flow in the char layer.

Continuity Equation $$W = W_p \varepsilon = \text{constant} \qquad (8)$$

Momentum Equation $$P = \left\{P_L^2 + 2R\left[\int_Z^L \left(\frac{\mu}{\gamma}\right)(W)\left(\frac{T}{M_w}\right)dz + \int_Z^L \beta\left(\frac{T}{M_w}\right)(W)^2 dz\right]\right\}^{1/2} \qquad (9)$$

Heat Flux Equation $$q_{cz} = (q_L - q_o) = \sum_{i=1}^{K} \int_{T_o}^{T_L} \varepsilon W_p C_{pi} x_i dT \quad (10)$$

Energy Equation $$\varepsilon \bar{C}_p W_p \frac{dT}{dz} = \frac{d}{dz}\left[k_e \frac{dT}{dz}\right] \quad (11)$$

The numerical solution of these equations will be discussed in a later section.

Equilibrium flow.-The equilibrium flow in the char zone gives an upper limit on the amount of heat that can be absorbed within the char zone. The reason is that the reactions occuring within the char are predominately endothermic. The set of equations used to describe flow for this case is the same as the equations developed previously: continuity (8), momentum (9), energy (3), and heat flux (4). The distinguishing feature lies in the method used to calculate the energy absorption by chemical reactions:

$$\sum_{i=1}^{K+1} H_i \bar{R}_i \neq 0 \quad (12)$$

Rewriting the species continuity equation, (1), in terms of the mole flux of species i gives:

$$R_i = \frac{d}{dz}(\rho v) = \frac{d}{dT}(W x_i) \frac{dT}{dz} \quad (13)$$

Therefore, in order to evaluate the term, $\sum_{i=1}^{K+1} H_i \bar{R}_i$, the mass flux, W, and the mass fraction, x_i, of the species in the gas and solid phases must be known as a function of temperature. The species composition and molal ratio of gases to carbon are a function of temperature, pressure and elemental composition of the virgin plastic and can be calculated by one of the many approaches in the literature (27,28). In this study, the free energy minimization technique was used (26).

Non-equilibrium flow.-The equations of change for non-equilibrium flow are the same as those developed for equilibrium flow. The evaluation of the energy absorption by chemical reaction, however, is dependent on the finite reaction rates of each reaction occurring within the char zone. Therefore, in addition to temperature and pressure, the reaction rate, R_i, is also a function of the mass flux and composition entering the char layer. This requires a knowledge of the specific reactions taking place within the char and the associated kinetic data; i.e., frequency factor and activation energy. The following paragraphs will present a method for determining the important reactions and the technique for using the kinetic data to predict the actual behavior within the char zone.

Reaction rate and rate constant equation.-In general, a chemical reaction can be written in the following form:

$$\sum_{i=1}^{q} r_{ij}A_i \rightleftarrows \sum_{i=1}^{q} p_{ij}A_i;\ j = 1,2,3,\ldots,m \tag{14}$$

For this j-th chemical reaction, r_{ij} and p_{ij} are the stoichiometric coefficients of the reactants and products respectively for species A_i. There are a total of q chemical species and m chemical reactions in the system.

The rate of reaction of the i-th species, R_i, is given by the following equation for the m chemical reactions:

$$R_i = \sum_{j=1}^{m} (p_{ij} - r_{ij})\left[k_{f_j} \prod_{k=1}^{q} c_i^{r'_{ij}} - k_{r_j} \prod_{k=1}^{q} c_i^{p'_{ij}}\right];$$

$$i = 1,2,3,\ldots,q \tag{15}$$

where c_i is the concentration of component i and r'_{ij} and p'_{ij} represent the power on the concentrations. It is not necessary for these to be equal to r_{ij} and p_{ij}. The forward and reverse reaction rate constants are k_{fj} and k_{rj}. This is the equation for R_i that is used in the computer implemented numerical solution of the transport equations. Equation (15) is a very convenient and general formulation for the reaction rate of the j-th species in m simultaneous chemical reactions. The stoichiometric coefficients and the powers on the concentrations are each conveniently represented as a matrix.

In addition to the above, the reaction rate constants are also required. A general form for the rate constant of the i-th chemical reaction is:

$$k_j = A_j T^{s_j} \mathrm{Exp}\ (-E_j/RT)\ ;\ j = 1,2,3,\ldots,m \tag{16}$$

where A_j is the frequency factor and E_j, the energy of activation.

With these mathematical generalizations the analysis is resolved to one of selecting the important chemical reactions taking place in the char zone along with precise values of the rate constants. These equations and associated rate constants can then be used in equation (15) to calculate the reaction rate, R_i, which is needed to solve the transport equations.

The non-equilibrium flow model is an order of magnitude more complex than the chemical equilibrium computations. The latter case involves the solution of a set of algebraic equations with the energy and momentum equations. The former requires the solution of a set of non-linear, ordinary differential equations (species continuity equations) simultaneously with the energy equation. There is also the additional difficulty of determining all of the important chemical reactions that take place in the system and the initial composition of pyrolysis products entering the char zone. For equilibrium

flow, only the elemental composition is required. Finally, there is the laborious task of collecting and evaluating reaction kinetic data appearing in the literature.

Chemical reactions in the char layer.-The general nature of the reactions occurring in the char zone of a charring ablator has been qualitatively established (29). Between 500°F (533°K) and 3000°F (1925°K), the primary reactions occurring are hydrocarbon cracking reactions of high molecular weight species to lower molecular weight species (ultimately H_2, CO_2, CO, H_2O, etc.). From 3000°F (1925°K) to about 6000°F (3590°K), free radical and recombination reactions take place, with ionization reactions beginning to appear at the upper end of this temperature region. This study is concerned with the reactions occurring below 3000°F (1925°K); i.e., hydrocarbon cracking reactions, primarily. Free radical, recombination and ionization reactions are not considered as they do not take place. Fortunately, this greatly simplifies the already complex system of reactions that could occur. Establishing the fact that reacting flow in the char zone can be accurately described in the temperature range from 500° (533°K) to 3000°F (1925°K) establishes the basis for extending the investigation to temperatures in the 3000°F (1925°K) to 6000°F (3590°K) range.

Pike (30), in an effort to condense the large assortment of reaction kinetic data available in the literature, has compiled a detailed listing of reactions and the corresponding kinetic data for the C-H-O-N system. In a subsequent report (31) this and other kinetic data were analysed. The calculation of the isothermal conversion for each reaction possible in the char zone over a wide range of temperatures was included. This formed one method for determining the important reactions taking place in the char zone as discussed below.

Criterion for reaction selection.-The rate of a chemical reaction increases with temperature. For a particular reaction, if a significant conversion of reactants to products is obtained with the char at a uniform and specified temperature, then it can be assumed that there may be a significant conversion when a temperature gradient exists in the char layer with the front surface at this specified temperature. Thus, this reaction is considered important. An example of this behavior is the reaction illustrated in Figure 3 as a plot of conversion versus temperature. For another reaction if there is no conversion in the char at a uniform higher temperature (1925°K), there will be no conversion when there is a temperature gradient in the char. Therefore, this reaction can be omitted when there is a temperature gradient in the char with a front surface temperature of 1925°K. However, the products formed by the reaction may indeed be included as important components subject to further reactions. This logic forms the basis of the isothermal analysis of reaction kinetics data in the literature (31).

Although the reactions postulated to take place over a given temperature range (533°K to 1925°K) could occur, they are also restricted by the components initially present in the pyrolysis gas stream. For example, the reaction of butane and oxygen forming carbon dioxide and water is a likely candidate between 500°F (533°K) and 3000°F (1925°K); however, the absence of either butane or oxygen eliminates the reaction from consideration. A considerable amount of

caution must be exercised to make certain that the components are not formed at some time within the char, making the reaction an important part of the system.

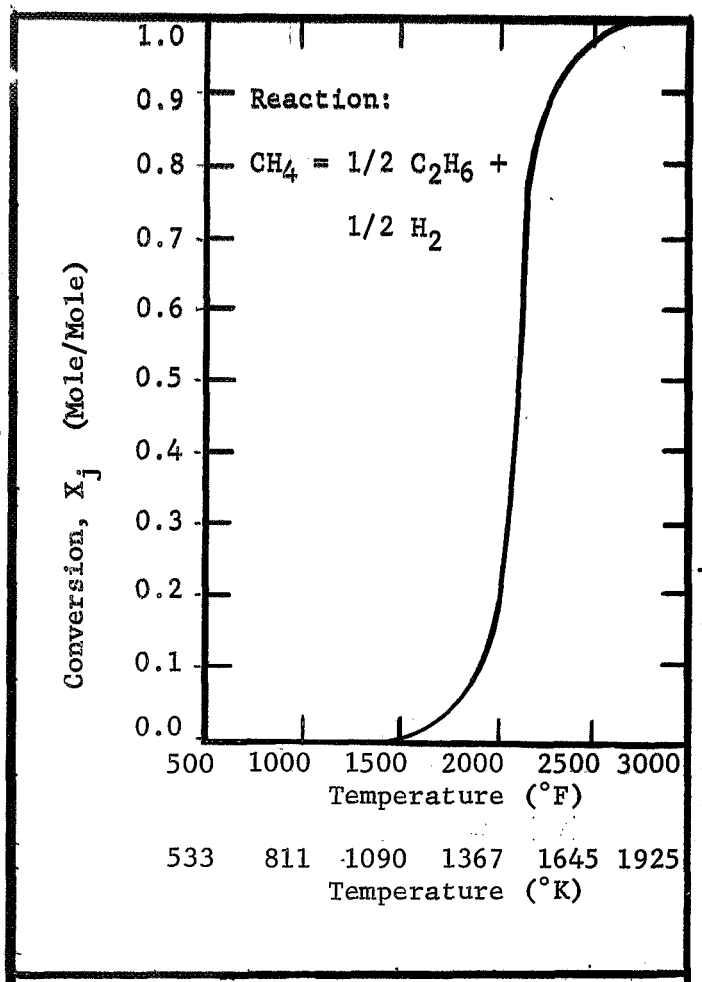

Figure 3. Isothermal Conversion of Methane to Hydrogen and Ethane Between 533°K and 1925°K.

The ten chemical reactions which accurately describe the energy transfer associated with reacting pyrolysis gas flow through the char zone of a charring ablator between 500°F (533°K) and 3000°F (1925°K) are listed in Table 5. In addition to the criterion just discussed for eleminating reactions, the composition of the pyrolysis products entering the char at the back surface was also considered.

Composition of pyrolysis products.-As discussed above, the pyrolysis product composition at the back surface of the char is important in reducing the total possible reactions likely to occur within a specified temperature range. First attempts to study the non-equilibrium flow of pyrolysis products through a porous char layer relied on two separate sources for estimating the gas composition entering the char at the back surface. The first method which served as an order of magnitude analysis was the equilibrium compositions calculated by the free energy minimization method (26). The second was analyses of the degradation products of low density nylon-phenolic resin composites by pyrolysis gas chromatography (32, 33). The unavailability of accurate analytical procedures and thermo-physical data for the high molecular weight pyrolysis products (i.e., phenol, cresol, toluene, etc.) left a region of definite uncertainty. As a result, the major components of the pyrolysis products were methane, hydrogen, carbon dioxide, carbon monoxide and nitrogen by many (34,35) with unknown quantities of water and high molecular weight residues completing the analysis.

Subsequent research by Sykes (36) confirmed the presence of phenol-based materials as primary constituents in the high molecular weight residues.

Table 5. Important Reactions and Associated Kinetic Data for the Pyrolysis Product Species in the Char Zone Between 533 - 1925°K.

General Form of the Reactions: $aA + bB + \ldots + = rR + sS + \ldots +$

General Rate Constant Equation: $k = k^{\circ}T^{-s} \exp(-E/RT)$

Reaction Number	Reaction	Rate Law	Activation Energy E,(KJ/Kg-mole)	Frequency Factor	s	References
1	$CH_4 = 1/2\ H_2 + 1/2\ C_2H_6$	k_fA	38.0	7.6×10^{14} *	0	42,43,44,45, 46,47
2	$C_2H_6 = C_2H_4 + H_2$	k_fA	28.0	3.1×10^{14} *	0	42,48,44,45, 46,49
3	$C_2H_4 = C_2H_2 + H_2$	k_fA	16.0	2.6×10^{8} *	0	42,43
4	$C_2H_2 = 2C + H_2$	k_fA^2	4.0	2.1×10^{7} **	0	42,50,55
5	$C + 2H_2 = CH_4$	k_f	7.0	2.0×10^{12} ***	0	56,57,51,52, 53,54,58
6	$C_6H_6O + H_2 = H_2O + C_6H_6$	k_fA	18.0	2.0×10^{13} *	0	72
7	$C_6H_6 = 3\ C_2H_2$	k_fA	14.0	1.4×10^{9} *	0	59
8	$C + H_2O = CO + H_2$	k_fAB	33.0	1.2×10^{9} **	-1	66,71,60,61, 62,63,64,67
9	$CO + H_2O = H_2 + CO_2$	k_fAB	12.0	1.0×10^{9} **	0	65,60,61,62, 63,64,67,68
10	$C + CO_2 = 2\ CO$	$k_fA-k_rR^2$	20.0 24.0	1.0×10^{6} * 1.0×10^{-12} **	-1 0	69,70,60,61, 62,63,64,68

* 1st Order (sec^{-1}) ** 2nd Order (M^3/Kg-mole-sec) *** 0^{th} Order (Kg-mole/M^3)

Table 6 represents a more precise pyrolysis gas composition obtained by Sykes (36). Very good agreement was obtained by comparing the reported experimental results with an overall energy balance technique using heats of formation and heats of combustion data for the virgin plastic and the experimentally determined pyrolysis product composition.

The simultated pyrolysis gas composition used in the experimental program is also listed in Table 6.

Table 6. Pyrolysis Products Resulting From the Thermal Decomposition of Nylon-Phenolic Resin Composites Including the High Molecular Weight Species.

Component	Sykes (36) Mole % (Nylon-Phenolic Resin)		Sykes (33) Mole % (Phenolic Resin Only)	Simulated Pyrolysis Product Composition
	By Flash Pyrolysis at 1073°K	By Pyrolysis at 50°C Increments to 900°C (1475°K)		
Phenol	8.0	7.6	6.7	[
Methylphenol	4.0	4.0	2.1	
Dimethylphenol	2.8	3.2	0.0	
Trimethylphenol	2.4	2.7	0.0	6.2
Benzene	0.4	0.4	0.2	
Toluene	0.0	0.2	0.4	
Cyclopentanone	1.2	2.5	0.0	]
Hydrogen	30.2	32.2	47.1	33.4
Methane	3.8	4.0	9.4	6.7
Carbon Monoxide	5.3	3.6	5.2	3.7
Carbon Dioxide	12.1	6.8	1.5	1.1
Water	20.1	23.3	22.0	48.9
Ammonia	0.8	0.4	0.0	0.0
Unidentified	9.2	10.1	5.2	0.0
Totals	100.0	100.0	100.0	100.0

Physical and thermodynamic properties.-In any real problem where the temperature gradient varies over a wide range (>1000°K), changes in the physical and thermodynamic properties as a function of temperature occur. For the multicomponent flow of a reacting gas within a porous char, composition change by chemical reaction is also important. The equations used in this research for calculating the variation in physical and thermodynamic properties are shown in Table 7.

Table 7. Equations Expressing the Physical and Thermodynamic Properties as a Function of Temperature

Gas Phase Properties:

1. Thermal conductivity:
   of a pure gas component

$$kg_i = \frac{2.6693 \times 10^{-5} \left(\frac{T}{Mw_i}\right)^{1/2} (Cv_i + 4.47)}{\sigma^2 \Omega_v} \quad (17)$$

   of a gas mixture

$$\bar{kg} = \sum_{i=1}^{k} n_i kg_i / \sum_{i=1}^{k} n_i \quad (18)$$

2. Viscosity:
   of a pure gas component

$$\mu_{gi} = \frac{2.6693 \times 10^{-3} \left((M_{vi})T\right)^{1/2}}{\sigma^2 \Omega_v} \quad (19)$$

   of a gas mixture

$$\bar{\mu}_g = \sum_{i=1}^{K} \mu_i \left[1 + \sum_{\substack{j=1 \\ j \neq i}}^{K} \phi_{ij} (n_j/n_i)\right]^{-1} \quad (20)$$

   where

$$\phi_{ij} = \frac{\left[1 + (\mu_i/\mu_j)^{1/2} (M_{wj}/M_{wi})^{1/4}\right]^2}{\left[\sqrt{8}(1 + (M_{wi}/M_{wj})\right]^{1/2}} \quad (21)$$

3. Heat capacity

$$C_{pi}/R = a_i + b_i T + c_i T^2 + d_i T^3 + e_i T^4 \quad (22)$$

4. Free energy

$$\frac{(F^\circ T)_i}{RT} = a_i (1 - \log_e T) - \frac{b_i}{2} T - \frac{c_i T^2}{6} - \frac{d_i}{12} T^3 - \frac{e_i}{20} T^4 - \frac{f_i}{T} - g_i \quad (23)$$

5. Enthalpy

$$\frac{(H^\circ T)_i}{RT} = a_i + \frac{b_i}{2} T + \frac{c_i}{3} T^2 + \frac{d_i}{4} T^3 + \frac{e_i}{5} T^4 + \frac{f_i}{T} \quad (24)$$

Char Properties:

1. Porosity	Assumed constant and equal to the average effective porosity.
2. Permeability	Average values obtained from a Carman - Cozeny plot of reported experimental data (26).
3. Thermal Conductivity	Linear least squares fit of available experimental data (26).

Numerical Solution of the Equations of Change

Prior to the selection of a numerical method, the accuracy of the numerical solution desired must be specified. This determines the interval size needed in the analysis which effects the round-off errors associated with the calculation of the solution. If a relatively small interval size is used, the round-off errors may be intolerable. On the other hand, a very large interval size could produce large truncation errors which results in a solution that does not approach the true solution. One technique used to determine if a specific interval size is a reasonable choice involves the computation of the solution for the particular interval selected, and interval sizes reduced by a factor of one half of each preceeding value. Comparison of the solutions for each interval chosen should reveal when the approximate solution approaches the true solution or when round-off errors make the calculated solution invalid.

In general, increased accuracy requires increased complexity in (or order of) the numerical method used. Therefore, there is an optimum decision to be made between the nearness of the approximate solution to the real solution and the computational time required to obtain the solution. The best approach is obviously the one that minimizes truncation and round-off errors.

Numerical solution of the differential energy equation.-The energy equation describing the flow of pyrolysis gases through the char zone of a charring ablator is a second order, non-linear differential equation with variable coefficients. In order to obtain a solution to this equation, a numerical integration technique must be used. This requires the equation to be transformed into a finite difference form which can be integrated stepwise on a digital computer. Of the various methods available, all require the specification of the order and stepsize to achieve the desired solution. Two general types of numerical integration schemes are commonly used; the self-starting methods, ranging from the Euler equation to the Runge-Kutta series, and, the predictor-corrector methods which require the specification or calculation of several initial points to start the procedure. The number of points is proportional to the order of the particular equation used. Because of the accuracy and relatively straightforward nature of the self-starting methods, a fourth order Runge-Kutta formula was selected.

The formulae as they apply to the differential energy equation are presented in Table 8. The truncation error is of the order $0(h^5)$ where h is the step size (37). The parameters A_1, A_2, A_3, and A_4 in equation (28) correspond to the Runge-Kutta parameters generated by the numerical integration of the energy equation.

Therefore, in the non-equilibrium flow analysis, the solution of the energy and continuity equations are calculated simultaneously because of the interdependence of the temperature and the mole flux (composition).

Numerical solution of the species continuity equation.-In the non-equilibrium flow analysis, the species continuity equation expressing the mole (or mass) flux of each species as a function of temperature must be solved simultaneously with

the differential energy equation. Rewriting equation (13) in terms of the mole flux, N_i, of species i gives:

$$\frac{dN_i}{dT} = \left(\frac{R_i}{M_{wi}}\right)\left(\frac{1}{dT/dz}\right) \tag{25}$$

Table 8. Fourth Order Runge-Kutta Formulae for Solving the Differential Energy Equation for Flow of Pyrolysis Gases Through the Char Zone

Formulae for the Flow of Pyrolysis Gases Through Chars

$$T_{N+1} = T_N + h\left[T'_N + \frac{1}{6}(A_1 + A_2 + A_3)\right] \tag{26}$$

$$T'_{N+1} = T'_N + \frac{1}{6}(A_1 + 2A_2 + 2A_3 + A_4) \tag{27}$$

$$A_1 = h(T'_o)\left[\frac{W_p\bar{C}_p\varepsilon}{k_e} - \frac{dk_e/dT}{k_e}(T'_o) + \frac{\Sigma H_i\bar{R}_i}{k_e}\right]_{T_o}$$

$$A_2 = h(T'_o+1/2\ A_1)\left[\frac{W_p\bar{C}_p\varepsilon}{k_e} - \frac{dk_e/dT}{k_e}(T'_o + 1/2\ A_1) + \frac{\Sigma H_i\bar{R}_i}{k_e}\right]_{T_o+\frac{h}{2}T'_o+\frac{h}{8}A_1}$$

$$A_3 = h(T'_o+1/2\ A_2)\left[\frac{W_pC_p\varepsilon}{k_e} - \frac{dk_e/dT}{k_e}(T'_o+1/2\ A_2) + \frac{\Sigma H_i\bar{R}_i}{k_e}\right]_{T_o+\frac{h}{2}T'_o+\frac{h}{8}A_2}$$

$$A_4 = h(T'_o + A_3)\left[\frac{W_pC_p\varepsilon}{k_e} - \frac{dk_e/dT}{k_e}(T'_o+A_3) + \frac{\Sigma H_i\bar{R}_i}{k_e}\right]_{T_o+hT'_o+\frac{h}{2}A_3} \tag{28}$$

where the temperature gradient, dT/dz, is calculated in the energy equation solution. Substitution for R_i from equation (15) results in the final form of the equation used to calculate the species mole flux, N_i, in the TEMPRE system.

$$\left(\frac{dN_i}{dT}\right) = \sum_{j=1}^{m} \frac{(p_{ij} - r_{ij})}{M_{wi}} \left[k_{fj} \prod_{i=1}^{K+1} c_i^{r'_{ij}} - k_{rj} \prod_{i=1}^{K+1} c_i^{p'_{ij}} \right];$$

$$i = 1,2,3,\ldots, K+1 \qquad (29)$$

The solution of the K+1 first order differential equations for the mole flux, N_i, is obtained by numerical integration using a fourth order Runge-Kutta formula (37) shown in Table 9.

Table 9. Fourth Order Runge-Kutta Formulae for Solving The Species Continuity Equation.

$$N_{i_{M+1}} = N_{i_M} + \frac{1}{6}(B_{i,1} + 2B_{i,2} + 2B_{i,3} + B_{i,4}) \qquad (30)$$

where

$$B_{i,1} = hf(T_0, N_{1,0}, N_{2,0}, N_{3,0}, \cdots, N_{K+1,0})$$

$$B_{i,2} = hf\left(T_0 + \frac{h}{2}T'_0 + \frac{h}{8}A_i,\ N_{i,0} + 1/2B_{2,1},\ N_{I+1,0} + 1/2B_{K+1,1}\right)$$

$$B_{i,3} = hf\left(T_0 + \frac{h}{2}T'_0 + \frac{h}{8}A_2,\ N_{1,0} + 1/2B_{1,2},\ N_{2,0} + 1/2B_{2,2},\ \ldots,\ N_{K+1,0} + 1/2B_{K+1,2}\right)$$

$$B_{i,4} = hf(T_0 + hT'_0 + \frac{h}{2}A_3,\ N_{i,0} + B_{1,3},\ N_{2,0} + B_{2,3},\ \ldots,\ N_{K+1,0} + B_{K+1,3}) \qquad (31)$$

The interdependence of the energy and species continuity equations can be seen by noting the presence of the A_j values in the above equations (31). These values are the Runge-Kutta parameters calculated for the energy equation solution at the same position within the char. A one-to-one correspondence between the A_j and $B_{i,j}$ values must exist to obtain a non-equilibrium flow solution. To start the integration, the initial composition, temperature and temperature gradient at the back surface are used to calculate the first intermediate temperature and Runge-Kutta parameter, A_1. These values are then used to estimate the mole flux of each species at the same

intermediate position within the char zone. The intermediate flux values are then substituted into the energy equation for the calculation of the next intermediate temperature. This procedure is continued until the four (for a fourth order analysis) parameters associated with each differential equation (continuity and energy) are calculated. At this point the temperature and concentration at a position advanced one interval unit into the char are calculated using equations (26) and (30).

This technique is repeated to the second boundary of the problem. If a non-iterative set of boundary conditions is specified (i.e., one boundary completely specified), the solution to the energy equation is obtained in one cycle and the calculation of the pressure and heat flux distributions can be started. If, however, a two point boundary value problem is being solved, a guessed value of the gradient must be used to start the solution. When the temperature at the front surface is calculated, it must be compared with the specified value. A calculated value which is too high or low requires an adjustment of the initial gradient and repetition of the entire procedure. Therefore, in addition to the Runge-Kutta logic, a convergence procedure to approach the known front surface temperature is also required.

Convergence techniques for the iterative Runge-Kutta analysis.-The specific convergence scheme used in the Iterative TEMPRE System is subdivided into three main parts. These include: (1) a gross correction procedure, (2) a fine correction procedure, and, (3) a limit or check procedure. Each method uses a simplified formula which bases the corrected adjustment on the relative overshoot or undershoot of the fromt surface temperature.

Gross correction procedure.-This method is used when the absolute value of the difference in the calculated and true front surface temperature exceeds a specified tolerance limit (usually $\geq$ 5% of the specified front surface temperature). When this condition is met, adjustment of the initial slope is made using the following equation:

$$T'_{O_{new}} = T'_{O_{old}} \left(1 + \lambda \left[\frac{T_{L_{true}} - T_{L_{calculated}}}{T_{L_{true}}} \right]\right) \qquad (32)$$

where λ is an adjustable parameter from 0 to 1.

Fine correction procedure.-This method is employed when the calculated front surface temperature falls between tolerance limits of $0.05 > 1 - T/T_L > 0.01$ of the specified value or when two complete cycles have been calculated. In this case a more precise adjustment is used taking advantage of the previous calculations to rapidly approach the specified front temperature and to prevent oscillations around that point. The specific equation used to adjust the initial gradient for the next iteration is:

$$T'_{O_{new}} = T'_{O_{old}} + \left[\frac{T_{L_{true}} - T_{L_{calc.\ this\ cycle}}}{T_{L_{calc.\ this\ cycle}} - T_{L_{calc.\ last\ cycle}}}\right] \left[T'_{O_{last\ cycle}} - T'_{O_{this\ cycle}}\right] \tag{33}$$

Very good convergence is obtained with these simple equations over a range of front surface temperatures between 1500 - 3000°F (1090 - 1925°K) and mass flux values between 0.0003 - 0.1 lb/ft^2-sec (0.00015 - 0.5 kg/m^2-sec). Three iterations are required to obtain a solution within the stated tolerance range.

Limit or check procedure.-A limit corresponding to a 20% overshoot of the front surface temperature is used to terminate the calculations at any point within the char where this condition is violated. A reduction in the initial gradient is made according to equation (32) and the procedure is restarted.

In addition to the above, several checks are included in the Runge-Kutta analysis to insure the calculated and/or adjusted values of the gradient remain non-negative and non-zero. The program logic includes an adjustment calculation similar to equation (32) which, on repeated violations, instructs the system to print pertinent information for diagnosis of the problem. With these simple adjustment equations, the iterative solution is obtained very quickly and with sufficient accuracy to insure a good approximation to the real solution.

A comparison of the temperature profiles obtained for the frozen flow energy equation (11) at various interval sizes is presented in Table 10. Based on the presented results, an interval size of one hundred units (or 1/400 ths of an inch for a one-quarter thick char) was used.

Numerical Solutions of the Heat Flux and Momentum Equations

The heat flux and momentum equations are solved after a valid temperature profile is calculated. Both heat flux and pressure are uncoupled from the energy equation by considering the energy dissapation by PV work small in comparison with other modes of energy transfer in the system. The equations for the heat flux and pressure are first order differential equations with variable coefficients.

$$q_{c_z} = \sum_{i=1}^{K} \int_{T_o}^{T_L} \epsilon W_p C_{p_i} x_i \, dT + \sum_{i=1}^{K+1} \int_{z}^{L} H_i \bar{R}_i dz \tag{4}$$

$$P = \left[P_L^2 + 2R\left(\int_z^L \left(\frac{\mu}{\gamma}\right)(W)\left(\frac{T}{M_w}\right)dz + \int_z^L \beta\left(\frac{T}{M_w}\right)(W)^2 dz\right)\right]^{1/2} \tag{2}$$

Table 10. Comparison of Various Runge-Kutta Increment Sizes for the Frozen Flow Variable Physical Properties Model

Dimensionless Char Distance (z/L)	Temperature (°K) Runge-Kutta Increment Size 10	50	100	400
0.0	533.0000	533.0000	533.0000	533.0000
0.2	606.0118	602.7934	602.7104	602.6779
0.4	713.1568	710.5278	710.4730	710.4393
0.6	869.7659	867.8951	867.8761	867.8412
0.8	1085.5353	1084.6029	1084.5700	1084.5336
1.0	1366.3333	1366.3333	1366.3333	1366.3333

Conditions: $W = 0.25$ Kg/m^2-sec $L = 0.0063$ M $\epsilon = 0.8$

Gas Composition (Mole/Mole Gas):

CO = 0.245, CO_2= 0.046, N_2= 0.073, CH_4= 0.570, C_6H_6= 0.068

A Simpson's Rule integration technique is used to obtain solutions for the integral terms in these equations. The general formula for the Simpson's Rule analysis is (37):

$$\int_{z_o}^{z_{2n}} f\,dz = \frac{h}{3}\left[f_o + 4\,(f_i + f_3 + \ldots + f_{2n-1}) + 2(f_2 + f_4 + \ldots + f_{2n-2}) + f_{2n} \right] - \frac{nh^5}{90} f^{(4)} \tag{34}$$

where $\frac{nh^5}{90} f^{(4)}$ represents the truncation error.

In terms of the heat flux and pressure equations, the Simpson's Rule functions are:

$$\int f_{p_1} dz = \int \left(\frac{\Psi}{\gamma}\right) (W) \left(\frac{T}{M_w}\right) dz \tag{35}$$

$$\int f_{p_2} dz = \int \beta \left(\frac{T}{M_w}\right) (W)^2 dz \tag{36}$$

$$\int f_{h_1} dz = \int \epsilon W_p C_p x_i dT \tag{37}$$

$$\int f_{h_2} dz = \int H_i \bar{R}_i dz \tag{38}$$

Once again the step-size is an important parameter that must be specified. A similar procedure as that described for the Runge-Kutta analysis to obtain the optimum value of the interval size was used. This minimizes the errors and maximizes the accuracy of the approximate solution. A comparison of the solutions for various step sizes is presented in Table 11. An interval size of twenty steps was used in this analysis. Calculation of the pressure profile within the char is made from the front surface where $P = P_L$ to the rear surface pressure. Results are reported as a pressure distribution and a surface heat flux which correspond to the total heat transferred within the char zone.

Summary of the Theoretical Development of the Equations of Change for Flow in the Char Zone

The equations of change (continuity, momentum, and energy) were developed for modeling the reacting flow of pyrolysis gases through the char zone of a charring ablator. The particular application to frozen, equilibrium, and non-equilibrium flow were discussed along with methods for determining the heat absorption by chemical reaction for the latter two models.

Table 11. Comparison of Various Simpson's Rule Increment Sizes for the Frozen Flow, Variable Physical Properties Model

Dimensionless Char Distance (Z/L)	Pressure (Kg/m^2) Simpson's Rule Increment Size 20	50	100	200
0.00	10877.9605	10877.9590	10877.9565	10877.9560
0.33	10867.0735	10867.0720	10867.0695	10867.0690
0.67	10843.6865	10843.6840	10843.6820	10843.6820
1.00	10800.0000	10800.0000	10800.0000	10800.0000

Conditions: $W = 0.25\ Kg/m^2\text{-sec}$ $L = 0.0063\ M$ $\epsilon = 0.8$

Gas Composition (Mole/Mole Gas):

$CO = 0.245$, $CO_2 = 0.046$, $N_2 = 0.073$, $CH_4 = 0.570$, $C_6H_6 = 0.068$

Similarly, the momentum and heat flux equations were integrated using Simpson's Rule. The solutions were presented as a pressure distribution across the char and a heat flux at the char front surface. A fourth order Runge-Kutta integration of the species continuity equation, coupled with the energy equation, produced concentration gradients for each pyrolysis gas species as a function of the char distance.

Specific values of the solutions will be presented and compared with experimental data obtained on the Char Zone Thermal Environment Simulator in a subsequent section. The experimental apparatus and procedure follows.

CHAR ZONE THERMAL ENVIRONMENT SIMULATOR

Experimental Equipment

The experimental data presented in this study were obtained using an apparatus that simulated the flow of pyrolysis gases through the char layer of a charring ablator during reentry. Low density nylon-phenolic resin chars, graphite and carbon were obtained from the National Aeronautics and Space Administration's Entry Structures Branch at the Langley Research Center. These specimens were placed in a metal holder with the front surface exposed to a bank of infrared quartz lamps used to simulate the high temperatures experienced by a reentering vehicle. Simulated pyrolysis gases were passed through the char from the rear surface to the heated front surface. The exit gases were sampled and analyzed for comparison with the inlet gas composition to determine whether chemical reactions had occurred within the char. These results were also compared with the calculated exit gas compositions for frozen, equilibrium and non-equilibrium flow conditions in the TEMPRE system. This was the method used to determine the accuracy of the non-equilibrium model for predicting the heat transfer for the flow of reacting pyrolysis products in the char zone. A schematic diagram of the Char Zone Thermal Environment Simulator is shown in Figure 4. A detailed description of the apparatus, including dimensions, materials of construction and assembly diagrams are included in reference (26).

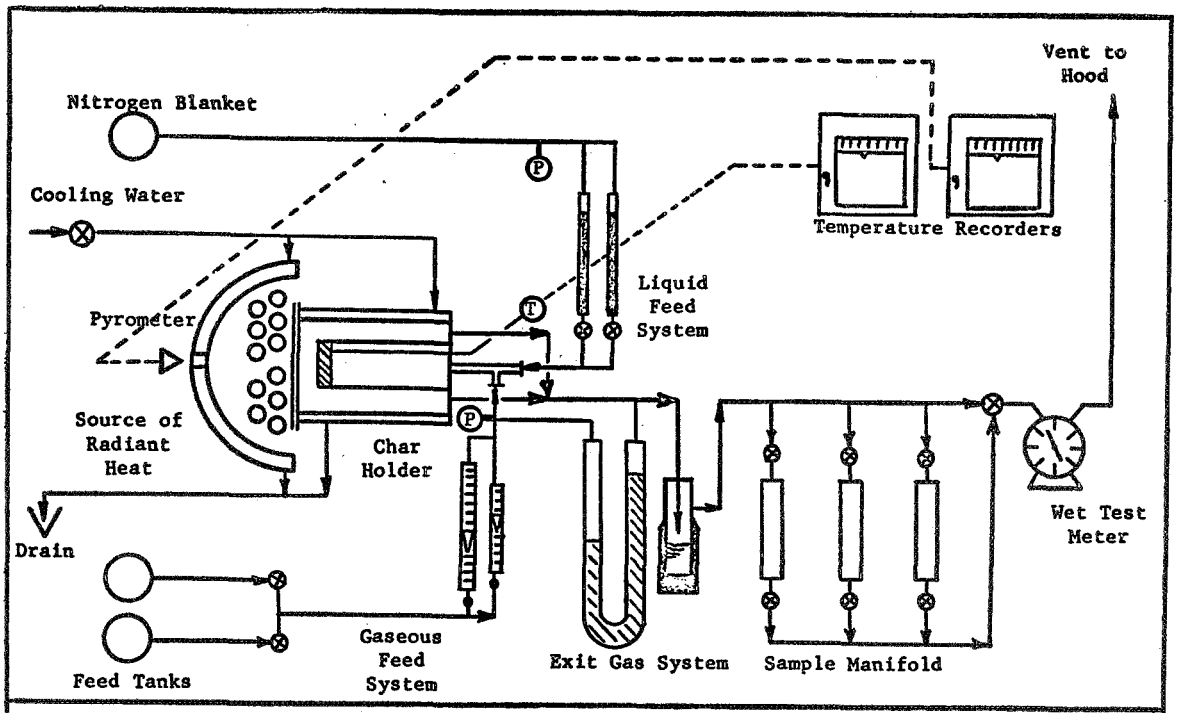

Figure 4. Schematic Diagram of the Char Zone Thermal Environment Simulator

Experimental Procedure

The procedure used for all experiments with the Char Zone Thermal Environment Simulator considered safety as the prime requisite. The recommendations for safe handling of hazardous materials outlined in Dangerous Properties of Industrial Materials by N. I. Sax (38) and "Chemical Safety Data Sheets" by the Manufacturing Chemists' Association (39, 40, 41) were used as guides. Proper ventilation of the laboratory and various safety devices including exhaust hoods, eye wash basin, safety shower, fire extinguisher and self-contained breathing equipment were available and employed.

The experimental procedure for the operation of the Char Zone Thermal Environment Simulator was divided into five main portions and are summarized in Table 12.

Table 12. Experimental Procedure for the Operation of the Char Zone Thermal Environment Simulator.

Phase	Function(s)
Pre-startup	Test instrumentation and equipment with helium (Argon) flow.
Startup	Turn lamps on. Obtain steady state with lamps on full power.
Experimental	Introduce pyrolysis gases. Record results of steady state runs.
Shutdown	Turn lamps off. Turn pyrolysis gas feed off. Introduce helium (Argon) to flush system.
Analytical	Analyse gas, liquid and radioactive labeled samples.

The analytical phase was carried out one day after the experiment and involved those analyses listed in Table 13. Reference to the original research report (26) is made for greater detail and explanation of the various procedures summarized in the above paragraphs.

Table 13. Typical Analyses of Samples From the Char Zone Thermal Environment Simulator

Gases:	H_2, CO, CH_4	Activated Charcoal Argon Gas Carrier (30cc/min) Temperature 280°F (410°K)
	H_2, CH_4, CO_2, C_2H_4, C_2H_2	Porapak S Argon Carrier (20cc/min) Temperature 165°F (350°K)
Liquids:	Phenol in aqueous solutions	ASTM Bulletin D 2145
Radioactive:		
Liquids & Gases:	Effluent from gas chromatograph is combusted forming CO_2 and H_2O. CO_2 is absorbed in one molar Hyamine Hydroxide solution and analysed on a liquid scintillation spectrometer.	
Solids:	Chars are combusted in a tubular furnace to CO_2 and H_2O. CO_2 is absorbed in one molar Hyamine Hydroxide solution and analysed on a liquid scintillation spectrometer.	

RESULTS OF THE NON-EQUILIBRIUM ANALYSIS OF PYROLYSIS GAS FLOW IN THE CHAR ZONE

Comparison of the Non-Equilibrium Flow Results with Experimental Data using Low Density Nylon-Phenolic Resin Chars.

In order to obtain solutions to the equations of change, the important chemical reactions occurring within the char, and the pyrolysis gas composition entering at the back surface must be specified. This information is summarized in Tables 5 and 6, respectively. The values of the activation energy and frequency factor for each reaction is compared to literature values in reference (26). In all cases very good agreement was obtained. The use of these data in the non-equilibrium flow model allows the calculation of the solutions to the energy, momentum and heat flux equations describing reacting flow in the char zone.

The basis for evaluating the non-equilibirum flow model as an accurate and realistic analysis of energy transfer in the char layer is by comparison of the experimentally determined exit product compositions from the Char Zone Thermal Environment Simulator with the calculated compositions in the non-equilibrium flow model. This was done for seventeen experiments using low density nylon-phenolic resin chars in which front surface temperatures of 1575-2300°F (1130-1535°K) and pyrolysis gas mass flux values of 0.00003-0.108 lb/ft^2-sec) (0.00015-0.540 kg/m^2-sec) were studied.

In order to obtain a significant conversion of the pyrolysis gases over the temperature range investigated, the residence time within the porous char was increased by decreasing the mass flux. Thus the combination of the highest temperature and lowest mass flux produced a maximum conversion resulting from chemical reactions.

Typical experimental results for the entire range of parameters studied are presented in Table 14. Also listed are the exit gas compositions resulting from the frozen (or initial composition) equilibrium and non-equilibrium calculated results. The excellent agreement of the calculated non-equilibrium compositions with the experimentally determined exit gas compositions obtained in the Char Zone Thermal Environment Simulator prove the analysis to be realistic and accurate over the entire range of temperature and mass fluxes investigated. In addition, a definite transition from a frozen condition, corresponding to relatively low temperatures and high mass flux values, to a non-equilibrium condition, corresponding to higher temperature and lower mass fluxes is noted. Also, in all cases except for those in which the mass flux values are extremely small (less than 0.00015 kg/m^2-sec), the compositions predicted by the equilibrium flow model are inaccurate and unrealistic. A more direct comparison of the three models (frozen, equilibrium and non-equilibrium) will be discussed in the following section with emphasis on the limitations of the two ideal flow models (frozen and equilibrium).

Table 14. Comparison of Calculated and Experimental Exit Gas Compositions from the Char Zone Thermal Environment Simulator for Mass Flux Rates Between 0.00655 and 0.540 Kg/M^2-sec and Front Surface Temperatures Between 1195 and 1545°K.

RUN NUMBER MASS FLUX FRONT TEMP BACK TEMP	FLOW MODEL	H_2 MOLE %	CH_4 MOLE %	CO MOLE %	CO_2 MOLE %	N_2 MOLE %	H_2O MOLE %	C_6H_6O MOLE %	C_2H_4 MOLE %	C_2H_2 MOLE %	MODEL ΔP	MODEL q_{cz}
XVIII-56	FROZEN	28.9	6.4	3.3	0.8	0.0	53.3	6.9	0.0	0.0	2.0	10.23
0.01040	EQUILIBRIUM	59.7	3.3	26.7	4.0	0.0	6.3	0.0	0.0	0.0	2.0	175.4
1200°K	NON-EQUILIBRIUM	23.0	11.1	2.8	2.1	0.0	53.8	7.1	0.0	0.0	2.0	10.95
810°K	EXPERIMENTAL	24.8	10.3	3.4	1.3	0.0	53.7	6.5	0.0	0.0	4.0	-
XVIII-57	FROZEN	30.6	6.1	3.5	0.9	0.0	52.1	6.8	0.0	0.0	10.0	53.90
0.0505	EQUILIBRIUM	60.2	3.2	27.1	3.7	0.0	5.9	0.0	0.0	0.0	9.0	609.3
1200°K	NON-EQUILIBRIUM	29.1	7.2	3.4	1.1	0.0	52.3	6.9	0.0	0.0	10.0	55.04
790°K	EXPERIMENTAL	28.7	7.5	3.4	1.2	0.0	51.7	7.5	0.0	0.0	13.0	-
XVIII-58	FROZEN	30.6	6.2	3.5	1.0	0.0	51.9	6.8	0.0	0.0	110.	768.0
0.5400	EQUILIBRIUM	59.5	3.5	26.0	4.4	0.0	6.5	0.0	0.0	0.0	94.	3085.0
1195°K	NON-EQUILIBRIUM	30.6	6.2	3.5	1.0	0.0	51.9	6.8	0.0	0.0	110.	768.2
640°K	EXPERIMENTAL	30.8	6.1	3.4	1.1	0.0	50.8	5.8	0.0	0.0	88.	-
XIX-60	FROZEN	29.3	6.0	3.3	0.9	0.0	53.7	6.8	0.0	0.0	3.5	12.8
0.01240	EQUILIBRIUM	62.7	0.8	35.2	1.5	0.0	0.9	0.0	0.0	0.0	3.0	143.0
1390°K	NON-EQUILIBRIUM	38.2	17.2	25.2	8.8	0.0	4.9	5.1	0.0	0.5	3.0	26.4
1020°K	EXPERIMENTAL	41.3	18.2	23.4	7.6	0.0	5.0	4.6	0.0	0.0	3.5	-
XIX-61	FROZEN	28.7	5.4	3.4	1.0	0.0	53.9	7.6	0.0	0.0	2.5	17.6
0.01100	EQUILIBRIUM	63.1	0.5	35.7	0.2	0.0	0.5	0.0	0.0	0.0	2.5	300.3
1450°K	NON-EQUILIBRIUM	36.6	18.3	31.2	7.3	0.0	0.6	5.2	0.0	0.7	2.0	32.3
860°K	EXPERIMENTAL	36.4	18.4	31.2	7.0	0.0	2.1	4.9	0.0	0.0	4.5	-
XX-63	FROZEN	28.6	5.5	3.4	1.0	0.0	53.8	7.7	0.0	0.0	3.0	19.8
0.01120	EQUILIBRIUM	63.1	0.3	36.4	0.1	0.0	0.2	0.0	0.0	0.0	2.5	565.4
1520°K	NON-EQUILIBRIUM	30.7	21.4	38.6	3.4	0.0	0.0	4.6	0.3	1.0	2.5	35.2
905°K	EXPERIMENTAL	30.4	19.8	38.0	5.7	0.0	0.0	5.0	0.5	0.6	3.0	-
XX-64	FROZEN	28.4	5.4	3.4	1.0	0.0	46.0	15.8	0.0	0.0	1.0	11.6
0.00515	EQUILIBRIUM	65.9	0.3	33.6	0.0	0.0	0.2	0.0	0.0	0.0	1.5	356.4
1545°K	NON-EQUILIBRIUM	25.2	25.6	38.5	0.9	0.0	0.0	7.9	0.5	1.3	1.0	13.0
910°K	EXPERIMENTAL	26.7	26.4	40.3	0.6	0.0	0.0	7.1	0.4	1.0	1.0	-

Comparison of the Non-Equilibrium Flow Results with the Results of the Frozen and Equilibrium Flow Analyses

The frozen and equilibrium flow models bracket the non-equilibrium case. Frozen flow corresponds to a system in which no chemical reactions occur, while equilibrium flow refers to a system of species undergoing chemical reactions which are at equilibrium (a function of temperature and pressure only). Since the non-equilibrium flow model predicts the actual behavior, comparison of the exit gas compositions, temperature and pressure distributions, and surface heat flux for each model will determine the accuracy of the two limited flow analyses in predicting the energy transfer within the char layer.

These results are presented in Figure 5 and Table 15 for a mass flux rate of 0.05 lb/ft^2-sec (0.25 kg/m^2-sec), a front surface temperature of 1500°F (1090°K) and a back surface temperature of 500°F (533°K). The char porosity is 0.8 and the char thickness is 0.25 inches (0.0064 m). As seen the temperature profile of the non-equilibrium flow analysis is identical to the frozen flow temperature profile. The relative closeness of these two models is likewise seen by comparing the exit gas composition, pressure drop across the char and surface heat flux in Table 15. Therefore, at the above conditions there is little evidence of chemical reactions in the char and the energy transfer is closely predicted by the frozen flow model.

In Figure 6 and Table 16 the same results are presented for a front surface temperature of 2000°F (1367°K). Although the reported non-equilibrium values are again very nearly equal to the frozen flow results, a noticeable change, especially in the concentration profile and surface heat flux is observed. This indicates chemical reactions among the species within the char layer.

A continuation of the analysis for a front surface temperature of 2500°F (1645°K) and 3000°F (1925°K) in Figures 7 and 8 and Tables 17 and 18, respectively, shows a more dramatic change which is reflected by a downward shift of the temperature profile toward the equilibrium curve and corresponding rapid changes in the concentration profile. Chemical reactions are obviously a very important mode of energy contribution under these last two sets of conditions.

It is not possible to extend the analysis to temperatures above 3000°F (1925°K) since the chemical behavior within the char will not be predicted by the chemical reactions of Table 5 . In this event additional reactions must be included to accurately describe the energy transfer within the char zone. This extension is discussed by del Valle, et.al. (73).

In addition to the above comparisons, the temperature profile, surface heat flux and pressure drop across the char are compared in Figures 7 and 9 for two pyrolysis product compositions. The results for the first simulated pyrolysis product composition, which was based

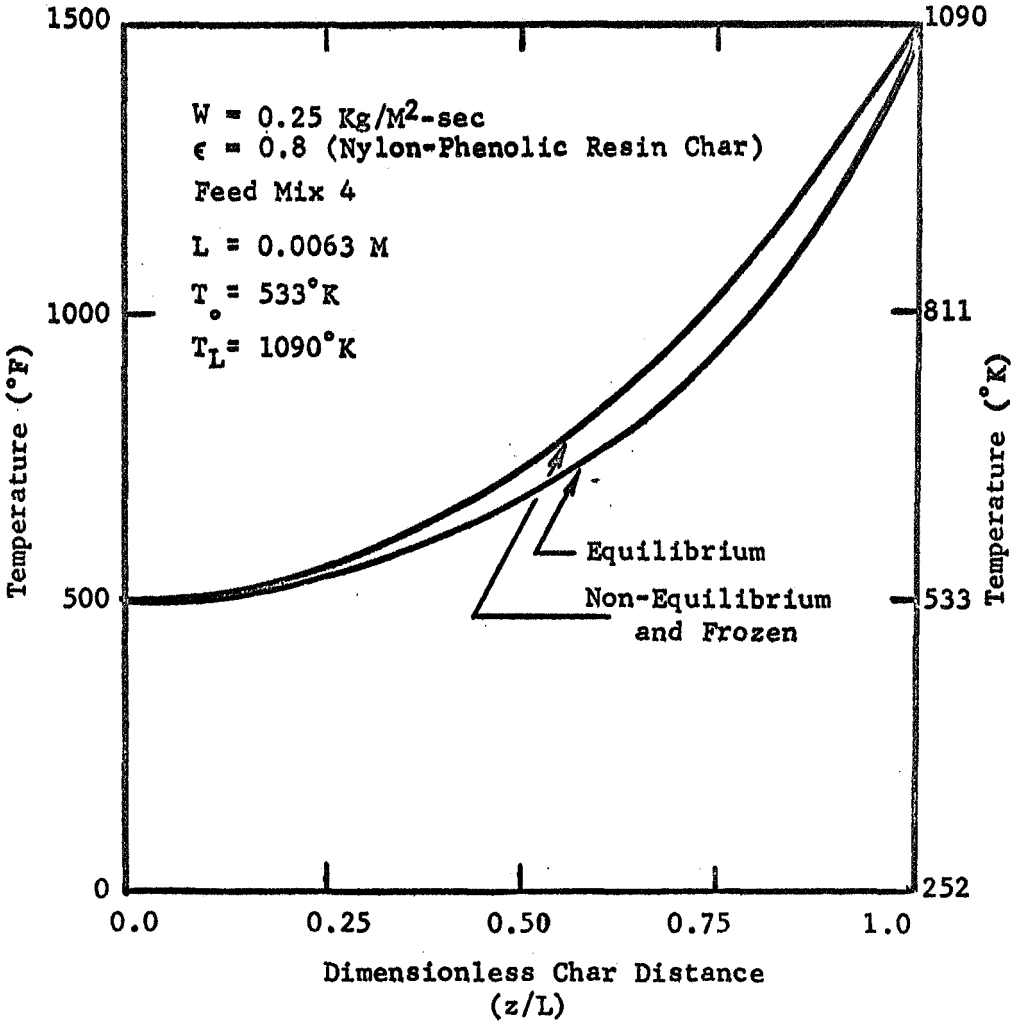

Figure 5. Temperature Profile for the Frozen, Equilibrium, and Non-Equilibrium Flow of Pyrolysis Gases Through the Char Zone of a Nylon-Phenolic Resin Ablator.

Table 15. Results of the Analyses of Frozen, Equilibrium and Non-Equilibrium Flow of Pyrolysis Gas Products Through a One-Quarter Inch Thick Low Density Nylon-Phenolic Resin Ablative Heat Shield Char at 1090°K.

Conditions: $W = 0.25$ Kg/M^2-sec $\epsilon = 0.8$ $T_o = 533$°K $L = 0.0063$ M Feed Mix 4

Char Distance	Inlet	At z/L = 0.5			At z/L = 1.0		
Flow Model(s)	(All)	FF	EF	NEF	FF	EF	NEF
Mass Flux (Kg/M^{2}voids-sec)	0.3125	0.3125	0.3125	0.3125	0.3125	0.3135	0.3125
Temperature (°K)	533.0	630.0	615.0	630.0	1090.0	1090.0	1090.0
Composition (Mole%):							
Hydrogen	33.4	33.4	2.9	33.4	33.4	9.2	33.4
Methane	6.7	6.7	35.4	6.7	6.7	33.3	6.7
Phenol	6.2	6.2	0.0	6.2	6.2	0.0	6.2
Water	48.9	48.9	54.8	48.9	48.9	48.4	48.9
Carbon Monoxide	3.7	3.7	0.0	3.7	3.7	0.1	3.7
Carbon Dioxide	1.1	1.1	6.9	1.1	1.1	8.9	1.1

Model	Pressure Drop Across Char Kg/M^2	Heat Flux at Surface KJ/M^2-sec
Frozen Flow	29.0	340.02
Non-Equilibrium Flow	29.5	350.35
Equilibrium Flow	26.5	509.74

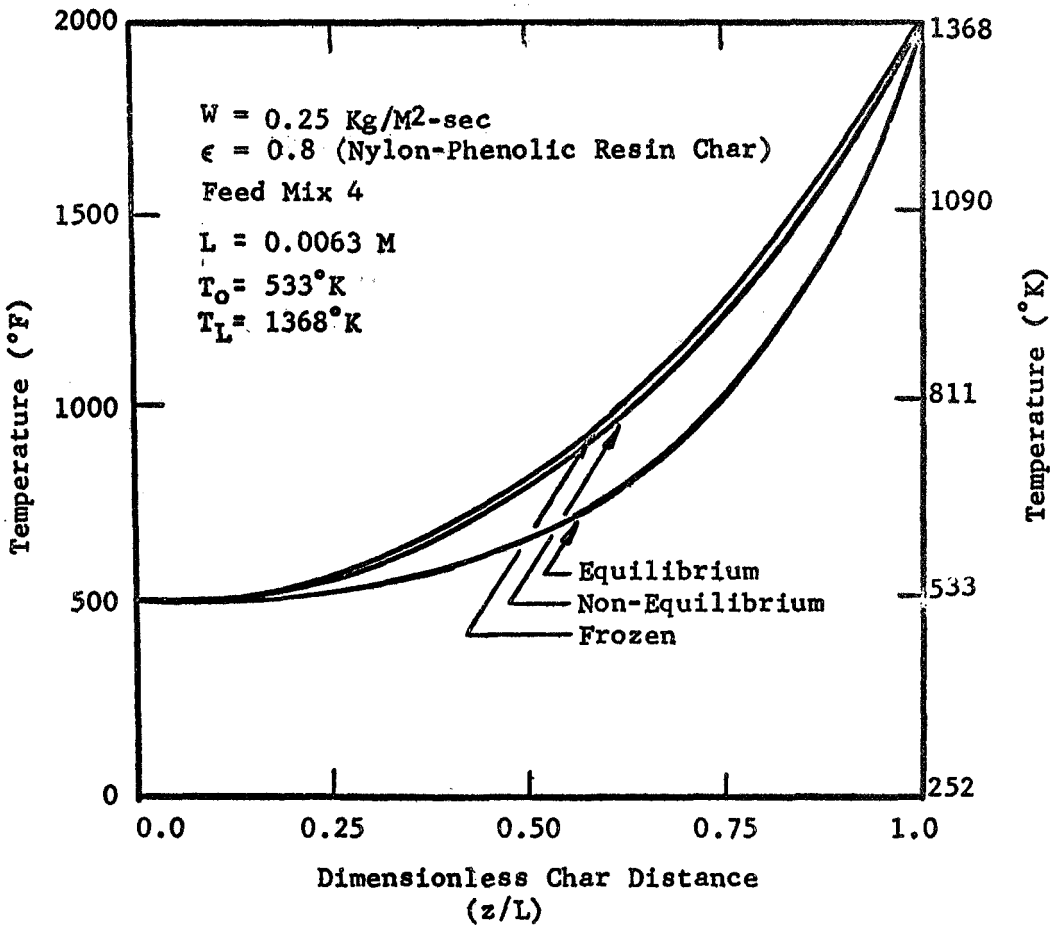

Figure 6. Temperature Profile for the Frozen, Equilibrium, and Non-Equilibrium Flow of Pyrolysis Gases Through the Char Zone of a Nylon-Phenolic Resin Ablator.

Table 16. Results of the Analyses of Frozen, Equilibrium and Non-Equilibrium Flow of Pyrolysis Gas Products Through a One-Quarter Inch Thick Low Density Nylon-Phenolic Resin Ablative Heat Shield Char at 1368°K.

Conditions: $W = 0.25\ Kg/M^2\text{-sec}$ $\epsilon = 0.8$ $T_o = 533°K$ $L = 0.0063\ M$ Feed Mix 4

Char Distance	Inlet	At z/L = 0.5			At z/L = 1.0		
Flow Model(s)	(All)	FF	EF	NEF	FF	EF	NEF
Mass Flux (Kg/M^2_{voids}-sec)	0.3125	0.3125	0.3135	0.3125	0.3125	0.3140	0.3140
Temperature (°K)	533.0	690.4	650.7	690.0	1368.0	1368.0	1368.0
Composition (Mole%):							
Hydrogen	33.4	33.4	3.2	33.4	33.4	18.2	33.5
Methane	6.7	6.7	35.3	6.7	6.7	28.8	6.8
Phenol	6.2	6.2	0.0	6.2	6.2	0.0	6.2
Water	48.9	48.9	54.6	48.9	48.9	42.5	48.3
Carbon Monoxide	3.7	3.7	0.0	3.7	3.7	0.3	4.1
Carbon Dioxide	1.1	1.1	6.9	1.1	1.1	10.1	1.2

Model	Pressure Drop Across Char Kg/M^2	Heat Flux at Char Surface KJ/M^2-sec
Frozen Flow	36.0	550.77
Non-Equilibrium Flow	36.0	555.72
Equilibrium Flow	30.0	1081.52

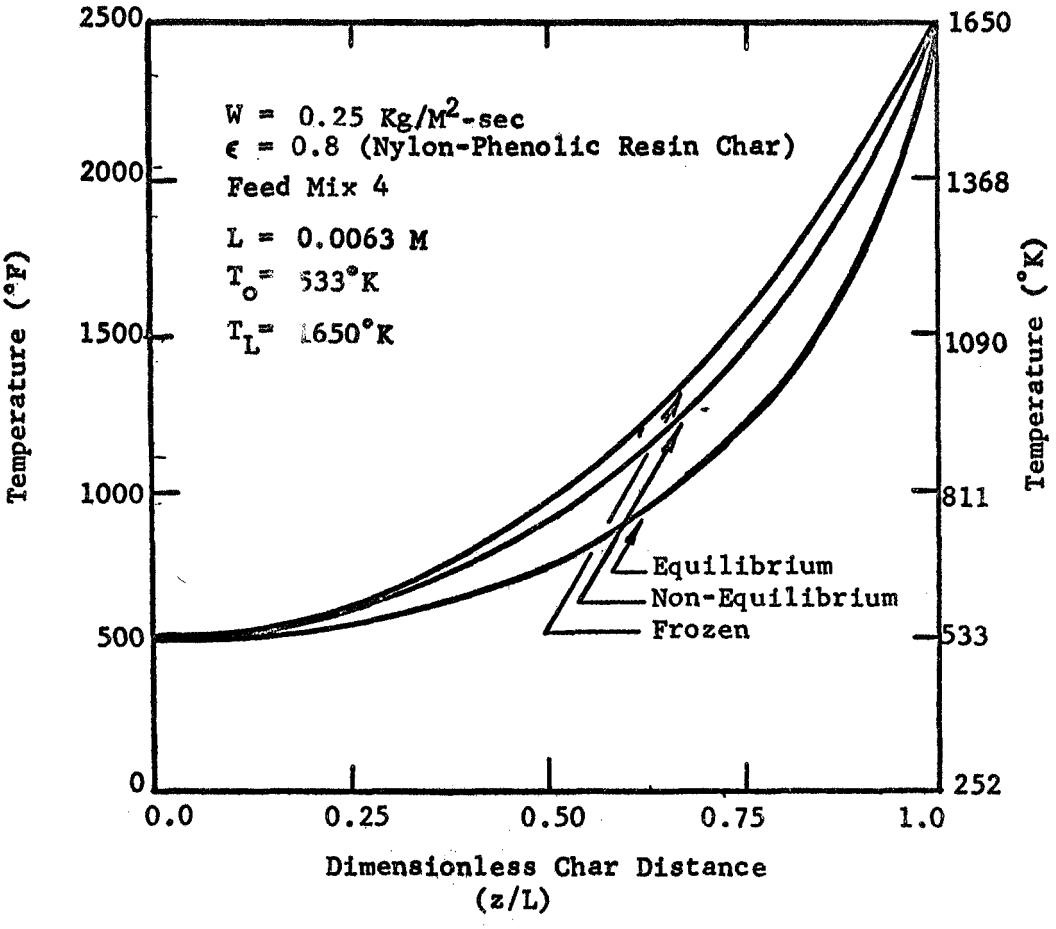

Figure 7. Temperature Profile for the Frozen, Equilibrium, and Non-Equilibrium Flow of Pyrolysis Gases Through the Char Zone of a Nylon-Phenolic Resin Ablator.

Table 17. Results of the Analyses of Frozen, Equilibrium and Non-Equilibrium Flow of Pyrolysis Gas Products Through a One-Quarter Inch Thick Low Density Nylon-Phenolic Resin Ablative Heat Shield Char at 1650°K.

Conditions: $W = 0.25\ Kg/M^2\text{-sec}$ $\epsilon = 0.8$ $T_o = 533°K$ $L = 0.0063\ M$ Feed Mix 4

Char Distance	Inlet	At z/L = 0.5			At z/L = 1.0		
Flow Model(s)	(All)	FF	EF	NEF	FF	EF	NEF
Mass Flux ($Kg/M^2_{voids}\text{-sec}$)	0.3125	0.3125	0.3140	0.3125	0.3125	0.3070	0.3855
Temperature (°K)	533.0	780.2	690.3	756.2	1650.0	1650.0	1650.0
Composition (Mole %):							
Hydrogen	33.4	33.4	3.3	33.4	33.4	36.5	51.1
Methane	6.7	6.7	35.4	6.7	6.7	18.8	5.3
Phenol	6.2	6.2	0.0	6.2	6.2	0.0	4.5
Water	48.9	48.9	54.1	48.9	48.9	31.4	8.3
Carbon Monoxide	3.7	3.7	0.0	3.7	3.7	1.9	29.4
Carbon Dioxide	1.1	1.1	7.1	1.1	1.1	11.5	1.2

Model	Pressure Drop Across Char Kg/M^2	Heat Flux at Char Surface $KJ/M^2\text{-sec}$
Frozen Flow	45.5	771.65
Non-Equilibrium Flow	45.0	1217.48
Equilibrium Flow	33.5	2118.71

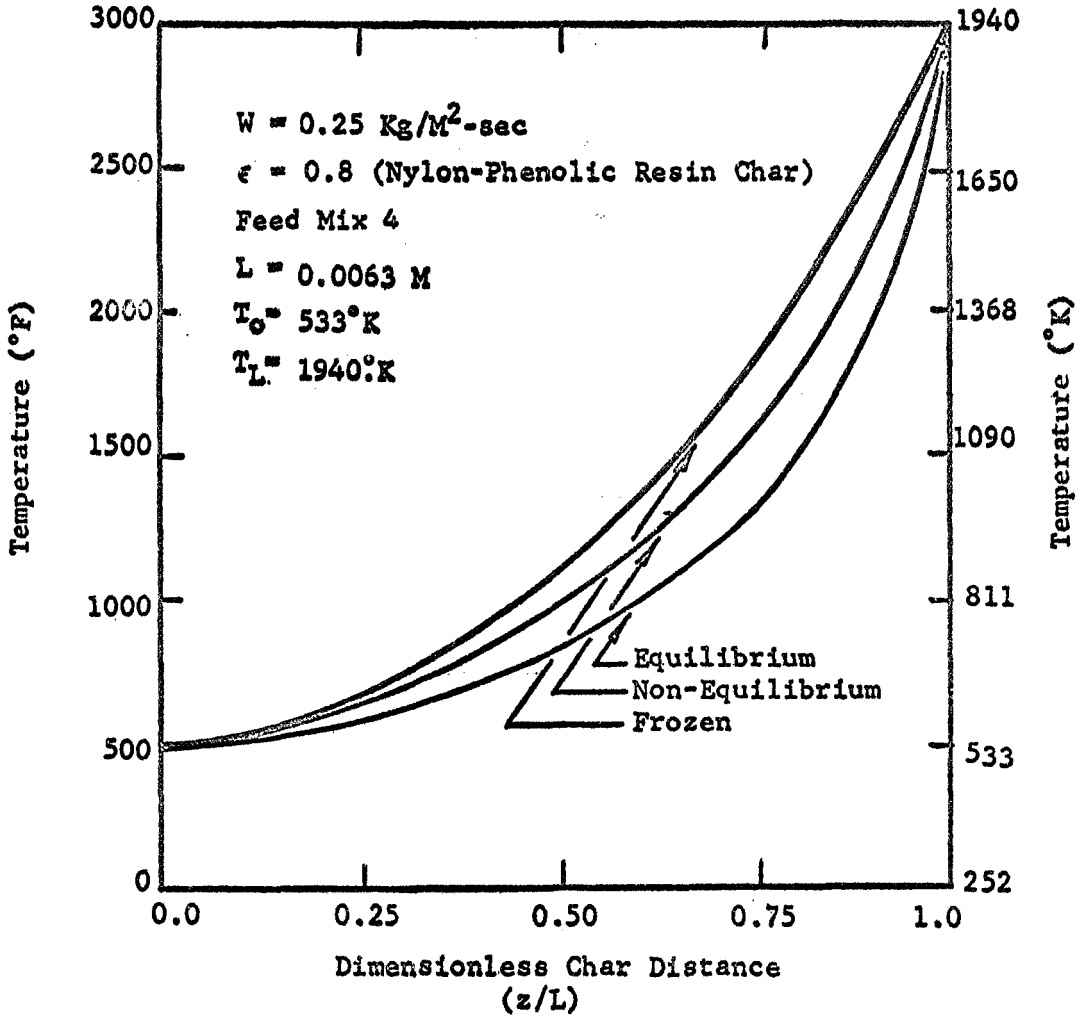

Figure 8. Temperature Profile for the Frozen, Equilibrium, and Non-Equilibrium Flow of Pyrolysis Gases Through the Char Zone of a Nylon-Phenolic Resin Ablator.

Table 18. Results of the Analyses of Frozen, Equilibrium and Non-Equilibrium Flow of Pyrolysis Gas Products Through A One-Quarter Inch Thick Low Density Nylon-Phenolic Resin Ablative Heat Shield Char at 1940°K.

Conditions: $W = 0.25$ Kg/M^2-sec $\epsilon = 0.8$ $T_0 = 533$°K $L = 0.0063$ M Feed Mix 4

Char Distance	Inlet	At z/L = 0.5			At z/L = 1.0		
Flow Model(s)	(All)	FF	EF	NEF	FF	EF	NEF
Mass Flux (Kg/m^{2}voids-sec)	0.3135	0.3135	0.3140	0.3135	0.3135	0.3570	0.5480
Temperature (°K)	533.0	895.0	720.3	785.8	1940.0	1940.0	1940.0
Composition (Mole %):							
Hydrogen	33.4	33.4	3.5	33.4	33.4	63.9	0.0[a]
Methane	6.7	6.7	35.4	6.7	6.7	1.1	54.0
Phenol	6.2	6.2	0.0	6.2	6.2	0.0	2.4
Water	48.9	48.9	53.9	48.9	48.9	2.2	0.0
Carbon Monoxide	3.7	3.7	0.0	3.7	3.7	31.2	28.9
Carbon Dioxide	1.1	1.1	7.2	1.1	1.1	1.6	17.4

Model	Pressure Drop Across Char Kg/M^2	Heat Flux at Char Surface KJ/M^2-sec
Frozen Flow	56.5	1017.28
Non-Equilibrium Flow	55.0	2126.85
Equilibrium Flow	36.5	3690.50

Note: (a) Non-Equilibrium Flow Model Requires Additional Important Reactions and Associated Kinetics Data to Accurately Describe the Energy Transfer Near 1940°C.

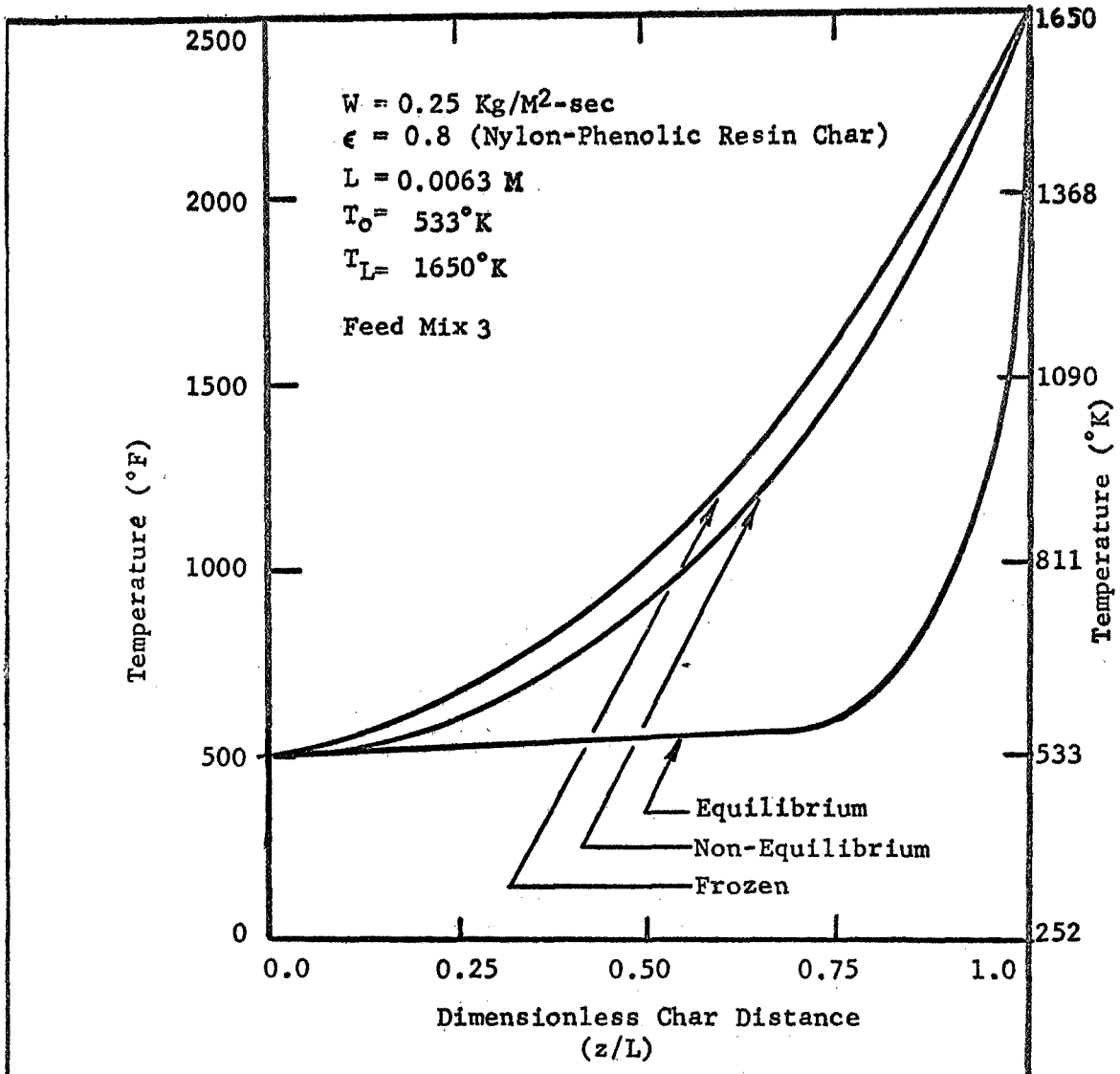

Model	Pressure Drop Kg/M^2	Surface Heat Flux KJ/M^2-sec
Frozen Flow	64.85	574.20
Non-Equilibrium	62.25	1184.04
Equilibrium Flow	48.75	2983.75

Figure 9. Temperature Profile, Pressure Drop and Surface Heat Flux for the Flow of Pyrolysis Gases Through A One-Quarter Inch Thick Nylon-Phenolic Char.

on experimentally measured and computed equilibrium compositions excluding the high molecular weight cyclic compounds, is shown in Figure 9. The results in Figure 7 are for the more accurate composition based on pyrolysis gas chromatographic analyses of Sykes (33). A mass flux rate of 0.05 lb/ft^2-sec (0.25 kg/m^2-sec), front and back surface temperature of 2500°F (1644°K) and 500°F (533°K), respectively, and a one-quarter inch (0.0064 m) thick low density nylon-phenolic resin char (ϵ = 0.8) were the conditions for each case presented.

Comparison of the temperature profiles for frozen and non-equilibrium flow show the same overall behavior; i.e., a downward shift by the non-equilibrium curves indicating a higher energy absorption due to chemical reactions between the pyrolysis products. On the otherhand, a noticeable difference in the equilibrium curves is observed. For the more accurate pyrolysis gas composition (Figure 7), the characteristically sharp downward shift of the equilibrium curve observed in Figure 9 does not occur.

The explanation for this difference will point out the inadequacy of the equilibrium flow model in predicting the true behavior within the char zone. Because the results of Figure 9 were calculated for a pyrolysis product composition largely based on equilibrium calculated values, the inlet gas composition to the char was very nearly equal to the values calculated using the equilibrium flow model. As a result, very little energy absorption was omitted from the analysis due to the very small change in the inlet compositions which were already approximated as an equilibrium composition. This resulted in the relatively flat curve over nearly three quarters of the total char thickness.

On the otherhand, the more accurate pyrolysis product composition estimated from experimental data and dependent on finite reaction rates governing plastic decomposition, is far removed from the equilibrium calculated compositions. However, as these concentrations of gases are introduced into the equilibrium flow analysis, an abrupt adjustment to the equilibrium compositions calculated by minimizing the free energy is experienced. This is especially noted for phenol and methane which have initial compositions of 6.2 mole % and 6.7 mole %, respectively, but are immediately changed to 0.0 mole % and 35.3 mole % at the back surface temperature of 500°F (533°K). This erroneous adjustment results in the loss of energy absorption which results from phenol decomposition at finite reaction rates and causes the curve to more closely approach the frozen and non-equilibrium curves.

These same conclusions regarding the inability of the equilibrium flow model to accurately predict the true behavior is further shown in Table 19. Here, the surface heat flux values are compared for each model and for each simulated pyrolysis product composition. In comparing the relative values, i.e., the ratio of the heat flux of any model to the actual or non-equilibrium flow heat flux, the characteristic under-predictive nature of the frozen flow model (ratio = 0.634) and the

Table 19. Comparison of the Surface Heat Flux Values for Each Flow Model and Two Pyrolysis Gas Compositions at a Front Surface Temperature of 1650°K.

Pyrolysis Gas Composition	Mole%	Flow Model	Surface Heat Flux KJ / M^2-Sec	Relative Heat Flux, ϕ_s
Hydrogen	31.7			
Methane	46.3	Frozen	574.20	0.485
Carbon Monoxide	5.5	Non-Equilibrium	1184.04	1.000
Carbon Dioxide	2.5	Equilibrium	2983.75	2.520
Nitrogen	14.0			
Water	0.0			
Phenol	0.0			
Hydrogen	33.4			
Methane	6.7	Frozen	771.65	0.634
Carbon Monoxide	3.7	Non-Equilibrium	1217.48	1.000
Carbon Dioxide	1.1	Equilibrium	2118.71	1.720
Nitrogen	0.0			
Water	48.9			
Phenol	6.2			

Note: The relative heat flux is defined as the ratio of the heat flux calculated by any model to the heat flux calculated by the non-equilibrium flow model. The relative closeness of this value, ϕ_s, to 1 determines the closeness with which the model (frozen or equilibrium) predicts the actual behavior. Values less than one show an underprediction, while values above one indicate an overprediction of the true state.

extremely overpredictive behavior of the equilibrium flow model (ratio = 1.720) are shown. It further illustrates that although the frozen flow model can accurately describe the true behavior in some cases (low temperatures or high mass flux rates), the equilibrium flow model is totally inadequate over the temperature (533-1925°K) and mass flux (0.00015-0.50 kg/m^2-sec) values studied in this research. Therefore, in order to obtain an accurate prediction of the energy transfer, a non-equilibrium flow model must be used within the transition region. This is only possible by considering chemical reactions between the species to occur at finite reaction rates as described by reliable kinetic data. Again the importance and application of the non-equilibrium flow model has been demonstrated and the limitations of the two ideal models shown. This discussion forms the basis for extending this research to higher temperatures involving more complex reactions and increased number ofspecies.

Parametric Study of the Flow of Pyrolysis Gases in the Char Zone

A comparison of the non-equilibrium flow results with the experimental data was important in determining the accuracy of the flow model. However, very little quantitative information, beyond the discrete sets of data for each experiment, was assembled regarding the effect of changing mass flux and/or temperature. As a result, a parametric study was undertaken to accurately relate the changes in these variables with variations in energy absorption within the char. To do this the non-iterative TEMPRE System (NIT) was used in which the back surface temperature and temperature gradient were specified as boundary conditions for various values of the mass flux. The results of the calculation were in the form of the net heat transfer at the surface, called the approximate aerodynamic heating, which was the sum of the surface heat flux and radiant heat flux resulting from the calculated front surface temperature:

$$q_a = -k_e \left.\frac{dT}{dz}\right|_{z=L} + \epsilon\sigma T_L^4 \tag{49}$$

where a value of 0.95 was used for the emissivity. This information is shown in Figure 10 in which the mass flux is plotted against the aerodynamic heating for various heats of pyrolysis, q_p, (function of the temperature and gradient at the back surface):

$$q_p = -k_e \left.\frac{dT}{dz}\right|_{z=0} \tag{50}$$

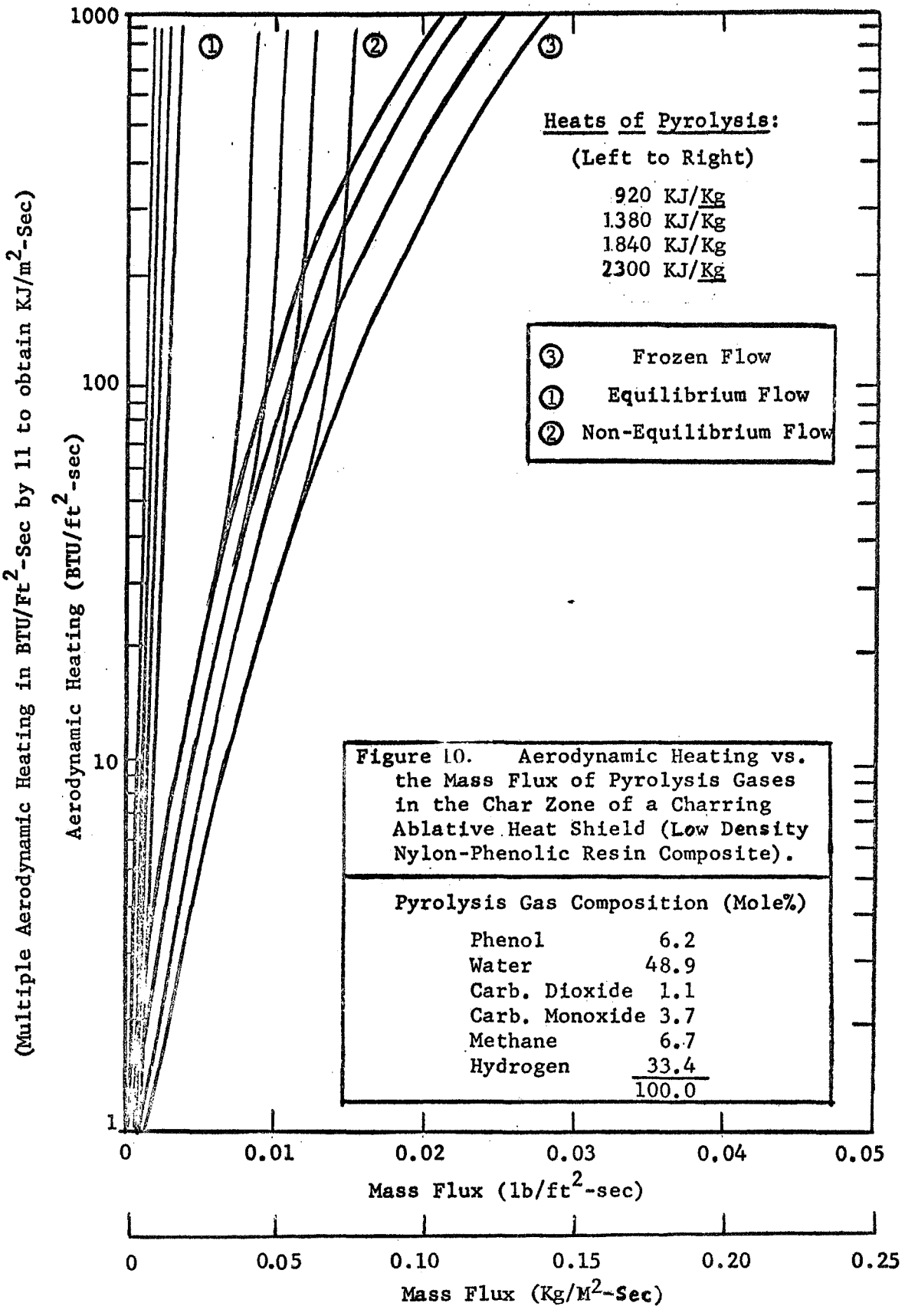

Figure 10. Aerodynamic Heating vs. the Mass Flux of Pyrolysis Gases in the Char Zone of a Charring Ablative Heat Shield (Low Density Nylon-Phenolic Resin Composite).

Pyrolysis Gas Composition (Mole%)	
Phenol	6.2
Water	48.9
Carb. Dioxide	1.1
Carb. Monoxide	3.7
Methane	6.7
Hydrogen	33.4
	100.0

where q_p is the sum of the energy absorbed by the decomposition of the polymer and the energy conducted through the virgin plastic. Results for the frozen, equilibrium and non-equilibrium flow models are presented. This form of presenting the results is a very convenient and informative method as will be seen.

In a reentry problem one of the important questions asked is what is the required heat shield weight for protection for a certain mission. Specification of the type of heat shield material to be used (e.g., nylon-phenolic resin) brackets the heat of pyrolysis value, while the trajectory calculations determine the amount of aerodynamic heating that can be expected. For example, an approximate aerodynamic heating rate of 500 BTU/ft^2-sec (5×10^6 J/m^2-sec) and a heat of pyrolysis of 400 BTU/lb (8×10^5J/kg)locates three distinctive points on Figure 9; one for each of the frozen, equilibrium and non-equilibrium flow models. This corresponds to three distinctive values of the mass flux; 0.017 lb/ft^2-sec (0.085 kg/m^2-sec) for frozen, 0.002 lb/ft^2-sec (0.01 kg/m^2-sec) for equilibrium and 0.009 lb/ft^2-sec (0.045 lb/m^2-sec) for non-equilibrium. The non-equilibrium flow model accurately predicted the behavior and would specify the exact heat shield weight (function of the mass flux) required. The frozen flow model shows an over-prediction because important endothermic reactions were omitted, and the equilibrium flow model shows an under-prediction, because reactions were assumed to occur at a greater extent than the actual behavior.

The results presented in Figure 10 also provide a way of determining at what point the non-equilibrium flow model changes from the frozen flow behavior to a truly non-equilibrium flow condition governed by finite reaction rates(6×10^5J/m^2-sec). This figure very graphically illustrates the differences in each model and permits the presentation of a large volume of information in a clear and readily accessible manner.

Calculation of the Reacting Gas Heat Capacity

In addition to the above information, the reacting gas heat capacity for the non-equilibrium flow of pyrolysis products through the char has been determined also. This term is very useful in the calculation of the one-dimensional, transient response of an ablative composite. The energy equation for the transient case can be put in the following form (18) for the char zone.

$$-\frac{\partial}{\partial z}\left(k\frac{\partial T}{\partial z}\right)+\left[\left(\frac{W}{W_o}\right)\bar{C}_p+\frac{\sum_{i=1}^{K+1}H_i\bar{R}_i}{W_o\left(\frac{\partial T}{\partial z}\right)}\right]W_o\frac{\partial T}{\partial z}=-C_p\frac{\partial T}{\partial t} \qquad (51)$$

where W is the mass flux of pyrolysis products at z and W_o is the mass flux of pyrolysis products entering the char. The term in brackets is referred to as the effective reacting gas heat capacity. Hence, the flow within the char zone can be considered frozen ($\Sigma H_i \bar{R}_i \neq 0$) by introducing the reacting gas heat capacity as an input function to the transient calculations. In Figure 11 a plot of the reacting gas heat capacity as a function of temperature is shown for frozen, equilibrium and non-equilibrium flow within the char layer up to 3000°F (1925°K). These curves were calculated for a mass flux of 0.05 lb/ft^2-sec (0.25 kg/m^2-sec), a back surface temperature of 500°F (533°K), and, char porosity and thickness of 0.8 and 0.25 inches (0.0064 m), respectively. The differences in the manner used to calculate the energy transfer by chemical reaction ($\Sigma H_i \bar{R}_i$) for equilibrium and non-equilibrium flow causes the curves to separate as shown.

Flow of Pyrolysis Products Through Porous Graphite

There are two important reasons for using porous graphite to simulate low density, nylon-phenolic resin chars used in ablative heat shield applications. These are availability and machinability of the graphite.

Nylon-phenolic resin chars were obtained from the National Aeronautics and Space Administration's Langley Research Center for use in the Char Zone Thermal Environment Simulator. Electric air arc jets were used to char the nylon-phenolic resins, and this represented a considerable effort in supplying just a few specimens for use in this research. Although two sections of char were usually obtained from each specimen, the demand for additional chars could not be met. In addition to the problem of obtaining the samples, the brittle nature of the chars caused serious problems in mounting on the char holder section. These complications led to the testing and use of graphite, especially, for use in radioactive tracer and catalyst evaluation studies. However, for the successful substitution of graphite for the chars to be complete, the chemical behavior of the two must be essentially the same. This is to say that the same reactions and kinetic data important in predicting the energy transport within porous chars, must also do the same for energy transport in porous graphite. This will be shown in the following sections by comparing the exit gas compositions from the Char Zone Thermal Environment Simulator with the composition predicted by the non-equilibrium flow model, and, by direct comparison of char and graphite experimental results over a range of mass flux rates and front surface temperature common to both systems.

Comparison of reacting flow through chars and graphite.-Other than the differences in the structural properties of chars and graphite, the one most important consideration that must be accounted for is the change in mass flux rates caused by differences in material porosity. Therefore,

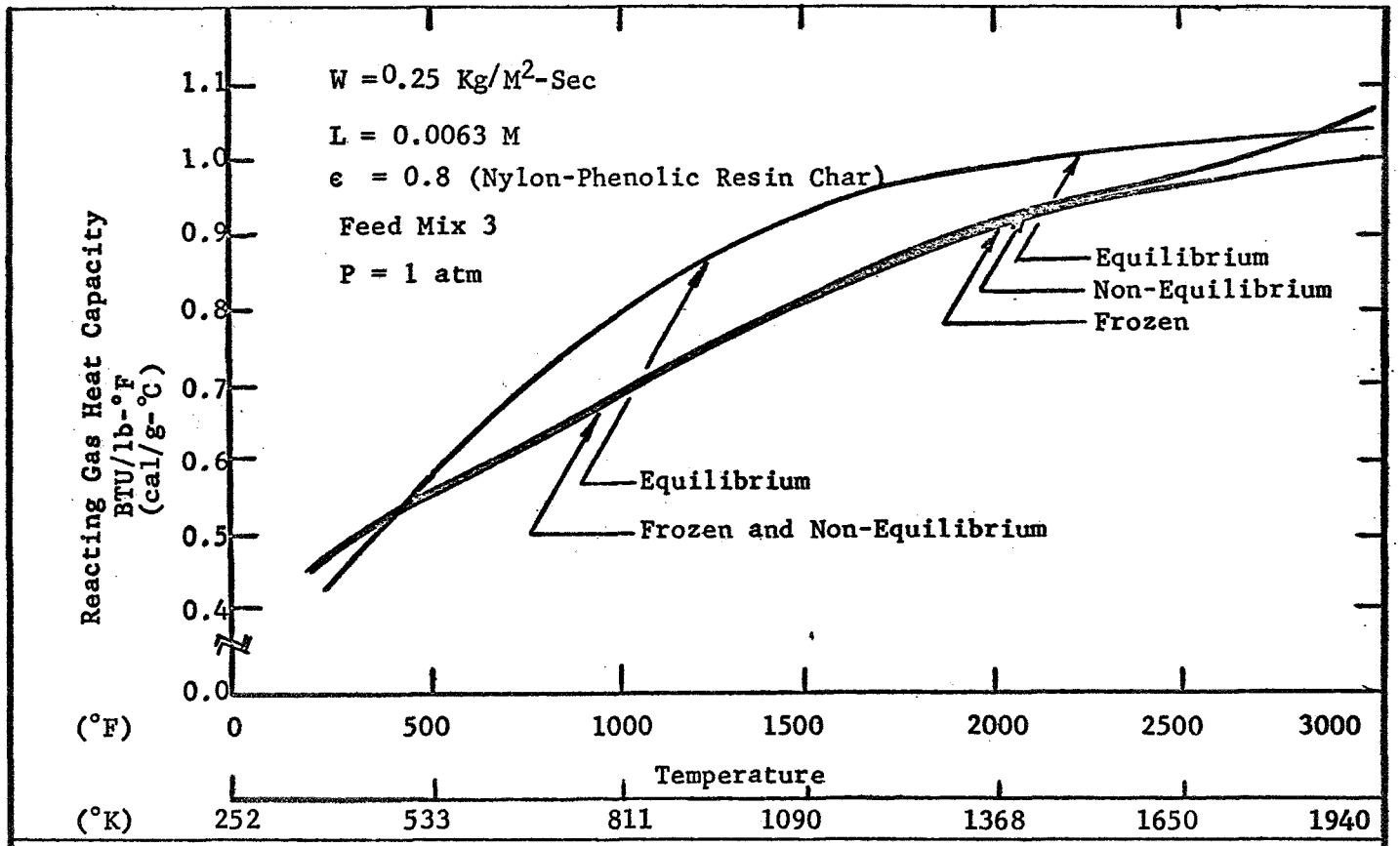

Figure 11. Plot of the Reacting Gas Heat Capacity for Frozen, Equilibrium and Non-Equilibrium Flow of Pyrolysis Gases Through the Char Zone.

to put the materials on a common basis for discussion, the mass flux rates previously discussed in terms of the total area (kg/m^2_{total}-sec) must be divided by the porosity to obtain rates within the pores (kg/m^2_{voids}-sec). Even though the superficial mass flux rates are different for each porous medium, the mass flux rate within the pores will be the same. Again, the porosity of the chars and graphite were 0.8 and 0.5, respectively.

The foregoing discussion is not intended to mean that chemical reactions will not be influenced by other structural properties beside the porosity (e.g., crystallicity, permeability, etc.). However, it emphasizes that the mass flux within the pore spaces must be equivalent for a valid comparison. Differences in the chemical reaction rates resulting from differences in structural makeup could eliminate graphite as a suitable substitute. However, this could only be determined by a comparison of experiments conducted over the range of conditions for which the proposed flow model is valid.

In Table 20 the exit gas composition from the Char Zone Thermal Environment Simulator for the flow of pyrolysis products through graphite are presented for mass flux rates of 0.0034 to 0.0059 lb/ft^2-sec (0.017-0.030 kg/m^2-sec) at a front surface temperature of approximately 1950°F(1340°K). As in the case with chars, there is a significant amount of chemical reactions occurring in the porous medium for the lower mass flux (0.05 kg/m^2-sec). More importantly, however, is the agreement within experiment error between the measured exit gas compositions and the predicted values by the non-equilibrium flow model using the same kinetic data employed for the char experiments.

A similar comparison is presented in Table 22 for an average mass flux rate of 0.0035 lb/ft^2-sec (0.017 kg/m^2-sec) and front surface temperatures of 1950 (1340°K) and 2065°F (1410°K). Again, excellent agreement within the experimental accuracy of the analyses was obtained between the non-equilibrium flow model compositions and the experimental values. However, a closer inspection of the graphite experiments in Table A-2 of Appendix A shows that the non-equilibrium predicted compositions do not agree in some cases with the experimental data. This is especially true for experiments XXI-66, XXIII-72, XXIII-73, and XXIV-76. These differences were a result of experimental difficulties associated with maintaining a steady liquid (water and phenol) feed rate as indicated in the experimental summary sheets of Table A-1; and, therefore, should not be interpreted as a failure of the model to predict the flow behavior in porous graphite.

In addition to these irregularities in the water-phenol-gas experiments, similar disagreement was also observed in several water-phenol free pyrolysis product investigations. In experiments IX and XI shown in Table 22, increases in methane and corresponding decreases in hydrogen concentrations clearly deviated from the predicted frozen flow behavior. These observations were attributed to problems associated with the fabrication of the graphite specimens. In the earlier experiments, the dust-like graphite "fines" which resulted from the milling process

Table 20. Flow of Pyrolysis Gases Through Graphite. Effect of Changing Mass Flux Rates at a Front Surface Temperature of 1340°F.

RUN NUMBER MASS FLUX FRONT TEMP BACK TEMP	FLOW MODEL	H_2 MOLE %	CH_4 MOLE %	CO MOLE %	CO_2 MOLE %	N_2 MOLE %	H_2O MOLE %	C_6H_5O MOLE %	C_2H_4 MOLE %	C_2H_2 MOLE %	MODEL ΔP	MODEL q_{cz}
XXVIII-93	FROZEN	25.8	7.2	4.3	1.3	0.0	50.1	11.3	0.0	0.0	1.0	21.12
0.0170	EQUILIBRIUM	62.7	1.3	33.5	0.8	0.0	1.7	0.0	0.0	0.0	1.0	31.24
1340°K	NON-EQUILIBRIUM	32.8	10.0	11.8	4.1	0.0	32.6	10.2	0.0	0.3	1.0	25.63
860°K	EXPERIMENTAL	32.2	11.2	9.2	4.0	0.0	33.2	9.8	0.2	0.2	1.5	-
XXVIII-92	FROZEN	27.5	5.3	3.1	1.0	0.0	52.5	10.6	0.0	0.0	1.5	26.84
0.0220	EQUILIBRIUM	62.5	1.2	33.9	0.8	0.0	1.6	0.0	0.0	0.0	1.5	390.28
1320°K	NON-EQUILIBRIUM	29.3	7.7	8.0	2.5	0.0	42.2	10.1	0.0	0.2	1.5	30.25
866°K	EXPERIMENTAL	30.0	8.7	8.0	3.4	0.0	39.9	9.6	0.2	0.2	2.0	-
XXIX-95	FROZEN	21.7	4.6	2.8	0.8	0.0	57.1	13.1	0.0	0.0	2.5	30.74
0.0295	EQUILIBRIUM	61.1	1.4	34.0	1.3	0.0	2.2	0.0	0.0	0.0	1.5	275.88
1325°K	NON-EQUILIBRIUM	22.9	5.1	4.7	1.2	0.0	53.1	12.9	0.0	0.1	2.5	84.15
780°K	EXPERIMENTAL	21.9	6.6	5.4	2.1	0.0	52.0	11.3	0.3	0.4	2.0	-

Table 21. Flow of Pyrolysis Gases Through Graphite. Effect of Changing the Front Surface Temperature at a Mass Flux Rate of 0.0160 Kg/m^2-sec.

RUN NUMBER MASS FLUX FRONT TEMP BACK TEMP	FLOW MODEL	H_2 MOLE %	CH_4 MOLE %	CO MOLE %	CO_2 MOLE %	N_2 MOLE %	H_2O MOLE %	C_6H_6O MOLE %	C_2H_4 MOLE %	C_2H_2 MOLE %	MODEL ΔP	MODEL q_{cz}
XXVIII-93 0.0170 1340°K 860°K	FROZEN	25.8	7.2	4.3	1.3	0.0	50.1	11.3	0.0	0.0	1.0	21.12
	EQUILIBRIUM	62.7	1.3	33.5	0.8	0.0	1.7	0.0	0.0	0.0	1.0	308.44
	NON-EQUILIBRIUM	30.8	10.0	11.8	4.1	0.0	32.6	10.2	0.0	0.3	1.0	25.63
	EXPERIMENTAL	32.2	11.2	9.2	4.0	0.0	33.2	7.8	0.2	0.2	1.5	-
XXIII-71 0.0155 1400°K 858°K	FROZEN	25.8	4.9	2.9	0.9	0.0	54.7	10.8	0.0	0.0	1.5	22.22
	EQUILIBRIUM	62.6	0.7	35.8	0.3	0.0	0.7	0.0	0.0	0.0	1.5	350.35
	NON-EQUILIBRIUM	41.4	8.4	23.9	5.1	0.0	12.5	8.2	0.0	0.6	1.5	35.53
	EXPERIMENTAL	39.3	8.8	27.2	5.9	0.0	11.2	7.6	0.0	0.0	8.5	-

Table 22. Flow of Pyrolysis Gases Through Porous Graphite. Effect of Having Graphite "Fines" in the Pore Spaces.

RUN NUMBER MASS FLUX FRONT TEMP BACK TEMP	FLOW MODEL	H_2 MOLE %	CH_4 MOLE %	CO MOLE %	CO_2 MOLE %	N_2 MOLE %	H_2O MOLE %	C_6H_6O MOLE %	C_2H_4 MOLE %	C_2H_2 MOLE %	MODEL ΔP	MODEL q_{cz}
IX-25	FROZEN	35.0	43.6	4.9	2.9	13.6	0.0	0.0	0.0	0.0	2.5	4.51
0.0045	EQUILIBRIUM	76.7	5.6	5.8	0.2	10.0	1.7	0.0	0.0	0.0	2.5	54.01
1000 °K	NON-EQUILIBRIUM	35.0	43.6	4.9	2.9	13.6	0.0	0.0	0.0	0.0	2.5	4.51
710 °K	EXPERIMENTAL	20.2	55.2	8.0	3.5	13.6	0.0	0.0	0.0	0.0	4.5	-
IX-26	FROZEN	35.0	43.6	4.9	2.9	13.6	0.0	0.0	0.0	0.0	10.0	19.80
0.0195	EQUILIBRIUM	77.6	4.9	6.0	0.2	9.9	1.4	0.0	0.0	0.0	8.0	211.42
1020 °K	NON-EQUILIBRIUM	35.0	43.6	4.9	2.9	13.6	0.0	0.0	0.0	0.0	10.0	19.80
700 °K	EXPERIMENTAL	24.6	52.2	6.2	3.4	13.6	0.0	0.0	0.0	0.0	11.0	-
IX-27	FROZEN	35.0	43.6	4.9	2.9	13.6	0.0	0.0	0.0	0.0	195.	310.75
0.2850	EQUILIBRIUM	77.0	5.2	5.9	0.2	10.0	2.7	0.0	0.0	0.0	124.	984.50
1000 °K	NON-EQUILIBRIUM	35.0	43.6	4.9	2.9	13.6	0.0	0.0	0.0	0.0	195.	310.75
650 °K	EXPERIMENTAL	27.0	51.5	5.5	2.9	13.6	0.0	0.0	0.0	0.0	141.	-
XI-31	FROZEN	35.0	43.6	4.9	2.9	13.6	0.0	0.0	0.0	0.0	2.5	4.51
0.0045	EQUILIBRIUM	76.3	6.0	5.6	0.2	10.0	1.9	0.0	0.0	0.0	2.5	52.69
995 °K	NON-EQUILIBRIUM	35.0	43.6	4.9	2.9	13.6	0.0	0.0	0.0	0.0	2.5	4.51
705 °K	EXPERIMENTAL	28.5	49.8	5.5	2.5	14.7	0.0	0.0	0.0	0.0	4.0	-
XI-32	FROZEN	35.0	43.6	4.9	2.9	13.6	0.0	0.0	0.0	0.0	10.5	18.48
0.0195	EQUILIBRIUM	78.1	4.6	6.1	0.1	9.8	1.3	0.0	0.0	0.0	9.0	206.58
1025 °K	NON-EQUILIBRIUM	35.0	43.6	4.9	2.9	13.6	0.0	0.0	0.0	0.0	10.5	18.48
740 °K	EXPERIMENTAL	29.8	49.2	4.9	2.9	13.6	0.0	0.0	0.0	0.0	10.0	-
XI-33	FROZEN	35.0	43.6	4.9	2.9	13.6	0.0	0.0	0.0	0.0	171.	368.50
0.2850	EQUILIBRIUM	77.2	5.2	5.9	0.2	10.0	2.5	0.0	0.0	0.0	104.	1070.3
1005 °K	NON-EQUILIBRIUM	35.0	43.6	4.9	2.9	13.6	0.0	0.0	0.0	0.0	171.	368.50
570 °K	EXPERIMENTAL	32.3	46.2	5.0	2.9	13.6	0.0	0.0	0.0	0.0	180.	-

were not removed from the pore spaces within the plug. These "fines" provided additional surface area which made them highly susceptible to reaction with hydrogen to form methane. After complete reaction of the "fines" (about five to ten minutes), the hydrogen and methane concentrations in the exit stream returned to their initial compositions indicating frozen flow behavior. This is illustrated graphically in Figure 12 in which hyrodgen and methane concentrations (in mole percent) are plotted against experimental run time (in minutes) for experiment IX.

Methane production of this kind was eliminated in subsequent experiments (XII, XIII, and XV in Table 23) by first passing nitrogen or helium through the graphite plugs prior to mounting in the char holder. This removed the "fines" from the pore spaces and eliminated the sharp increase in methane observed in Figure 12. The contrasting concentration profiles as a function of run time are shown in Figure 13 for experiment XIII.

As a final comparison, several char and graphite experiments are examined in Table 24. To accomplish this the mass flux rates based on the void area were calculated and are shown in brackets. The listing in Table 24 is, also, made in order of increasing chemical reactions; i.e., low temperatures and high mass flux rates appear first. As seen, the char and graphite experiments are indeed compatible and behave, from the overall chemical viewpoint, as one material.

This permits the use of the more easily workable graphite materials in experiments designed to study carbon deposition and product distribution using Carbon-14 tracers, and, to investigate the effect of catalysts in accelerating the rates of chemical reactions within the char layer. Details of the results from these additional experimental investigations follow.

Radioactive Tracer Studies Using Porous Graphite

Radioactive methane and phenol were used in separate experiments to determine the specific products of decomposition from each labeled species. Also, the amount and location of carbon deposition in the char due to the thermal cracking of each species was determined.

The method used involved the sampling of the exit gas stream followed by gas chromatographic analysis. The fractionated gas chromatographic effluent stream was then passed through a combustion furnace forming carbon dioxide and water. After trapping the water, the carbon dioxide was absorbed in a one molar hydroxide of hyamine (in methanol) solution. Collecting the carbon dioxide over small intervals (one half to one minute) produced radioactive concentrations corresponding to the separated gases indicated on the gas chromatogram. By comparing the two curves for

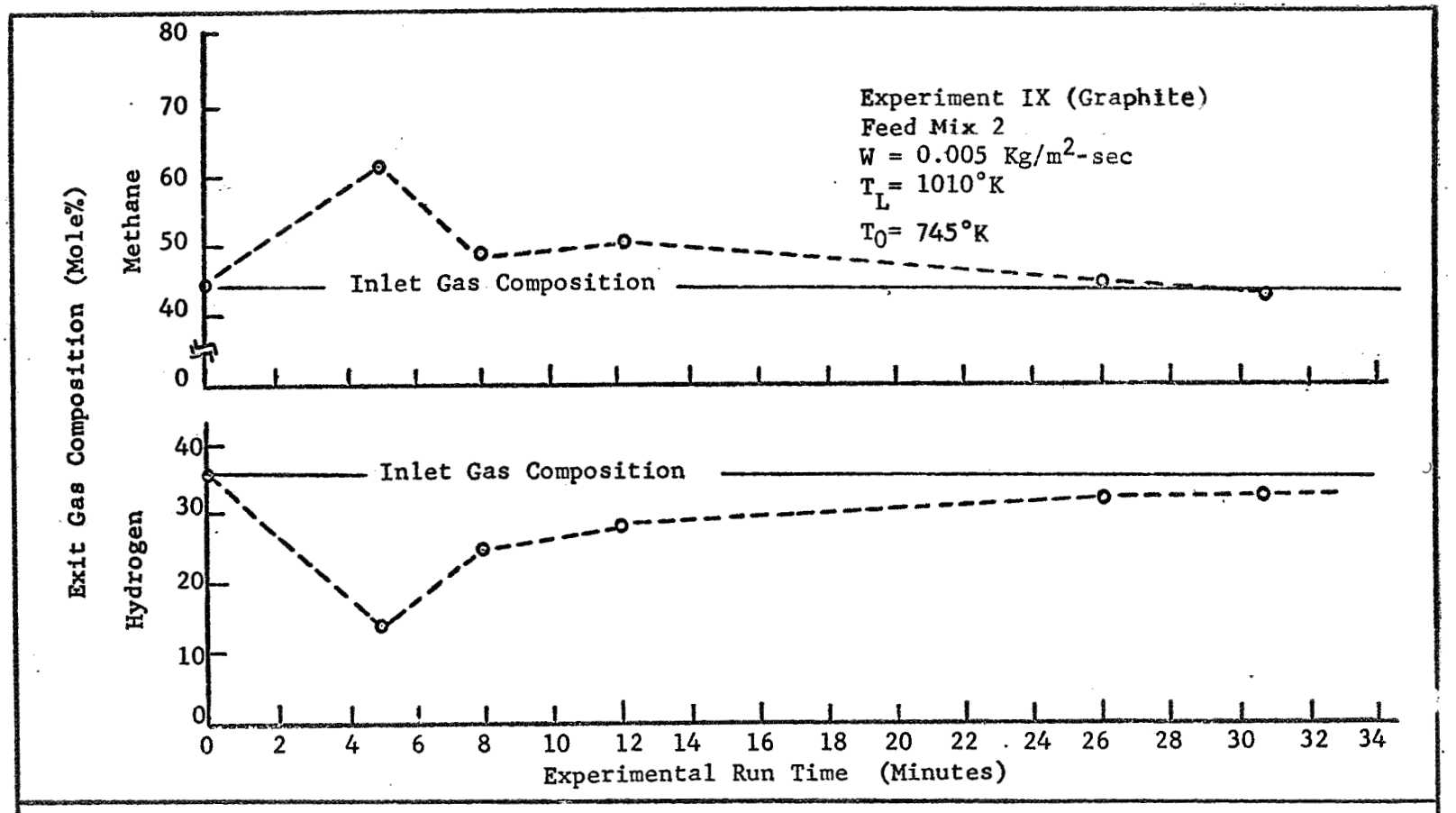

Figure 12. Typical Methane-Hydrogen Concentration Profile in the Exit Gas Stream from the Char Zone Thermal Environment Simulator for the Inclusion of Graphite "Fines" in the Pore Spaces.

Table 23 . Flow of Pyrolysis Gases Through Porous Graphite. Exit Gas Compositions Resulting From Experiments In Which The "Fines" Were Cleared From The Pore Spaces By Passing Helium Through the Specimens.

RUN NUMBER MASS FLUX FRONT TEMP BACK TEMP	FLOW MODEL	H_2 MOLE %	CH_4 MOLE %	CO MOLE %	CO_2 MOLE %	N_2 MOLE %	H_2O MOLE %	C_6H_6O MOLE %	C_2H_4 MOLE %	C_2H_2 MOLE %	MODEL ΔP	MODEL q_{cz}
XII-36	FROZEN	35.0	43.6	4.9	2.9	13.6	0.0	0.0	0.0	0.0	10.5	14.9
0.01950	EQUILIBRIUM	76.9	5.5	5.8	0.2	9.9	1.6	0.0	0.0	0.0	10.0	155.8
1005°K	NON-EQUILIBRIUM	35.0	43.6	4.9	2.9	13.6	0.0	0.0	0.0	0.0	10.5	14.9
765°K	EXPERIMENTAL	36.1	42.9	4.8	3.3	12.9	0.0	0.0	0.0	0.0	11.5	-
XIII-38	FROZEN	31.7	46.3	5.5	2.5	14.0	0.0	0.0	0.0	0.0	3.5	4.5
0.0045	EQUILIBRIUM	82.3	1.1	7.0	0.0	9.5	0.2	0.0	0.0	0.0	5.0	34.8
1195°K	NON-EQUILIBRIUM	31.7	46.3	5.5	2.5	14.0	0.0	0.0	0.0	0.0	3.5	4.5
930°K	EXPERIMENTAL	32.6	41.3	8.9	5.2	14.0	0.0	0.0	0.0	0.0	2.5	-
XIII-39	FROZEN	31.7	46.3	5.5	2.5	14.0	0.0	0.0	0.0	0.0	14.5	19.1
0.0195	EQUILIBRIUM	82.4	1.0	7.0	0.0	9.5	0.1	0.0	0.0	0.0	21.0	143.1
1210°K	NON-EQUILIBRIUM	31.7	46.3	5.5	2.5	14.0	0.0	0.0	0.0	0.0	14.5	19.3
940°K	EXPERIMENTAL	30.8	45.8	6.0	4.4	14.0	0.0	0.0	0.0	0.0	21.0	-
XIII-40	FROZEN	31.7	46.3	5.5	2.5	14.0	0.0	0.0	0.0	0.0	3.5	4.7
0.0450	EQUILIBRIUM	82.3	1.0	7.1	0.0	9.5	0.1	0.0	0.0	0.0	5.5	57.8
1230°K	NON-EQUILIBRIUM	31.7	46.3	5.5	2.5	14.0	0.0	0.0	0.0	0.0	3.5	4.6
920°K	EXPERIMENTAL	30.8	45.7	5.9	3.6	14.0	0.0	0.0	0.0	0.0	7.5	-
XV-45	FROZEN	31.7	46.3	5.5	2.5	14.0	0.0	0.0	0.0	0.0	3.0	5.2
0.0450	EQUILIBRIUM	82.3	1.1	7.0	0.0	9.5	0.1	0.0	0.0	0.0	4.5	57.8
1210°K	NON-EQUILIBRIUM	31.7	46.3	5.5	2.5	14.0	0.0	0.0	0.0	0.0	3.0	5.2
870°K	EXPERIMENTAL	31.7	46.8	4.5	3.0	14.0	0.0	0.0	0.0	0.0	6.0	-
XV-46	FROZEN	31.7	46.3	5.5	2.5	14.0	0.0	0.0	0.0	0.0	0.2	0.3
0.0005	EQUILIBRIUM	82.5	0.9	7.0	0.0	9.5	0.1	0.0	0.0	0.0	0.5	5.3
1230°K	NON-EQUILIBRIUM	31.7	46.3	5.6	2.4	14.0	0.0	0.0	0.0	0.0	0.2	0.3
905°K	EXPERIMENTAL	32.5	43.7	6.2	4.6	13.0	0.0	0.0	0.0	0.0	1.0	-

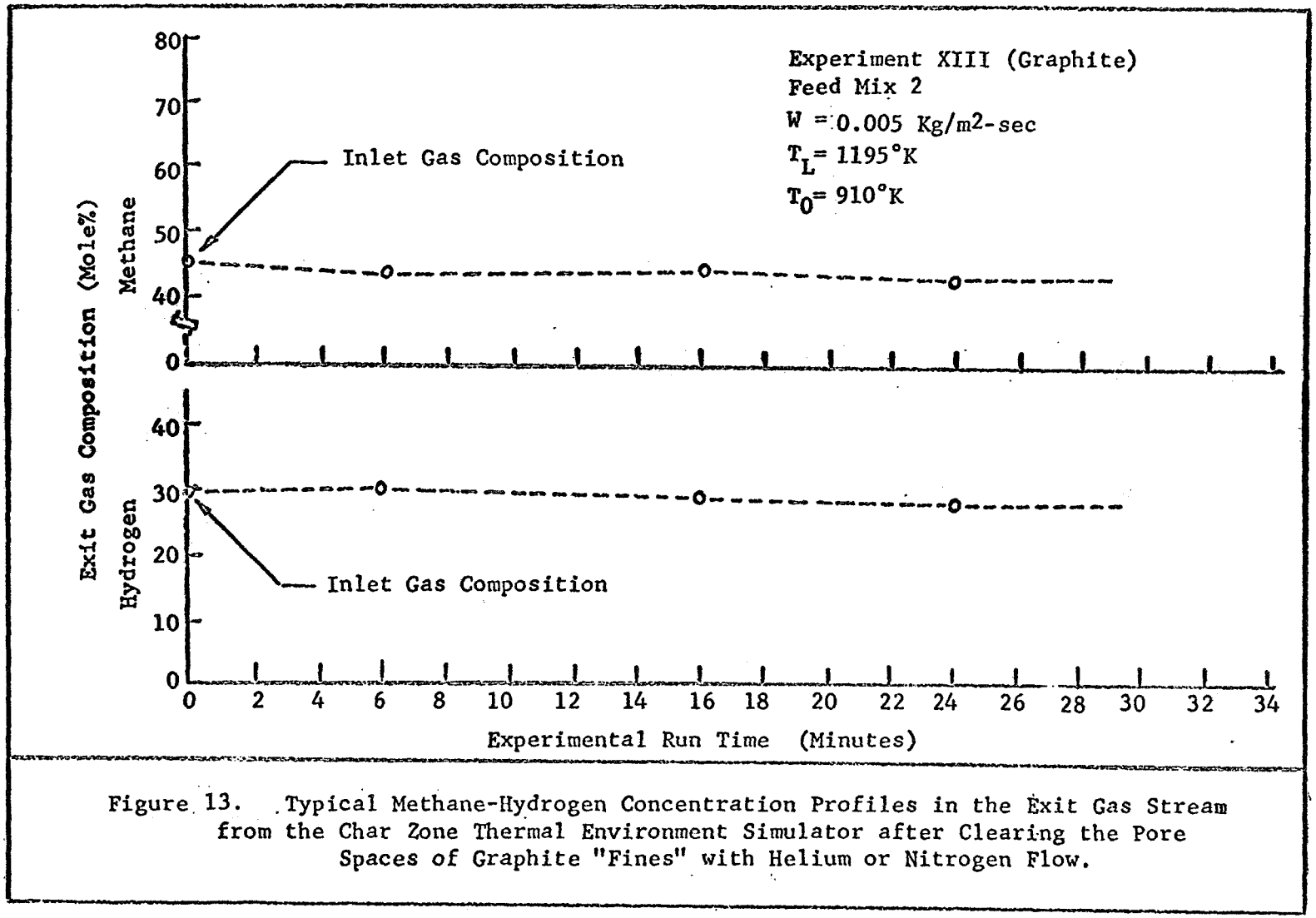

Figure 13. Typical Methane-Hydrogen Concentration Profiles in the Exit Gas Stream from the Char Zone Thermal Environment Simulator after Clearing the Pore Spaces of Graphite "Fines" with Helium or Nitrogen Flow.

Table 24. Flow of Pyrolysis Gases Through Graphite and Chars. Comparison of Results.

RUN NUMBER MASS FLUX: W (W_p) FRONT TEMP BACK TEMP	FLOW MODEL	H_2 MOLE %	CH_4 MOLE %	CO MOLE %	CO_2 MOLE %	N_2 MOLE %	H_2O MOLE %	C_6H_6O MOLE %	C_2H_4 MOLE %	C_2H_2 MOLE %	MODEL ΔP	MODEL q_{cz}
C-XVIII-56	FROZEN	28.9	6.4	3.3	0.8	0.0	53.3	6.9	0.0	0.0	2.0	10.2
0.01040	EQUILIBRIUM	59.7	3.3	26.7	4.0	0.0	6.3	0.0	0.0	0.0	2.0	174.2
(0.01300)	NON-EQUILIBRIUM	23.0	11.1	2.8	2.1	0.0	53.8	7.1	0.0	0.0	2.0	10.9
1190°K	EXPERIMENTAL	24.8	10.3	3.4	1.3	0.0	53.7	6.5	0.0	0.0	4.0	-
820°K												
G-XXVIII-93	FROZEN	25.8	7.2	4.3	1.3	0.0	50.1	11.3	0.0	0.0	1.0	21.9
0.0170	EQUILIBRIUM	62.7	1.3	33.5	0.8	0.0	1.7	0.0	0.0	0.0	1.0	312.4
(0.0340)	NON-EQUILIBRIUM	28.8	10.0	11.8	4.1	0.0	32.6	10.2	0.0	0.3	1.0	25.6
1340°K	EXPERIMENTAL	32.2	11.2	9.2	4.0	0.0	33.2	9.8	0.2	0.2	2.0	-
865°K												
C-XIX-60	FROZEN	29.3	6.0	3.3	0.9	0.0	53.7	6.8	0.0	0.0	3.5	12.9
0.01240	EQUILIBRIUM	62.7	0.8	35.2	1.5	0.0	0.9	0.0	0.0	0.0	3.0	143.0
(0.01550)	NON-EQUILIBRIUM	38.2	17.2	25.2	8.8	0.0	4.9	5.1	0.0	0.5	3.0	26.6
1370°K	EXPERIMENTAL	41.3	18.2	23.4	7.6	0.0	5.0	4.5	0.0	0.0	3.0	-
1020°K												
G-XXIII-71	FROZEN	25.8	4.9	2.9	0.9	0.0	54.7	10.8	0.0	0.0	1.0	22.0
0.01550	EQUILIBRIUM	62.6	0.7	35.8	0.3	0.0	0.7	0.0	0.0	0.0	1.0	350.4
(0.03100)	NON-EQUILIBRIUM	41.4	8.4	23.9	5.1	0.0	12.5	8.2	0.0	0.6	1.0	55.5
1380°K	EXPERIMENTAL	39.3	8.8	27.2	5.9	0.0	11.2	7.6	0.2	0.3	3.5	-
865°K												
C-XX-63	FROZEN	28.6	5.5	3.4	1.0	0.0	53.8	7.7	0.0	0.0	3.0	19.7
0.01120	EQUILIBRIUM	63.1	0.3	36.4	0.1	0.0	0.2	0.0	0.0	0.0	2.5	565.0
(0.01400)	NON-EQUILIBRIUM	30.7	21.4	38.6	3.4	0.0	0.0	4.6	0.3	1.0	2.5	34.9
1535°K	EXPERIMANTAL	30.4	19.8	38.0	5.7	0.0	0.0	5.0	0.5	0.6	3.0	-
905°K												

identical retention times, the relative amount of each carbon-containing species formed from the thermal degradation of the labeled pyrolysis product entering the char was determined.

Typical results for Carbon-14 labeled methane are shown in Figure 14, in which the gas chromatogram(s) and corresponding radioactivity curve are presented. The particular results are for experiment XXIX in which the front surface temperature was 1935°F (1333°K) and the gas mass flux was 0.00591b/ft^2-sec (0.030 kg/m^2-sec). By comparing the two curves, the products of methane decomposition were found to be unreacted methane, carbon monoxide, carbon dioxide, ethylene and acetylene. These results for methane are very important in the light of predicting the manner in which energy can be absorbed by chemical reaction. Ethylene and acetylene, for example, are indirect products of methane decomposition predicted by reactions (39) through (42) in Table 5 , while carbon monoxide and dioxide are formed by the reaction of steam with deposited carbon in reactions (46) through (48). This information established that the chemical reactions used to predict the phenomena occurring in any system are correct.

A similar discussion is presented for labeled phenol. These results are likewise shown in Figure 14. Conditions for the presented data were a front surface temperature of 1960°F (1350°K) and a mass flux rate of 0.0034 lb/ft^2-sec (0.017 kg/m^2-sec). The exit gas products for phenol degradation are methane, carbon monoxide, carbon dioxide, ethylene and acetylene, as well as unreacted phenol analysed in the liquid phase. Once again insight into the kind of reactions necessary to produce the products was obtained. The formation of hydrogen and carbon by reaction (44) and (45) is probable by the observed carbon deposition within the graphite. Hydrogenation of carbon by reaction (43) to form methane, followed by the steam-gas reactions (46,47,48) and the hydrocarbon cracking reactions (39, 40, 41, 42) accounts for each radioactive species observed.

In both methane and phenol degradation, thermal decomposition of the major species in the simulated pyrolysis product stream was described and accounted for by the reactions considered important between 500-3000°F (533-1925°K).

In addition to the product distribution resulting from the thermal degradation of methane and phenol, deposited carbon was also observed to occur. The location of the carbon deposition within the char layer is important in defining the temperature at which reactions become significant. This topic is discussed in detail in the next section.

Carbon Deposition Studies by Radioactive Tracer Methods

The location and extent of carbon deposition resulting from methane and phenol decomposition was determined using Carbon-14 labeled methane and phenol. In the specific cases studied, labeled methane and phenol were fed separately as components in the simulated pyrolysis product stream

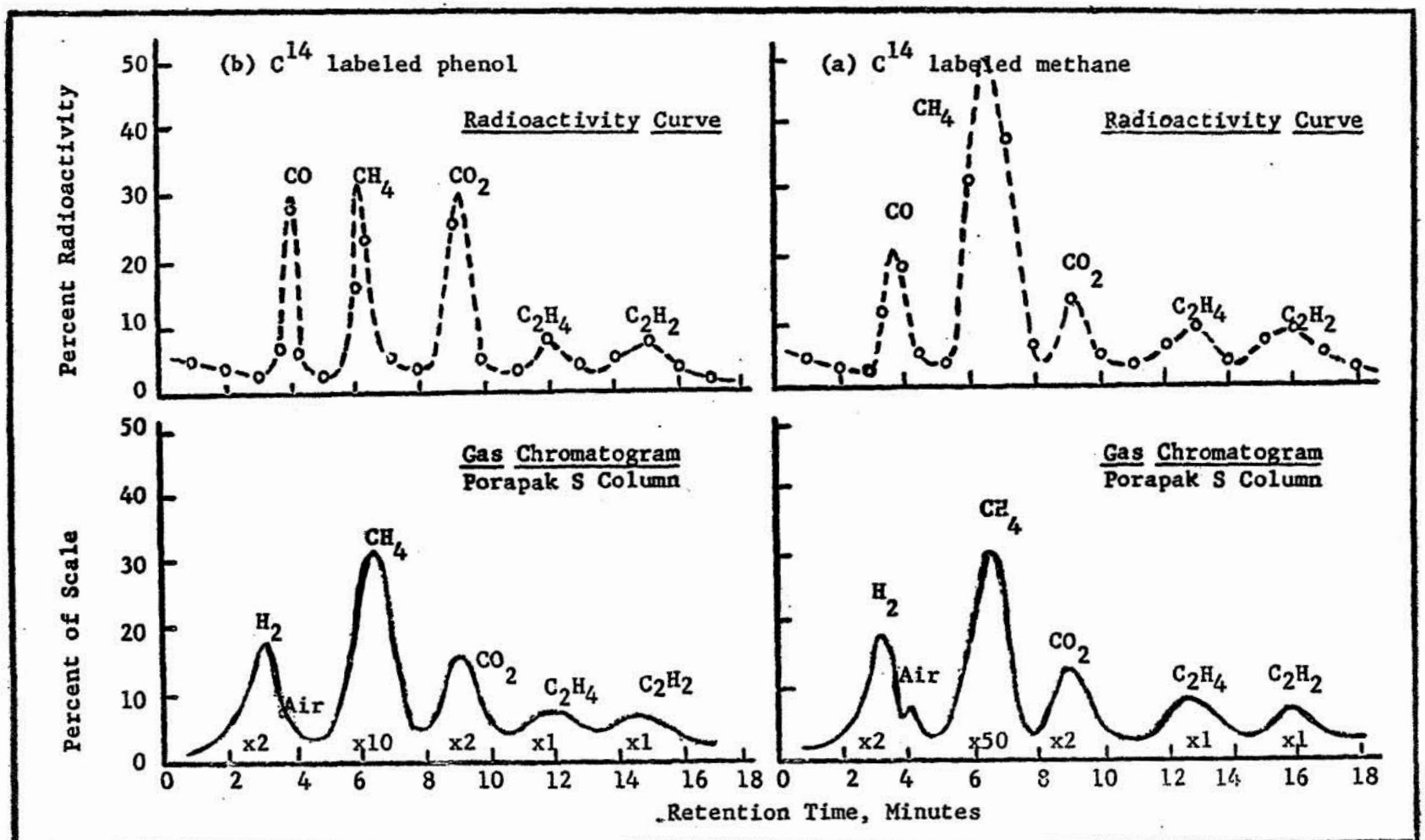

Figure 14. Gas Chromatograms and Radioactivity Curves of the Exit Product Stream from the Char Zone Thermal Environment Simulator; (a) C^{14} labeled methane, (b) phenol.

entering the char. The char was removed after each experiment and sectioned by removing thin layers using emery paper. These layers varied between one and ten percent (by weight) of the total char and were combusted separately with collection of the carbon dioxide in one molar hydroxide hyamine (in methanol) solution. The radioactivity of each thin layer was determined and plotted as a function of char depth. In Figure 15 such a curve is shown for the thermal degradation of phenol and Figure 16 is a similar curve for the decomposition of radioactive labeled methane. The hashed-in rectangular blocks represent the total percent radioactivity of the thickness of the individual slices analysed, while the dotted curve represents the percent radioactivity per unit thickness at a particular char depth. The results in Figure 15 are for phenol decomposition at a mass flux rate of 0.0059 lb/ft^2-sec (0.030 kg/m^2-sec) and a front surface temperature of 1960°F (1350°K). Deposition of carbon appears to start at a char depth of 0.38 corresponding to a temperature of 1300°F (978°K), and continues uniformly to 0.925 where the temperature is 1925°F (1325°K). At this point a rapid decrease is noted indicating either no further carbon deposition or disappearance of carbon by chemical reaction.

Similar results are observed for carbon deposition by methane decomposition in Figure 16. Since carbon deposition by methane and/or phenol degradation is an increasing function of temperature, and, since a substantial amount of phenol and methane is present in the exit gas stream, it is unlikely that carbon deposition reactions have terminated. Instead, the reaction of the deposited carbon with steam (or carbon dioxide) is a more probable explanation of the decline noted in Figure 16. This is also substantiated by the rapid decrease in water concentration at the same temperature where carbon deposition declines. Additionally, carbon was observed on the quartz cover plate and inside surfaces of the outer char holder section which indicated that the carbon deposition reactions were continuing after the gases had left the char surface. Therefore, a very comprehensive picture of carbon deposition with regard to its location, the causes for its appearance and disappearance, and its effect on the exit gas product distribution was obtained. This was one additional, important use of an accurate mathematical model in predicting phenomena very difficult and often impossible to determine with experimental techniques only.

The combination of the radioactive tracer techniques and the non-equilibrium flow analysis will be applied in evaluating various catalysts for accelerating the chemical reactions and, thereby, increasing the energy absorbed within the char zone. The effectiveness of each catalyst will be determined in the following section by comparing the results with data from non-catalytic experiments.

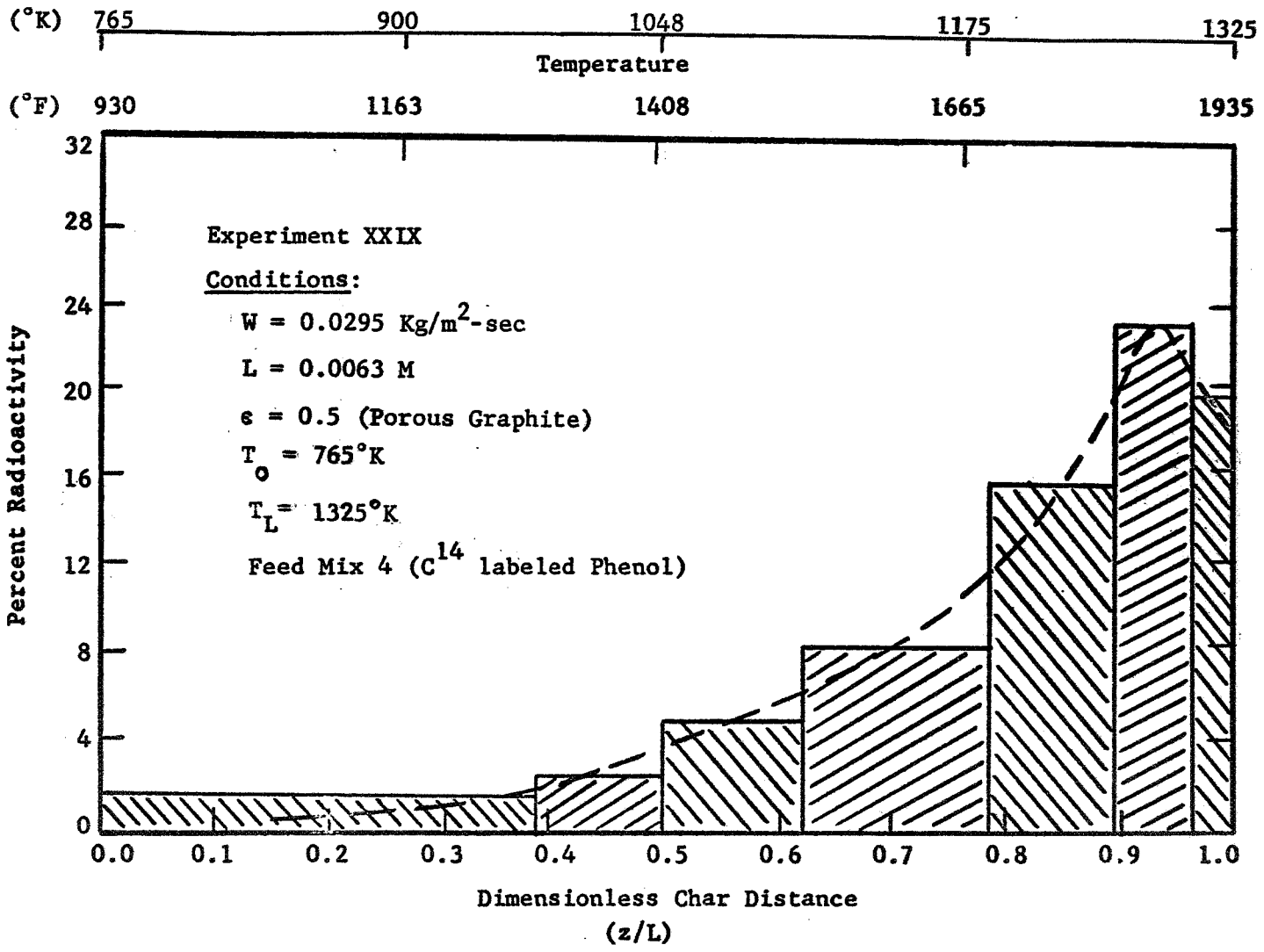

Figure 15. Carbon Deposition Profile for the Thermal Degradation of Phenol, a Major Component in the Pyrolysis Gas Stream.

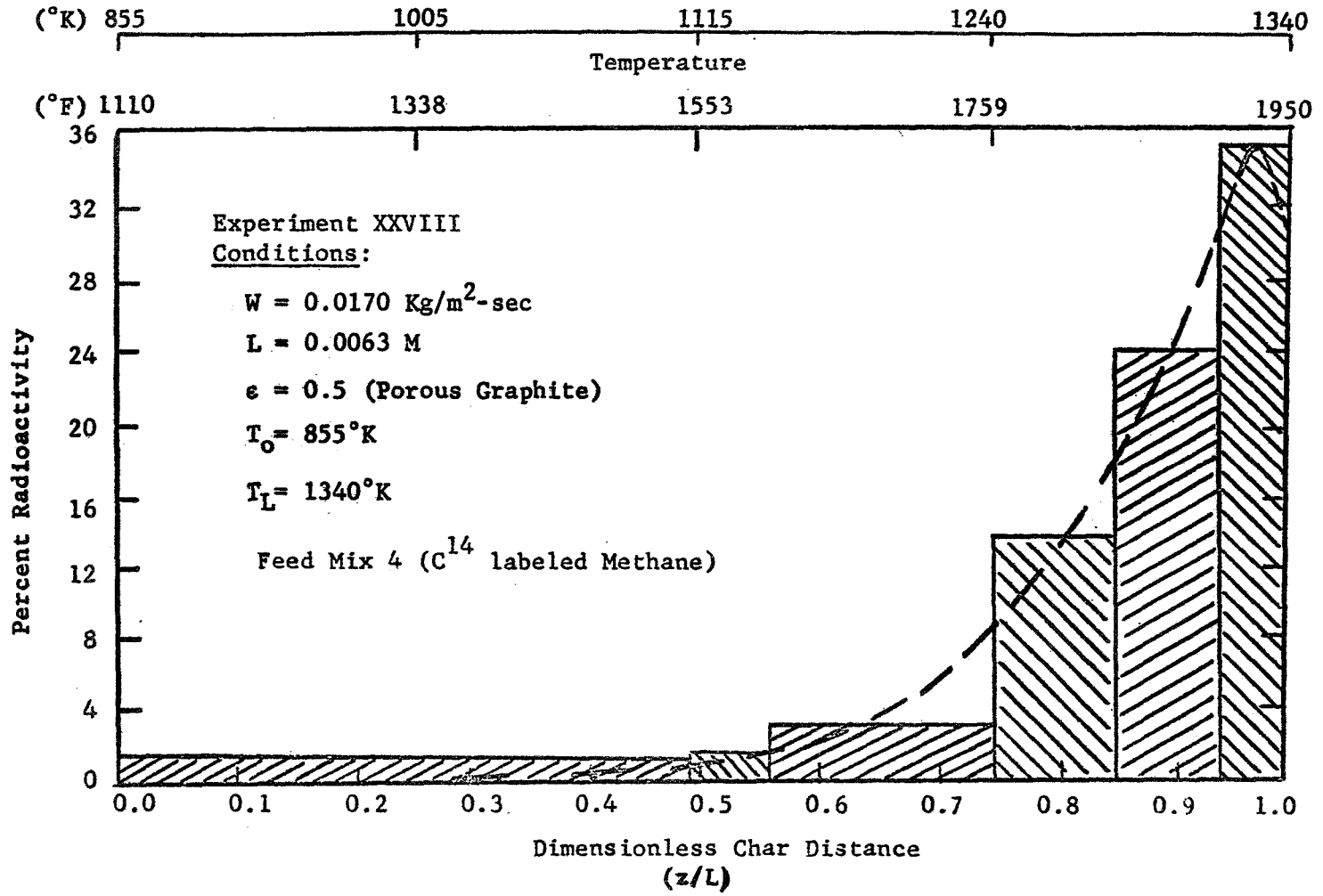

Figure 16. Carbon Deposition Profile for the Thermal Degradation of Methane, a Major Component in the Pyrolysis Gas Stream.

Catalytic Reactions of the Pyrolysis Products in the Char Zone

The discussion thus far has shown that chemical reactions within the char layer are very important modes of energy absorption. It was also pointed out that chemical non-equilibiium becomes important between 2000 - 2500 °F (1367 - 1644°K) for a mass flux rate of 0.05 lb/ft^2-sec (0.25 kg/m^2-sec) (Tables 15 through 18). Below this range, the flow of pyrolysis products through the char is essentially frozen, while above 2000°F (1367°K), the flow is best described by finite reaction rates for the important chemical reactions taking place within the char between the pyrolysis products.

In reentry applications where the temperature gradient across the ablator may vary from 500 - 5000°F (533 - 3033°K), the frozen state (less than 1367°K) can extend over nearly one third the entire thickness. Within this region heat absorption by conduction and convection are the only important modes of energy transfer. In order to increase the capacity of this region to absorb heat, and thus proportionately reduce the total heat shield weight requirement, the introduction of a catalyst to initiate chemical reactions in the lower temperature range (<1367°K) was evaluated.

There are two types of catalyst systems: homogeneous and heterogeneous. The first involves the introduction of a chemical compound which is in the same phase as the pyrolysis product stream. The homogeneous catalyst effectively reduces the energy of activation by interacting with the various species present. To illustrate this interaction the catalytic chlorination of nitrous oxide in the presence of bromine is used as an example (74) of the action of a homogeneous catalyst. The direct chlorination occurs by reaction (52):

$$2NO + Cl_2 \rightarrow 2NOCl \qquad (52)$$

Introducing bromine results in a two reaction sequence as follows:

$$2NO + Br_2 \rightarrow 2NOBr \qquad (53)$$

$$2NOBr + Cl_2 \rightarrow 2NOCl + Br_2 \qquad (54)$$

The reaction with the greatest activation energy between (53) and (54) is the rate determining step for the sequence. Bromine is considered a catalyst if, and only if, the energy of activation of the rate determining step is smaller than the energy of activation of reaction (52). Such is the case for this example. Other homogeneous catalysts are iodine, hydrogen bromide, hydrogen fluoride, nitric oxide, chlorine and mercury (75, 76, 77, 78, 79).

In the case of the halogens, incorporation of an organic halide into the composite which thermally degrades at or near the temperature for the nylon-phenolic resin could be used to introduce the catalyst into the pyrolysis product stream. One example for bromine is tribromobutane which vaporizes at 500°K (nylon-phenolic resin at 525°K) and forms HBr and cracked products of an olefin.

The second kind of catalyst system with application to flow of hydrocarbon products through porous media are the heterogeneous catalysts. These consist of a thin dispersion of an active metal on a porous solid, called a catalyst support. Gases are thus absorbed on the metal surfaces as they flow through the porous solid, undergo chemical reactions, and desorbe back into the gas stream. The kind of solid supports used vary from clays and alumina to porous carbon.

Heterogeneous catalysts are widely used in the petroleum and chemical industries for accelerating hydrogenation and dehydrogenation reactions, hydrocracking reactions and hydroforming reactions. Some typical active metals used in these applications are platinum, tungsten, molybdenum, palladium, etc. (80). One example involves the catalytic hydrogenation of benzene to cyclohexane at room temperature with platinum on porous carbon supports (80). Cyclohexane is then cracked to lower molecular weight compounds at 722°K (81). Details for the catalytic cracking of numerous organic compounds are presented by Vogh (82).

In many cases the use of heterogenous catalysts is restricted to applications which do not contain compounds that deactivate the metal surfaces. Some of these so called poisons are carbon monoxide, sulfur and deposits of carbon or coke. Although there is no sulfur in the pyrolysis product stream, carbon monoxide and deposited carbon are present requiring additional screening of the heterogeneous catalyst considered. The activity and selectivity of the catalyst chosen for this application is discussed in a subsequent section.

Because the heterogeneous catalyst exists in a different state, the solid phase, then the pyrolysis products, introduction into the system requires more detailed planning. There are two possible techniques that permit the placement of a finely dispersed metal catalyst on the char of a charring ablator. The first takes advantage of a nylon-platinum catalyst used to hydrogenate benzene to cyclohexane (83). The inclusion of this platinum impregnated nylon with nylon and phenolic resin during the molding process could be made. During ablation, the nylon would degrade and release the metal catalyst which would be distributed on the surface of the formed char layer. The presence of water and hydrogen at the lower temperatures (<750°K) would prevent coking, leaving the metal sites exposed to promote the pyrolysis reactions.

The second method is similar to the method used for introducing a homogeneous catalyst into the pyrolysis product stream. In this case an organo-metallic compound such as nickel stearate (84) could be included which would vaporize in the decomposition zone with deposition of nickel on the char surface. This action is commonly observed in vapor phase cracking processes (84,85) in which increased activity of the cracking catalyst results in excessive carbon and hydrogen formation. Other similar compounds are the carbonyl compounds of nickel, iron and cobalt (86). The combination of both catalysts systems may also be possible by using compounds containing both metal and halogen atoms, such as platinum iodide. The advantage of this type of co-catalyst would exist only if both groups were found to accelerate chemical reactions within the char layer.

The following sections will describe the results obtained in tests using the Char Zone Thermal Environment Simulator. Each catalyst system will be compared with non-catalytic data to determine the extent of chemical reaction due to the addition of the catalyst. The preparation of each catalyst and the procedure for introducing it into the experimental simulation will also be discussed.

Homogeneous catalysis of the pyrolysis products.-Unlike the heterogeneous catalysis systems, very little information regarding the activity of various homogeneous catalyst systems is contained in the literature. One source, however, reported the relative activity of several organic halides and halogen catalysts for the catalytic degradation of hydrocarbons to carbon monoxide, carbon dioxide and organic acids, aldehydes and ketones (87). A list of the relative activities of these catalysts are presented in Table 25 with iodine as a reference (relative activity of 100). No relative activities of nitrous oxide or mercury were found. Also hydrogen fluoride was omitted from the above list of relative activities.

Although the above may indeed be excellent homogeneous catalysts, certain aspects of the ablative process prohibit their use. For example, nitrous oxide, while exhibiting excellent catalytic activity for the thermal degradation of certain hydrocarbons requires a concentration too great to be practically included in the composite (75). Similarly, hydrogen fluoride and mercury are almost exclusively used as liquid phase catalysts (88, 89). As a result, attention in this research was given to the halides which were not only reported as good catalysts in hydrocarbon decomposition and oxidation reactions (90), but also required in small enough concentrations to be conviently and economically feasible for ablative heat shield applications.

Experimental results for homogeneous catalysis of the pyrolysis product reactions with bromine.-As a matter of convenience in the experimental simulation apparatus, bromine was selected as a representative halide catalyst. It was convenient to dissolve bromine in the water and feed the resulting solution to the char holder with phenol and the gaseous pyrolysis products. The concentration of bromine in the water solution was varied from 1.0 to 4.0% by weight.

Table 25. Relative Activity of the Halogens and Organic Halides as Catalysts in the Thermal Degradation of Pyrolysis Gas Products.

Conditions: Oxidation of Aldehydhes and Ketones at 400-500°C and one Atmosphere.

Component Name	Relative Efficiency
Iodine (Reference)	100
Isopropyl Iodide	70
Ethyl Iodide	40
Methyl Iodide	30
Hydrogen Bromide	20
Isopropyl Bromide	5
Ethyl Bromide	4
Dibromoacetylene	3
Chlorides	0

The selection of bromine as a suitable and typical catalyst was based on evidence of strong aromatic ring attack, such as with phenol, to form tribromophenol at ambient conditions. In addition it has excellent oxidative properties in decomposing hydrocarbons such as propane to carbon monoxide, carbon dioxide and other organic species such as organic acids, aldehydes and ketones (90). Furthermore, the formation of HBr from hydrogen and bromine occurs at moderate temperatures (475-575°K) by the following mechanism (91). This gives the additional catalytic benefit of HBr being present.

$$
\begin{aligned}
&Br_2 \rightarrow Br + Br \\
&Br + H_2 \rightarrow HBr + H \\
&H + Br_2 \rightarrow HBr + Br \\
&H + HBr \rightarrow H_2 + Br \\
&Br + Br \rightarrow Br_2^* \\
&Br_2^* \rightarrow Br + Br
\end{aligned}
\qquad (55)
$$

Also it established a reference to the remaining halide catalysts contained in Table 25 and thus makes an exhaustive investigation unnecessary if significant promotion of chemical reaction rates are found. The above mechanism is favored by low pressure and large surface area, both of which exist in the char zone during reentry.

Results of several experiments are shown in Table 26. The experimental exit gas compositions are no longer predicted by the non-equilibrium flow model within the experimental accuracy as observed for the non-catalytic experiments. Also the reactions are not at equilibrium as seen from the table.

The effect of bromine as a catalyst is better illustrated by comparing experiment XXVIII-92, in which the mass flux was 0.0044 lb/ft^2-sec (0.022 kg/m^2-sec), the front surface temperature of 1920°F (1322°K) and no bromine, with experiment XXV-81 (mass flux of 0.010 kg/m^2-sec, a front surface temperature of 1995°F (1370°K) and 4% (wt) bromine catalyst) in Table 27. The conditions are almost the same, and the extent of reaction is greater for the experiment with bromine present. The addition of bromine accelerated the chemical reactions as seen by the facts that significantly more of the water (17.6% rather than 25.4%) and phenol (7.2% rather than 9.5%) had been consumed than would have been if bromine had not been present. This is also seen by direct comparison of the experimental exit gas compositions from each of the similar experiments. A measured decrease in the water and phenol concentrations, with corresponding increases in methane, carbon monoxide, carbon dioxide, ethylene and acetylene are obtained in the bromine catalysed experiment. These same trends are observed in all investigations with bromine and are independent of the catalyst

Table 26. Flow of Pyrolysis Gases Through Graphite. Effect of Bromine Catalyst on the Exit Gas Compositions.

RUN NUMBER MASS FLUX FRONT TEMP BACK TEMP	FLOW MODEL	H_2 MOLE %	CH_4 MOLE %	CO MOLE %	CO_2 MOLE %	N_2 MOLE %	H_2O MOLE %	C_6H_6O MOLE %	C_2H_4 MOLE %	C_2H_2 MOLE %	CATALYSTS
XXV-82	FROZEN	36.9	7.2	4.2	1.3	0.0	42.3	8.1	0.0	0.0	Bromine
0.0325	EQUILIBRIUM	66.2	0.8	32.1	0.2	0.0	0.7	0.0	0.0	0.0	in Water
1380°K	NON-EQUILIBRIUM	40.6	9.7	14.1	2.7	0.0	25.2	7.3	0.0	0.0	4%
860°K	EXPERIMENTAL	41.6	11.8	18.9	3.4	0.0	16.4	7.1	0.3	0.5	(by weight)
XXVII-87	FROZEN	2.3	3.4	0.4	0.1	0.0	0.0	93.8	0.0	0.0	Bromine
0.0160	EQUILIBRIUM	73.7	1.5	24.1	0.3	0.0	0.4	0.0	0.0	0.0	in Water
1350°K	NON-EQUILIBRIUM	2.8	3.6	0.5	0.1	0.0	0.0	91.3	0.0	0.6	1%
845°K	EXPERIMENTAL	4.8	2.7	0.8	0.1	0.0	0.0	90.2	0.1	0.3	(by weight)
XXVII-89	FROZEN	2.1	3.2	0.4	0.1	0.0	94.2	0.0	0.0	0.0	Bromine
0.0254	EQUILIBRIUM	51.1	0.6	46.7	0.7	0.0	1.0	0.0	0.0	0.0	in Water
1365°K	NON-EQUILIBRIUM	18.3	2.8	13.3	2.0	0.0	63.6	0.0	0.0	0.0	1%
850°K	EXPERIMENTAL	28.2	3.4	21.5	6.0	0.0	40.8	0.0	0.4	0.5	(by weight)
XXVI-84	FROZEN	34.3	6.6	3.9	1.1	0.0	45.4	8.7	0.0	0.0	Bromine
0.0065	EQUILIBRIUM	65.0	1.0	32.5	0.4	0.0	1.0	0.0	0.0	0.0	in Water
1370°K	NON-EQUILIBRIUM	39.5	10.7	16.6	3.8	0.0	21.5	7.5	0.0	0.4	2%
755°K	EXPERIMENTAL	37.8	15.3	21.0	4.8	0.0	14.2	6.3	0.2	0.4	(by weight)

Table 27. Flow of Pyrolysis Gases Through Graphite. Comparison of Bromine Catalyzed and Non-Catalytic Exit Gas Compositions.

RUN NUMBER MASS FLUX FRONT TEMP BACK TEMP	FLOW MODEL	H_2 MOLE %	CH_4 MOLE %	CO MOLE %	CO_2 MOLE %	N_2 MOLE %	H_2O MOLE %	C_6H_6O MOLE %	C_2H_4 MOLE %	C_2H_2 MOLE %	COMMENTS
XXV-81	FROZEN	31.5	6.1	3.5	1.1	0.0	47.1	10.8	0.0	0.0	Bromine
0.0190	EQUILIBRIUM	64.7	0.9	33.2	0.4	0.0	0.9	0.0	0.0	0.0	in Water
1350°K	NON-EQUILIBRIUM	36.4	9.9	14.6	3.7	0.0	25.4	9.5	0.0	0.4	4%
903°K	EXPERIMENTAL	40.2	11.9	15.1	7.0	0.0	17.6	7.2	0.3	0.7	(by weight)
XXVIII-92	FROZEN	27.5	5.3	3.1	1.0	0.0	52.5	10.6	0.0	0.0	No
0.0220	EQUILIBRIUM	62.5	1.2	33.9	0.8	0.0	1.6	0.0	0.0	0.0	Bromine
1320°K	NON-EQUILIBRIUM	29.3	7.7	8.6	2.5	0.0	42.2	10.1	0.0	0.2	
855°K	EXPERIMENTAL	30.0	8.7	8.0	3.4	0.0	39.9	9.6	0.2	0.2	

concentrations used (1.0 to 4.0% by weight).

The effect of the bromine catalysis is also seen by inspecting the carbon deposition profiles for the thermal decomposition of phenol in the simulated pyrolysis product stream. This is presented in Figures 17 and 18. The carbon deposition profile for the non-catalytic experiment is shown in Figure 17 for a mass flux of 0.0059 lb/ft^2-sec (0.030 kg/m^2-sec) and 1935°F (1330°K). Deposition begins at a distance of 0.38 in the char where the temperature is 1312°F (980°K) with a uniform increase to a maximum value at 0.925 or 1915°F (1320°K). At this point the profile decreases. In contrast to this curve, Figure 18 represents the carbon deposition profile for the bromine catalysed experiment in which the mass flux was 0.0075 lb/ft^2-sec (0.038 kg/m^2-sec) and 1900°F (1315°K). There is a definite shift in the carbon deposition curve with the maximum value moving from 0.925 to 0.71 or from a temperature of 1915°F (1320°K) to 1630°F (1160°K). Deposition again starts at a distance of 0.38 (975°K). Also additional carbon deposition was noted near the front surface at a temperature of about 1925°F (1325°K).

Similar profiles are shown in Figure 19 and 20 for carbon-14 labeled methane decomposition. Although the results are not as pronounced as the phenol data, a detactable shift in the carbon deposition pattern is again observed. Deposition begins at 0.48 (1120°K) for the non-catalytic experiment compared with 0.42 (1090°K) for the bromine catalyzed case. The point of maximum deposition is shifted away from the front surface to a position corresponding to 1893°F (1300°K) or 0.85. The peak for the bromine-free experiment is located at 0.98 (1330°K).

In summary these results show that bromine is an active catalyst for the catalytic cracking of phenol in the presence of hydrogen (hydrocracking) and to a lesser extent for the hydrocracking of methane. A similar discussion regarding the cracking of the pyrolysis products using heterogeneous catalyst is presented in the following section.

Heterogeneous catalysis of the pyrolysis product reactions using a tungsten-molybdenum co-catalyst.-A great deal of research into heterogeneous catalysts, their applications and activities has been reported in the literature (80,81,82,83). These catalyst are excellent hydrogenation accelerators for a number of hydrocarbons common to the petroleum and chemical industries. However, they are also susceptible to deactivation by reaction, adsorption or coating by several poisons. The two poisons which are present in the pyrolysis gases are carbon monoxide and coke (or carbon) formation. These two poisons are present in the char zone and must be considered when selecting possible heterogeneous catalysts. These poisons rule out the use of platinum, paladium, rhodium, nickel and selenium since these are all poisoned by carbon monoxide. In light of this discussion, tungsten, because of its relatively good activity in systems containing carbon monoxide, and molybdenum, because of its

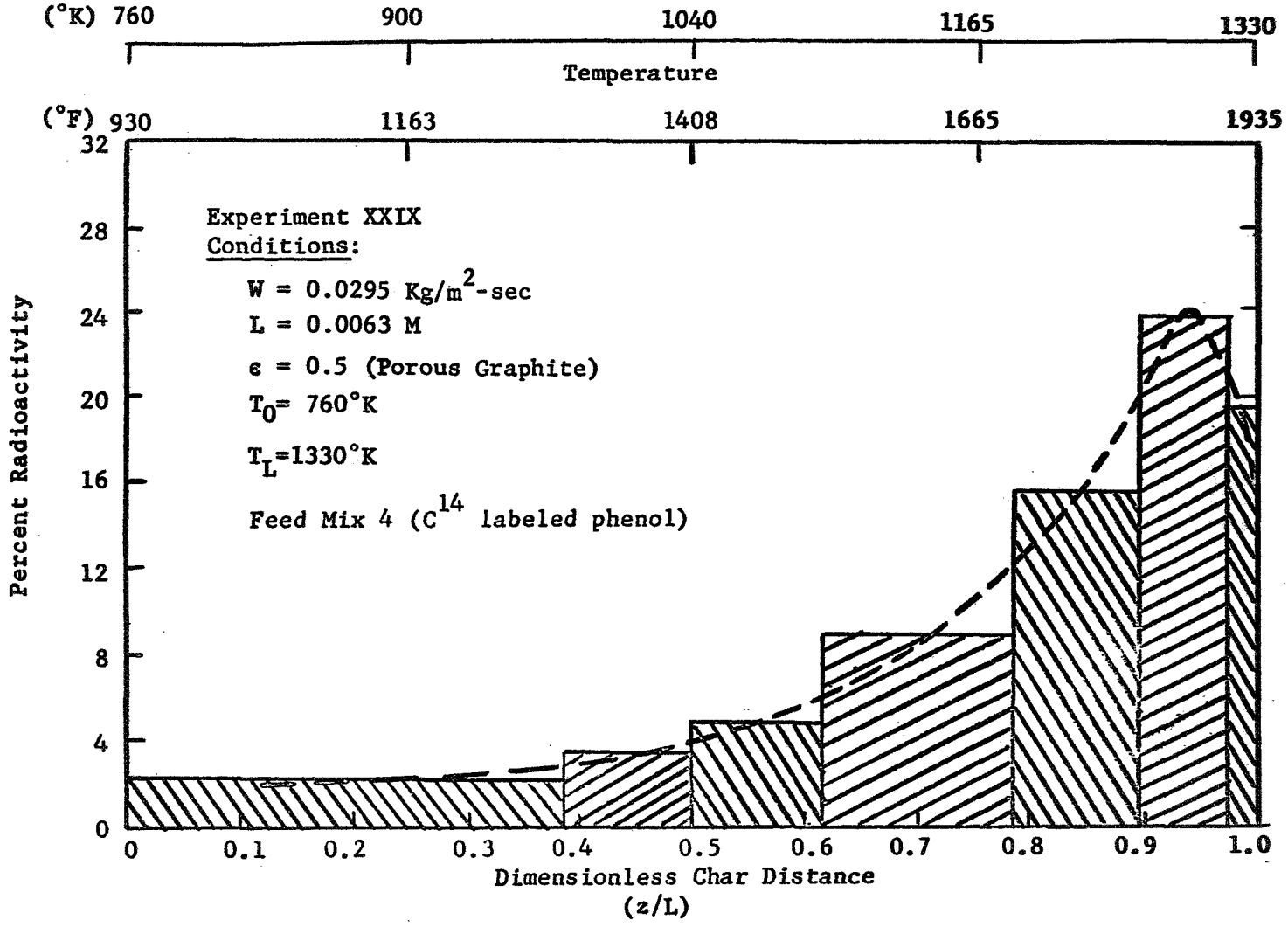

Figure 17. Carbon Deposition Profile for the Thermal Decomposition of Phenol, a Major Component in the Pyrolysis Gas Stream.

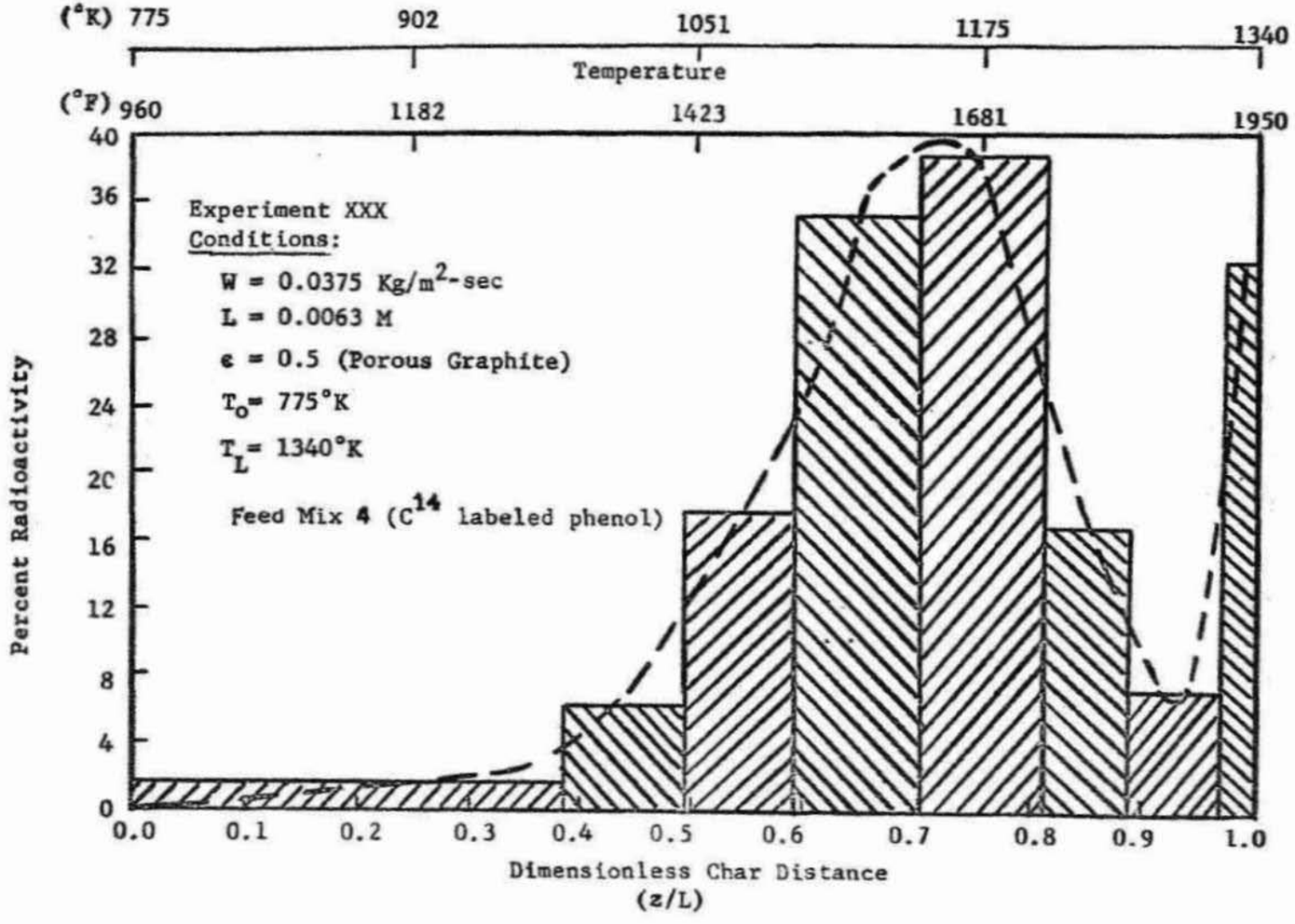

Figure 18. Carbon Deposition Profile for the Thermal Degradation of Phenol Catalyzed by Bromine in a Concentration of 4% (by weight).

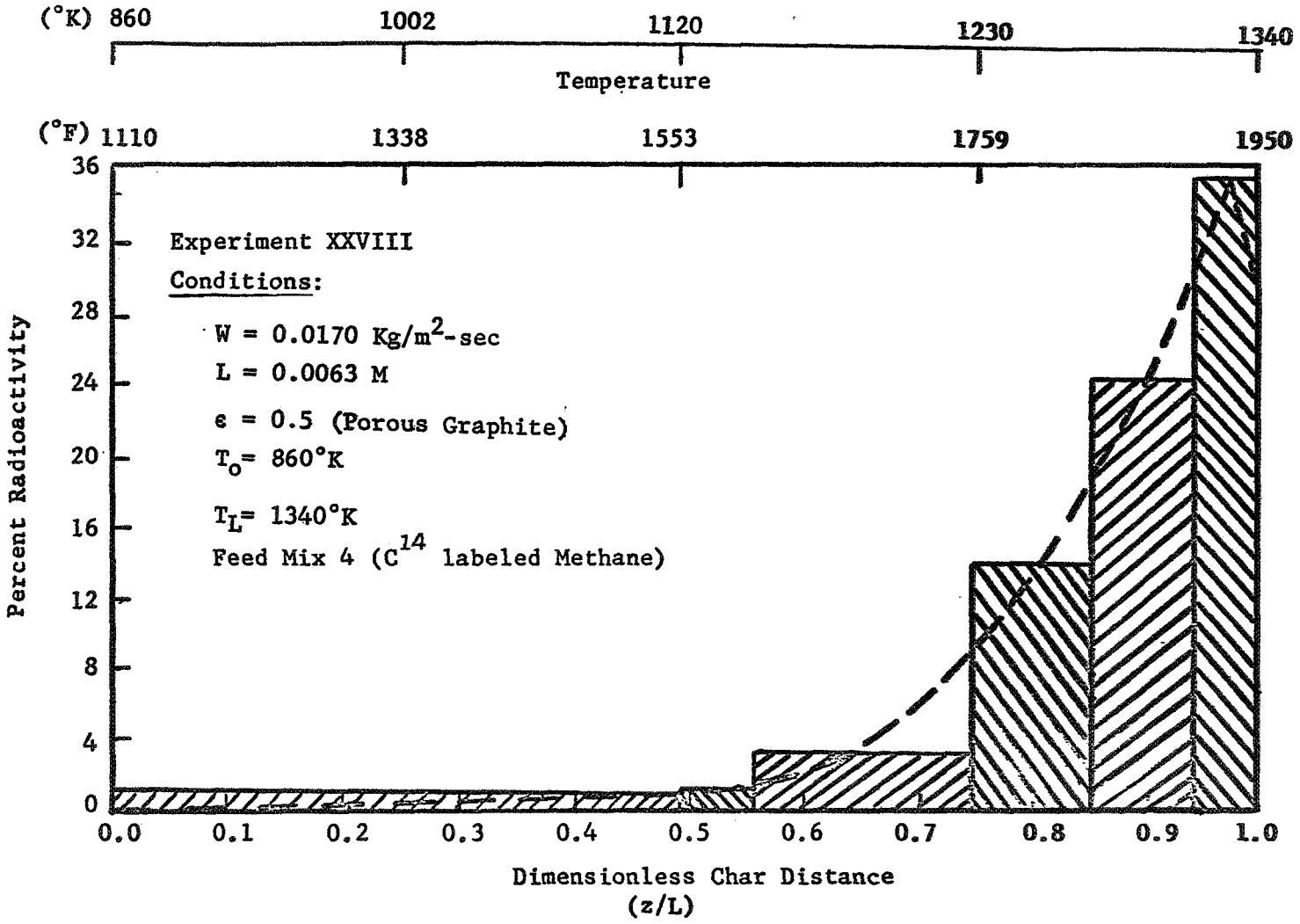

Figure 19. Carbon Deposition Profile for the Thermal Degradation of Methane, a Major Component in the Pyrolysis Gas Stream.

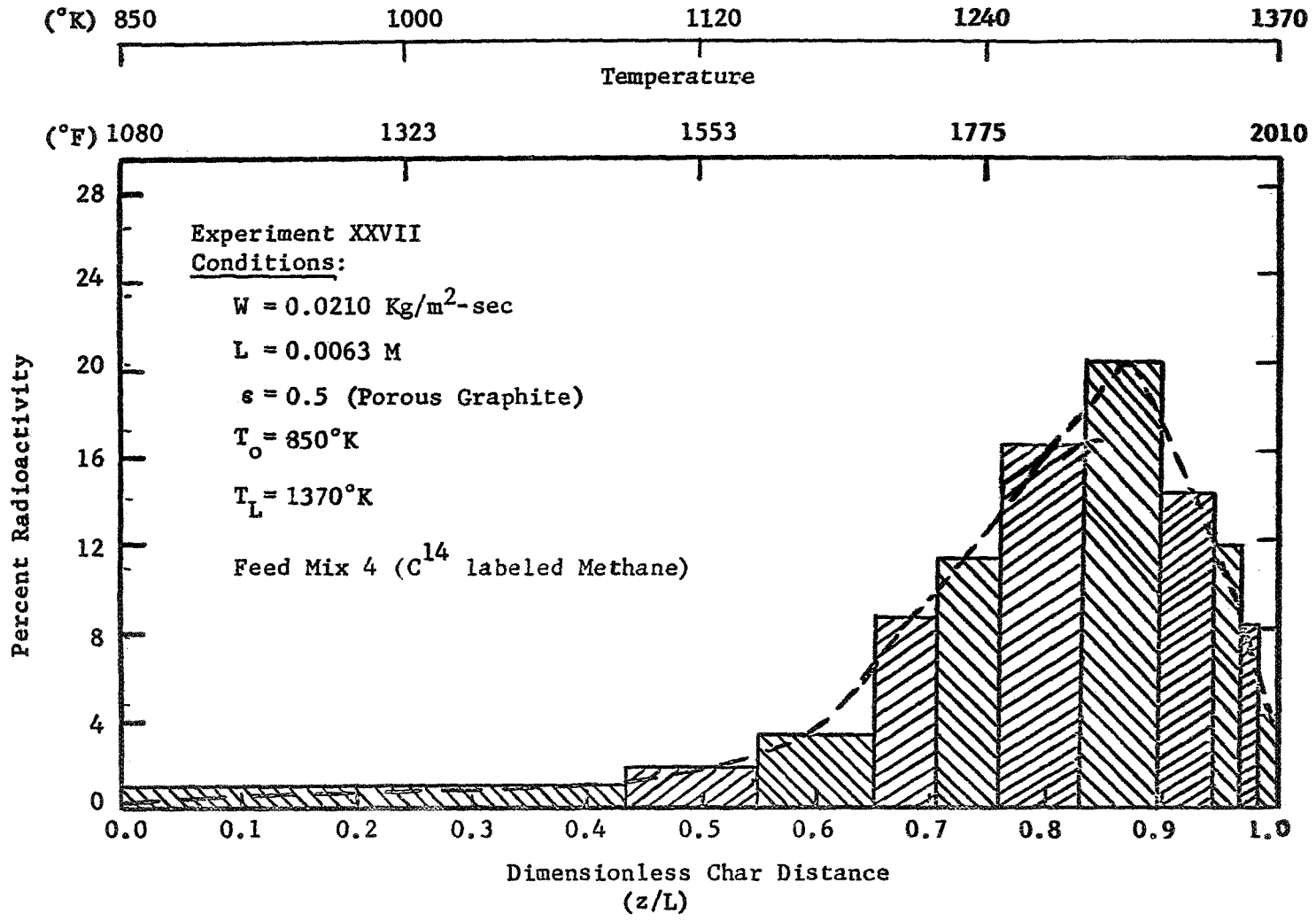

Figure 20. Carbon Deposition Profile for the Thermal Degradation of Methane Catalyzed by Bromine in a Concentration of 4% (by weight).

high selectivity in the thermal degradation of hydrocarbons, were selected as co-catalysts.

The method used to disperse these metals on the graphite specimens was the standard procedure to prepare heterogeneous catalysts and is as follows. First, the metals were obtained as metal acids (anhydrous) and added to hot (353°K) sulfuric acid. Molybdenum was completely dissolved while tungsten formed a saturated solution. The graphite specimens were placed in the hot solution and stirred vigorously for thirty minutes. The second phase of the procedure involved the passing of carbon disulfide vapors through the graphite to convert the metal oxides to sulfides which increases the catalytic activity of the metals. The specimens were then dried at 316°K and reweighed to determine the weight of catalyst dispersed within the pores. The catalyst concentration varied from 5 to 6 percent (by weight) of the co-catalyst (50:50). This is typical of the dispersed (metal) phase composition of heterogeneous catalysts.

The effect of this catalyst on the reactions of the pyrolysis products in the char zone is shown in Table 28. Although there are noticeable differences between the experimentally measured exit gas compositions and the computed values for the uncatalyzed case, they are not as pronounced as the results for bromine. This is better indicated by comparing the results of non-catalytic experiments (XXVIII-92 and XXIX-94) with the values obtained in the heterogeneous co-catalyst systems (XXXII-99 and XXXI-98). The exit gas compositions are shown in Table 29 for an average mass flux rate of 0.0048 lb/ft^2-sec (0.025 kg/m^2-sec) and a front surface temperature range of 1860° to 1945°F (1290°K-1336°K). No detectible difference between the four experiments is determined. Similarly, a comparison of the carbon deposition profiles for carbon-14 labeled phenol (XXVIII and XXXII) and methane (XXIX and XXXI) show no substantial shift in the position of the maximum deposition or the location where carbon deposition begins. These are shown in Figures 21 through 24. A slight difference in behavior near the front surface is observed. However, this represents no substantial change from the non-catalytic behavior.

A series of experiments with a platinum catalyst dispersed on the graphite specimens was also conducted using phenol-water free pyrolysis gases having a relatively low carbon monoxide concentration. These studies showed no catalytic activity over a temperature range of 1370° to 1755°F (1015°K to 1230°K). The results of these tests are summarized in Table 30. The flow remained frozen in each experiment studied.

Summary of the Catalytic Studies to Increase Reactions in the Char Zone

Results for adding bromine to the pyrolysis product stream as a homogeneous catalyst indicated increased chemical reactions within the char zone. This acceleration was shown by comparison of the exit gas composition

Table 28 Flow of Pyrolysis Gases Through Graphite. Effect of Molybdenum-Tungsten Co-catalyst on the Exit Gas Composition.

RUN NUMBER MASS FLUX FRONT TEMP BACK TEMP	FLOW MODEL	H_2 MOLE %	CH_4 MOLE %	CO MOLE %	CO_2 MOLE %	N_2 MOLE %	H_2O MOLE %	C_6H_6O MOLE %	C_2H_4 MOLE %	C_2H_2 MOLE %	CATALYST
XXXI-97	FROZEN	20.0	4.2	2.1	0.6	0.0	62.1	11.0	0.0	0.0	Molybdenum & Tungsten 5-6% by weight as sulfides
0.0320	EQUILIBRIUM	59.4	1.7	33.7	2.0	0.0	3.1	0.0	0.0	0.0	
1300°K	NON-EQUILIBRIUM	20.4	4.6	3.0	0.9	0.0	60.1	10.9	0.0	0.0	
740°K	EXPERIMENTAL	21.6	5.6	4.1	1.3	0.0	58.0	9.0	0.2	0.3	
XXXI-98	FROZEN	26.2	5.5	2.9	0.8	0.0	52.7	11.9	0.0	0.0	as above
0.0240	EQUILIBRIUM	62.6	1.4	33.1	1.0	0.0	1.9	0.0	0.0	0.0	
1340°K	NON-EQUILIBRIUM	28.4	6.5	6.9	1.5	0.0	45.2	11.4	0.0	0.2	
770°K	EXPERIMENTAL	29.2	11.1	8.7	3.6	0.0	38.0	8.8	0.3	0.3	
XXXII-99	FROZEN	25.4	5.4	2.8	0.8	0.0	53.9	11.7	0.0	0.0	as above
0.0245	EQUILIBRIUM	62.6	1.4	33.1	1.0	0.0	1.9	0.0	0.0	0.0	
1280°K	NON-EQUILIBRIUM	26.3	6.3	5.0	1.4	0.0	49.6	11.5	0.0	0.1	
730°K	EXPERIMENTAL	27.6	7.2	6.6	2.6	0.0	45.2	10.2	0.2	0.4	
XXXII-100	FROZEN	14.0	2.3	1.5	0.4	0.0	69.4	12.4	0.0	0.0	as above
0.0490	EQUILIBRIUM	62.6	1.4	33.1	1.0	0.0	1.9	0.0	0.0	0.0	
1330°K	NON-EQUILIBRIUM	15.2	2.4	2.8	0.6	0.0	66.8	12.2	0.0	0.0	
750°K	EXPERIMENTAL	16.6	3.2	3.7	0.8	0.0	64.0	10.8	0.4	0.5	

Table 29 . Flow of Pyrolysis Products Through Porous Graphite. Comparison of the Exit Gas Composition for Molybdenum-Tungsten Catalysed and Non-Catalyst Experiments.

RUN NUMBER MASS FLUX FRONT TEMP BACK TEMP	FLOW MODEL	H_2 MOLE %	CH_4 MOLE %	CO MOLE %	CO_2 MOLE %	N_2 MOLE %	H_2O MOLE %	C_6H_6O MOLE %	C_2H_4 MOLE %	C_2H_2 MOLE %	CATALYST
XXVIII-92	FROZEN	27.5	5.3	3.1	1.0	0.0	52.5	10.6	0.0	0.0	
0.0220	EQUILIBRIUM	62.5	1.2	33.9	0.8	0.0	1.6	0.0	0.0	0.0	no
1325°K	NON-EQUILIBRIUM	29.3	7.7	8.0	2.5	0.0	42.2	10.1	0.0	0.2	catalyst
855°K	EXPERIMENTAL	30.0	8.7	8.0	3.4	0.0	37.9	11.6	0.2	0.2	
XXIX-94	FROZEN	25.6	4.1	2.9	0.8	0.0	55.2	11.5	0.0	0.0	
0.0250	EQUILIBRIUM	61.8	1.1	34.9	0.7	0.0	1.5	0.0	0.0	0.0	no
1325°K	NON-EQUILIBRIUM	28.1	5.8	7.8	2.1	0.0	45.1	10.9	0.0	0.3	catalyst
760°K	EXPERIMENTAL	25.5	5.8	10.5	2.7	0.0	42.7	12.2	0.2	0.2	
XXXI-98	FROZEN	26.2	5.5	2.9	0.8	0.0	52.7	11.9	0.0	0.0	Molybdenum
0.0240	EQUILIBRIUM	62.6	1.4	33.1	1.0	0.0	1.9	0.0	0.0	0.0	Tungsten
1340°K	NON-EQUILIBRIUM	28.4	6.5	6.9	1.5	0.0	45.2	11.4	0.0	0.2	5-6% (wt)
770°K	EXPERIMENTAL	29.2	11.1	8.7	3.6	0.0	38.0	8.8	0.3	0.3	as sulfide
XXXII-99	FROZEN	25.5	5.3	2.8	0.8	0.0	53.9	11.7	0.0	0.0	Molybdenum
0.0245	EQUILIBRIUM	62.6	1.4	33.1	1.0	0.0	1.9	0.0	0.0	0.0	Tungsten
1290°K	NON-EQUILIBRIUM	26.3	6.3	5.0	1.4	0.0	49.6	11.5	0.0	0.1	5-6% (wt)
720°K	EXPERIMENTAL	27.6	7.2	6.6	2.6	0.0	45.2	10.2	0.2	0.4	as sulfide

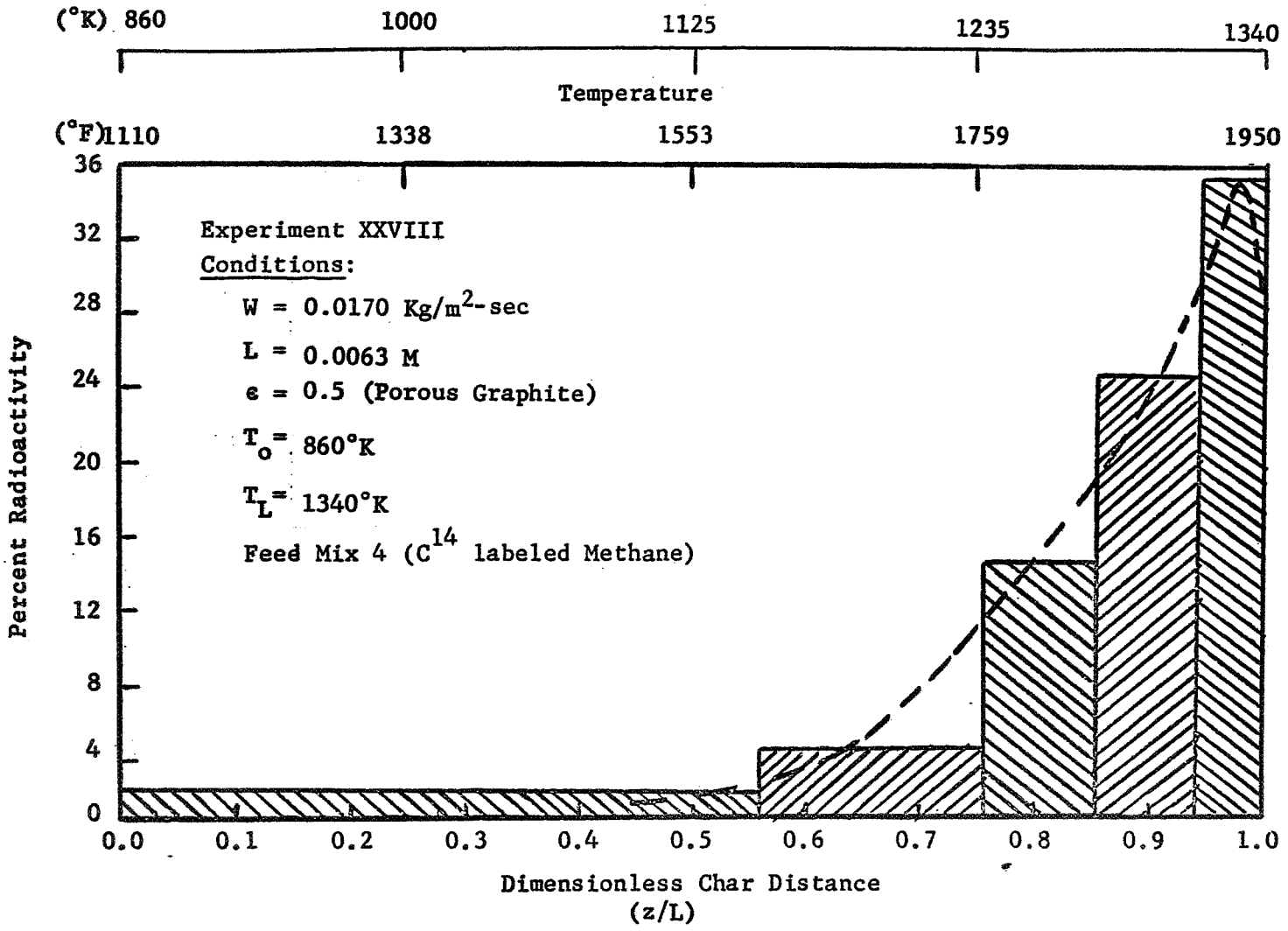

Figure 21. Carbon Deposition Profile for the Thermal Degradation of Methane, a Major Component in the Pyrolysis Gas Stream.

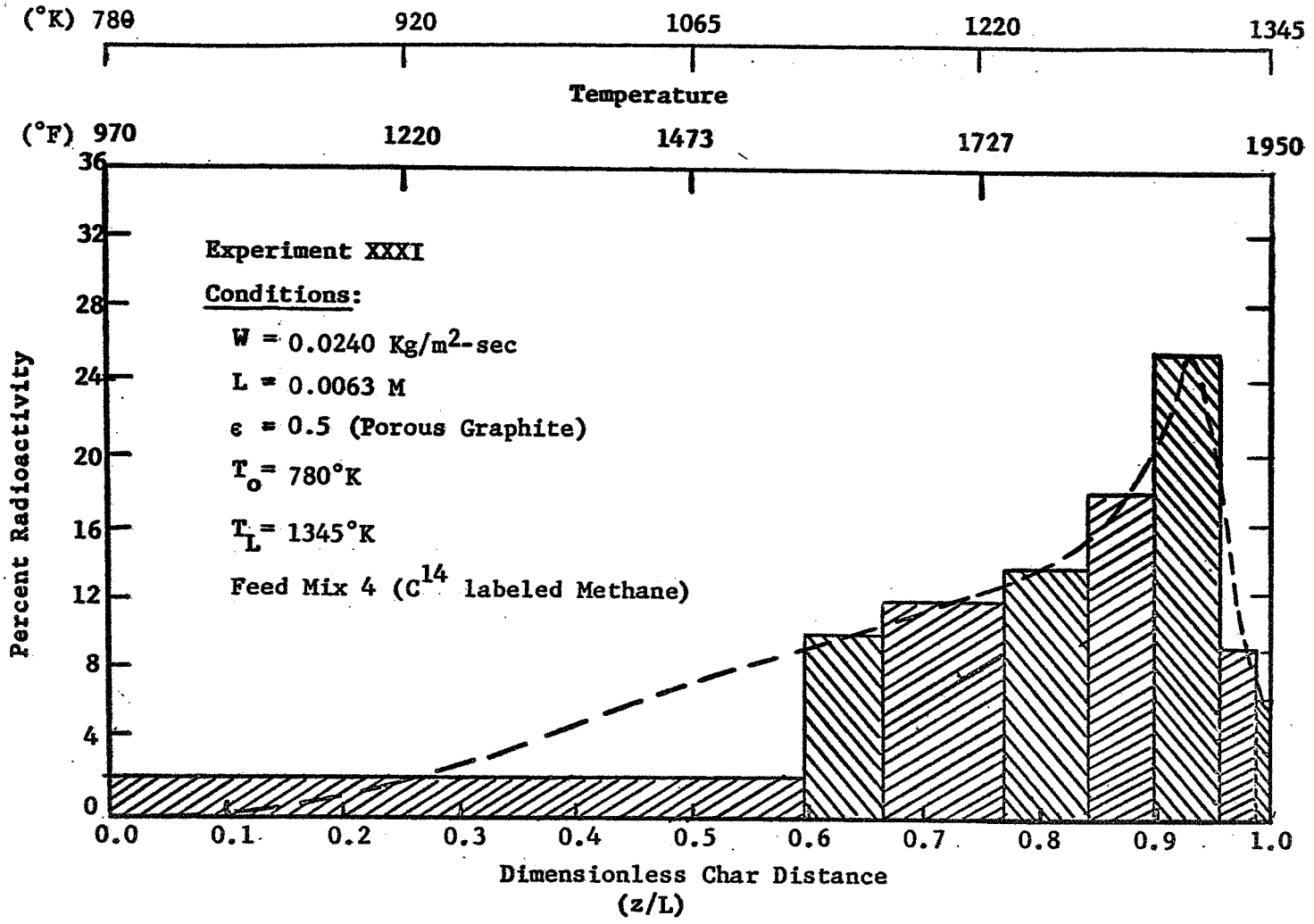

Figure 22 . Carbon Deposition Profile for the Thermal Degradation of Methane Catalyzed with a Molybdenum-Tungsten Co-Catalyst Coating on the Graphite.

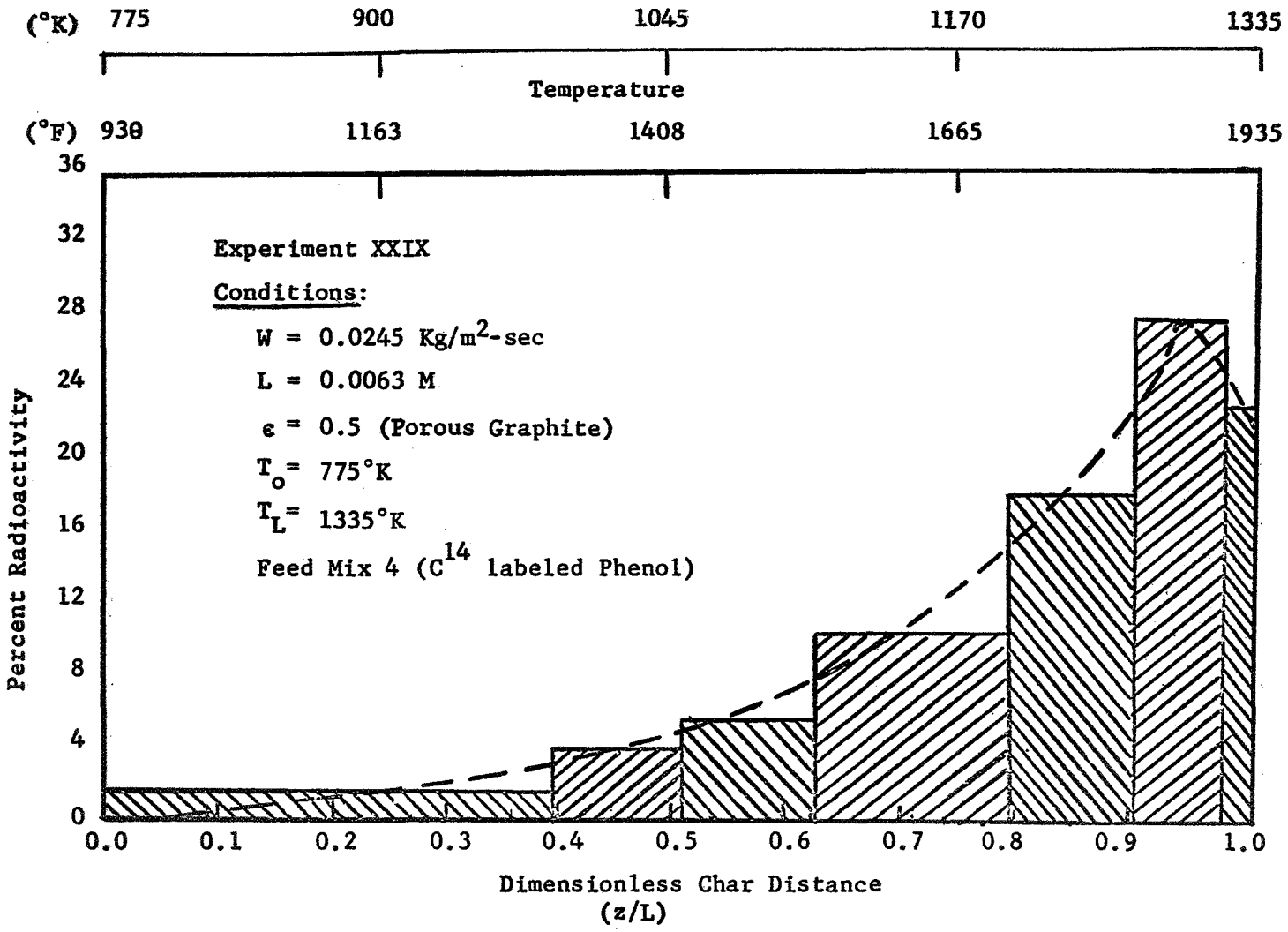

Figure 23. Carbon Deposition Profile for the Thermal Degradation of Phenol, a Major Component in the Pyrolysis Gas Stream.

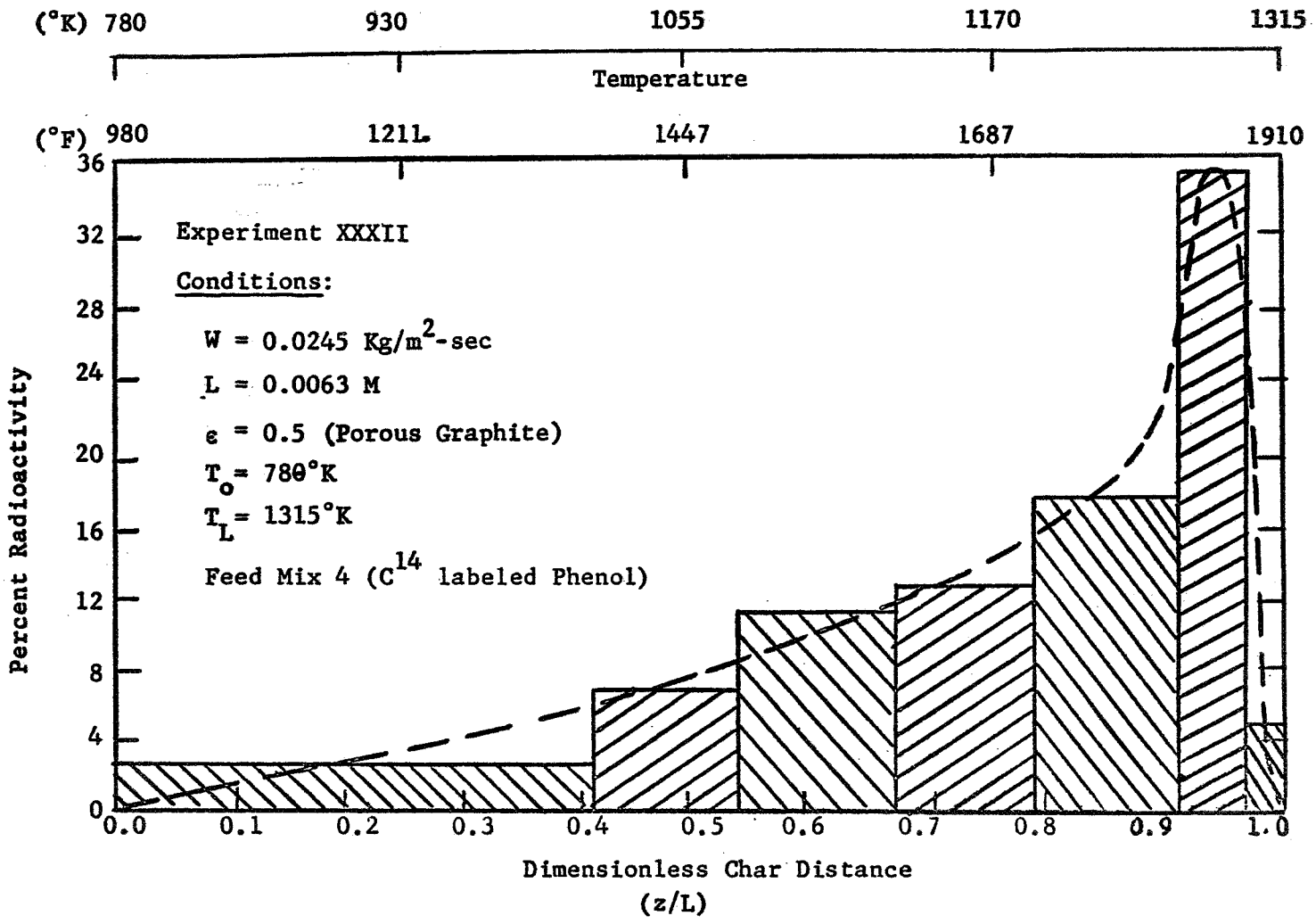

Figure 24. Carbon Deposition Profile for the Thermal Degradation of Phenol Catalyzed with a Molybdenum-Tungsten Co-Catalyst Coating on the Graphite.

Table 30. Flow of Pyrolysis Products Through Porous Graphite. Exit Gas Compositions of Platinum Catalysed Experiments.

RUN NUMBER MASS FLUX FRONT TEMP BACK TEMP	FLOW MODEL	H_2 MOLE %	CH_4 MOLE %	CO MOLE %	CO_2 MOLE %	N_2 MOLE %	H_2O MOLE %	C_6H_6O MOLE %	C_2H_4 MOLE %	C_2H_2 MOLE %	CATALYST
XIII-38	FROZEN	31.7	46.3	5.5	2.5	14.0	0.0	0.0	0.0	0.0	Platinum 5% (wt)
0.0045	EQUILIBRIUM	82.3	1.1	7.0	0.0	9.5	0.2	0.0	0.0	0.0	
1175°K	NON-EQUILIBRIUM	31.7	46.3	5.5	2.5	14.0	0.0	0.0	0.0	0.0	
924°K	EXPERIMENTAL	32.6	41.3	8.9	5.2	14.0	0.0	0.0	0.0	0.0	
XIII-39	FROZEN	31.7	46.3	5.5	2.5	14.0	0.0	0.0	0.0	0.0	Platinum 5% (wt)
0.0195	EQUILIBRIUM	82.4	1.0	7.0	0.0	9.5	0.1	0.0	0.0	0.0	
1215°K	NON-EQUILIBRIUM	31.7	46.3	5.5	2.5	14.0	0.0	0.0	0.0	0.0	
930°K	EXPERIMENTAL	30.8	45.8	6.0	4.4	14.0	0.0	0.0	0.0	0.0	
VIII-22	FROZEN	35.0	43.7	4.9	2.9	13.6	0.0	0.0	0.0	0.0	Platinum 5% (wt)
0.0190	EQUILIBRIUM	79.8	3.0	6.7	0.1	9.6	0.7	0.0	0.0	0.0	
1065°K	NON-EQUILIBRIUM	35.0	43.7	4.9	2.9	13.6	0.0	0.0	0.0	0.0	
660°K	EXPERIMENTAL	36.2	41.4	5.2	4.2	13.0	0.0	0.0	0.0	0.0	

based on the non-equilibrium (non-catalysed) flow model. Furthermore, carbon deposition profiles were used to locate the position and temperature where deposition resulting from methane and phenol thermal degradation occurred.

The use of bromine (or HBr) as a representative homogeneous catalyst made a detailed investigation unnecessary because of the relative activity of various halides to hydrogen bromide in Table 26. By comparison, iodine and organic iodides should have a greater influence on the pyrolysis product reactions, while chlorine or the organic chlorides should have a lesser influence.

No detectable change in the exit product composition, and, therefore, in the rates of chemical reaction of the pyrolysis products, were observed for tungsten and molybdenum co-catalysts and platinum over a temperature range of 1845° to 2300°F (1280°K to 1535°K).

Oxidative Degradation of Low Density Nylon-Phenolic Resin Chars in an Air Stream at Elevated Temperatures

The oxidative degradation of low density nylon-phenolic resin chars is important in reentry applications as a result of the hot, shock heated air streams flowing adjacent to the char front surface. It is believed that a portion of this air stream penetrates the char front surface forming large cavities and irregular shaped, erroded areas on the surface of the heat shield during reentry or in models tested in arc jets. In order to determine the extent of air oxidation, experiments were made in the Char Zone Thermal Environment Simulator in which air, at rates corresponding to reentry values, was injected into the char at the front surface. These experiments simulated a maximum air mass flux, because there is pyrolysis gas flow counter to the air during ablation.

To determine whether air reacted at the surface or in depth, samples of the exit gas stream were taken at short intervals to determine the oxygen conversion within the char. The result of these analyses for two separate experiments are shown in Figure 25. At an air mass flux of 0.0057 lb/ft^2-sec (0.029 kg/m^2-sec) and a front surface temperature of 1485°F (1080°K), the maximum conversion of oxygen at the back surface was 53% corresponding to an oxygen concentration of 10 mole percent leaving the back surface. A back surface temperature of (670°K) was measured for the 1/8 inch (0.0032 m) thick char. Increasing the air flow rate to 0.035 lb/ft^2-sec (0.18 kg/m^2-sec) and a front surface temperature of 2047°F (1393°K), increased the maximum conversion at the rear surface to 81% or a concentration of four percent leaving the char back surface. The back surface temperature was measured at (425°K). The char thickness was 1/4 inch (0.0064 m). The relatively low back surface temperatures indicate that the highly exothermic reaction probably occurs near the front surface. Although oxygen conversion at the back surface was never

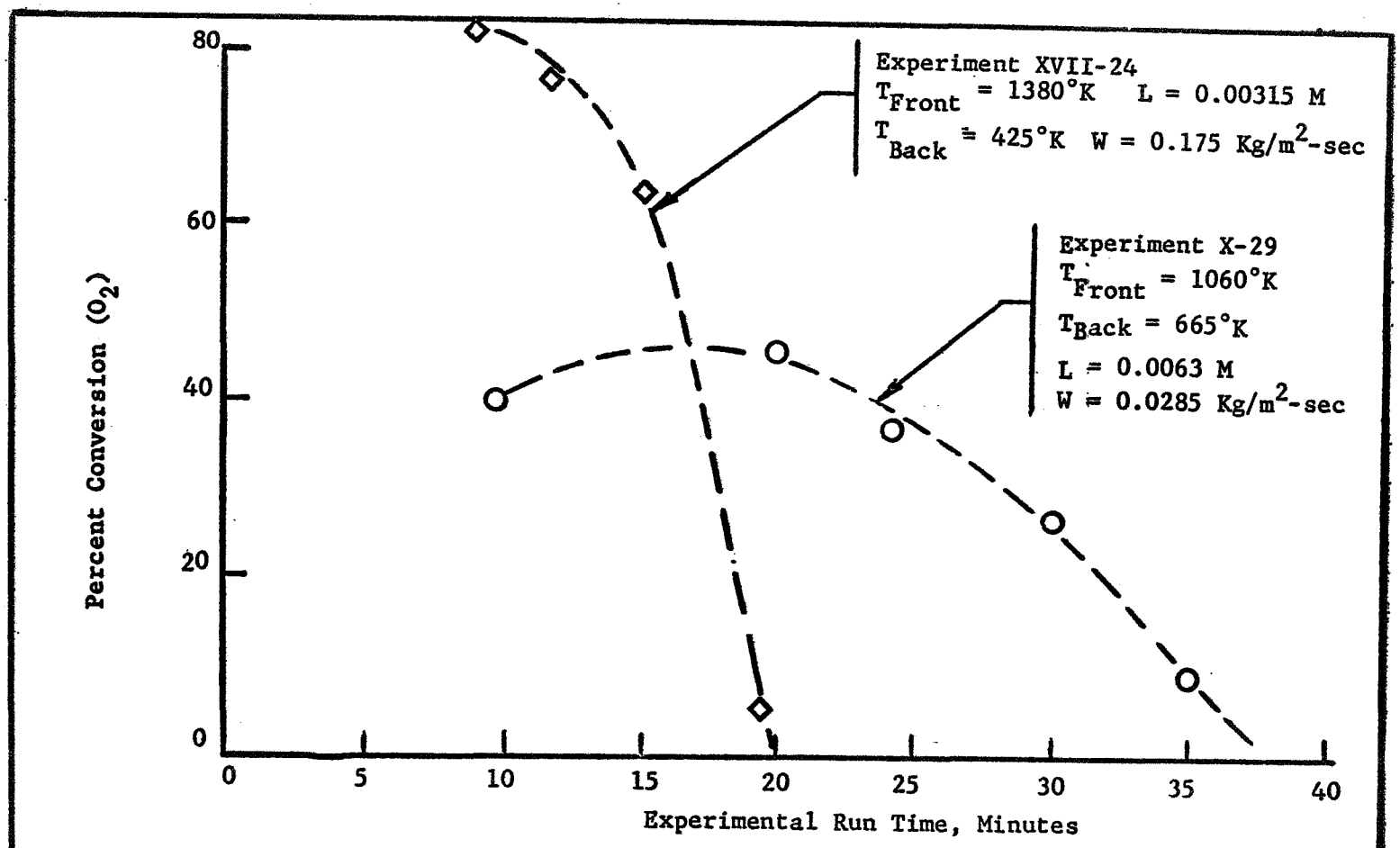

Figure 25. Conversion of Oxygen as a Function of Experimental Run Time for the Air Oxidation of Porous Graphite at High Temperatures.

complete indicating the presence of oxygen within the pores at all char depths the extent of oxidation in depth appears small in comparison to the surface oxidation. The three large erroded areas indicate strong surface attack. The rounded edges near the errosions further support the concept that oxidation occurs where there is the least resistance to flow. The time for these holes to be formed can be estimated by comparing the length of time necessary to obtain near zero oxygen conversion at the back surface in Figure 25.

In addition to the experimental data, a modification to the isothermal analysis was made by considering temperatures within the char linear with char distance. This approximation permits the calculation of the oxygen conversion for a given char depth (residence time) and front surface temperature. A comparison of the calculated and measured maximum conversions is shown in Table 31. The conversion of oxygen with char depth is also presented in Figure 26 for the linear approximation of the temperature and also the isothermal evaluations at the front and back surface temperatures. The data used to describe the air oxidation of graphite is presented in Table 31. Agreement of the calculated and experiment conversions at the back surface is within the experimental accuracy of the analyses.

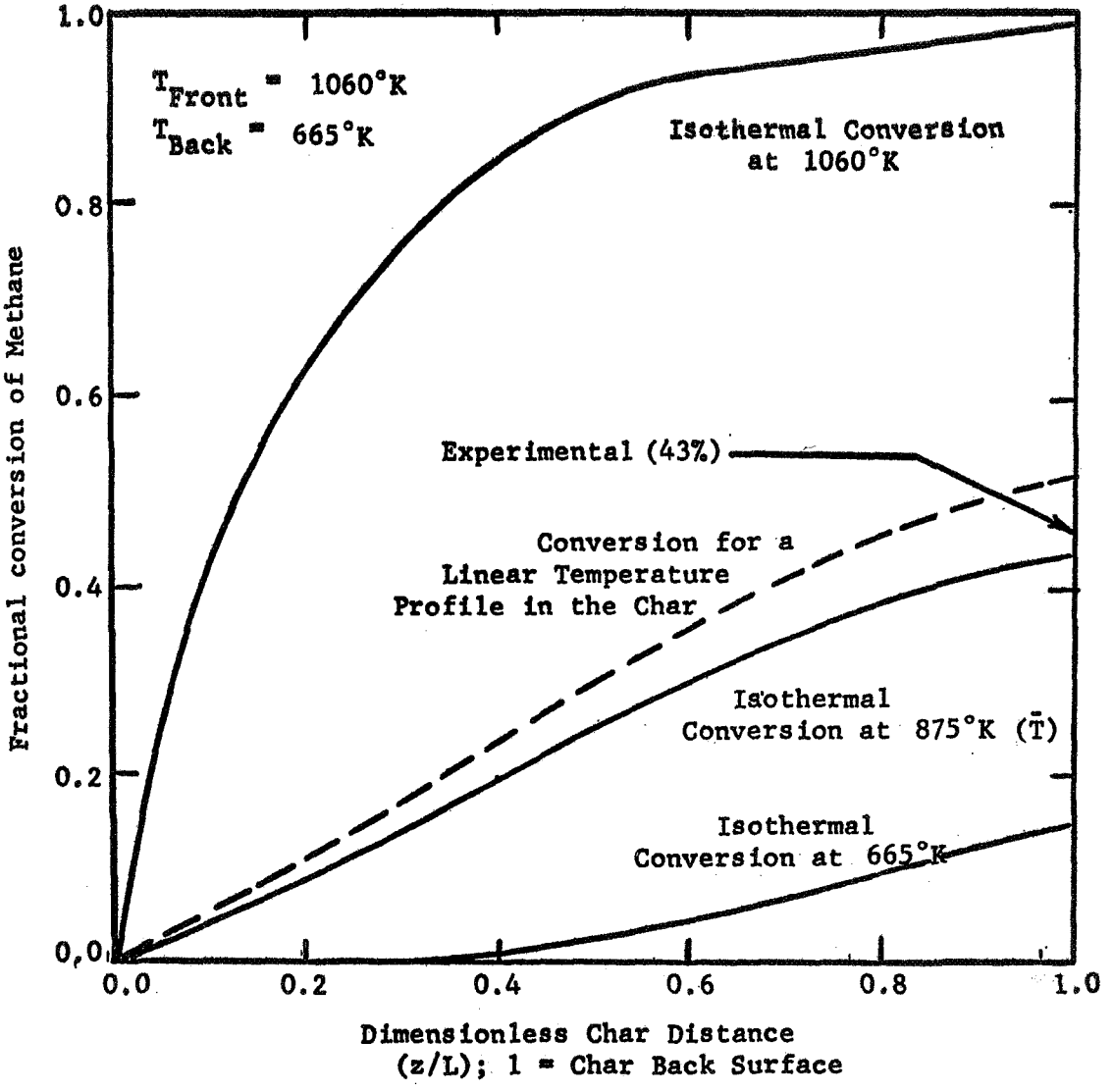

Figure 26. Conversion of Oxygen for the Flow of Air Through a Low Density Nylon-Phenolic Resin Char at a Mass Flux of 0.1750 Kg/m^2-sec and a Temperature of 1060°K.

Table 31. Air Oxidation of Low Density Nylon-Phenolic Resin Chars. A Detailed Comparison of the Calculated and Measured Oxygen Conversion at the Char Back Surface (Exit Surface).

Experiment Number:	X-29	XVII-54
Conditions:		
Mass Flux, Kg/m^2-sec	0.0285	0.1750
Front Temperature, °K	1060	1380
Back Temperature, °K	665	425
Char Thickness, M	0.0063	0.00315
Experiment Run Time, Min.	35	25
Measured Maximum Conversion: (%)	43	83
Calculated Maximum Conversion:		
(1) at the Front Temperature	96	100
(2) at the Back Temperature	8	22
(3) at a Temperature which varied linearly with char depth	45	86
(4) at the Average Temperature	41	81

CONCLUSIONS

Based on the experimental and theoretical results of this research the following conclusions are drawn:

Reacting Flow of Pyrolysis Products in the Char Zone

1. The reacting flow of pyrolysis products from nylon-phenolic resin composites in the char zone is accurately described by a non-equilibrium model employing reaction kinetic data of the important reactions occurring in the system. For the simulated pyrolysis product compositions in Table 6, mass flux values between 0.00003 - 0.10 lb/ft^2-sec (0.00015 - 0.5 Kg/m^2-sec) and a front surface temperature range of 1350 - 2300°F (1000°K - 1535°K), the reactions and associated kinetic data in Table 5 accurately describe the energy transfer in the char zone. These reactions are valid up to 3000°F (1925°K). Above this temperature, additional reactions must be considered to accurately describe the reacting flow system.

2. Under conditions of high mass fluxes (> 0.05 Kg/m^2-sec) and/or low temperatures (< 1365°K), the flow of pyrolysis products is essentially frozen. These conditions define the upper limitation of the frozen flow model.

3. The equilibrium flow model erroneously predicts the behavior in the char for all conditions except those in which the mass flux rate is smaller than 0.0001 lb/ft^2-sec (0.0005 Kg/m^2-sec). Mass flux rates greater than this value require the use of a non-equilibrium flow analysis to describe reactions occurring at finite rates.

Reacting Flow of Pyrolysis Products Through Porous Graphite

1. The same results are obtained for the reacting flow of pyrolysis products in porous graphite. The same important reactions and kinetic data that applied to the low density nylon-phenolic resin chars, likewise apply to the graphite between 1350 - 2300°F (1000°K - 1535°K) and 0.00003 - 0.10 lb/ft^2-sec (0.00015 - 0.5 Kg/m^2-sec). This permits the substitution of graphite for the brittle chars in studies requiring post-experimental analyses of the porous media; i.e., carbon deposition studies.

2. In order to compare the results from char and graphite experiments, the mass flux in the pores must be identical. This corrects for differences in the porosity of each material.

3. The inclusion of graphite "fines" in the pore spaces, during the fabrication procedure, results in reactions with hydrogen forming methane. Purging the graphite with helium or nitrogen prior to an experiment is sufficient to remove these dust-like particles from the pore spaces and eliminate the methane formed from this more reactive form of graphite.

Carbon Deposition Studies

1. The use of radioactive tracers is a very effective method of determining the extent of carbon deposition within the char from the cracking of the pyrolysis gases. A plot of the percent radioactivity as a function of char depth very graphically determines the position where deposition starts, ends and is maximum.

2. Carbon is deposited as a result of the thermal degradation of methane and phenol. Deposition starts near the middle of the char ($z/L = 0.5$) where the temperature is 1400°F (1035°K) and increases uniformly to a maximum value near the front surface at a temperature of 1900°F (1310°K).

Degradation Product Distribution

1. The products of methane degradation were determined by comparing radioactive tracer concentration profiles with the gas chromatograms of the exit gases leaving the Char Zone Thermal Environment Simulator. The species identified were carbon monoxide, carbon dioxide, ethylene, acetylene and unreacted methane.

2. Similarly, the products of phenol degradation were determined. The species were identified as methane, carbon monoxide, carbon dioxide and unreacted phenol.

3. The above methods provided excellent supporting evidence that the reactions considered important in the mathematical model were correct.

Catalysts Evaluation Studies

1. The effect of adding homogeneous catalysts (such as bromine) to the pyrolysis product stream to accelerate chemical reactions and, therefore, the heat absorption in the system was determined. Bromine (and the organic halides and other halogens) produced a catalytic effect which reduced the temperature at which carbon deposition starts from 1400°F (1035°K) to 1200°F (911°K). The position of maximum deposition was likewise shifted 300°F (150°C). A sharp decline in the carbon deposition probably indicated rapid depletion of carbon by reactions with water and/or carbon dioxide.

The product concentrations of the exit gas stream is likewise different from the non-catalytic experiemnts and not predicted by the non-catalytic kinetic data.

2. Molybdenum and tungsten heterogeneous catalysts did not affect a measurable change in the behavior of the system. A slight shift in the carbon deposition profiles were observed; however, the results were outside the experimental accuracy of

the analytical equipment. Platinum was used in earlier studies and, likewise, failed to produce a change.

Air Oxidation Studies

The effect of injecting air into low density nylon-phenolic resin chars at the front surface is rapid errosion near the edge regions of the chars. These experiments were conducted by passing air into the char from the front surface with no counter flow of pyrolysis products from the rear. The experimental results were bracketed by the isothermal analysis and values calculated using a linear description of the temperature profile within the char.

NOMENCLATURE

Symbol	Description	Units
A	area	L^2
	species identification in a general expression for a reaction	none
	Runge-Kutta parameter in the energy equation numerical solution method	T
	ratio of system parameter defined in equation (2-13)	none
a	formula number for chemical compounds	none
	coefficients in the polynomial defined in equation (2-28)	none
B	Runge-Kutta parameter in the species continuity numerical solution method	M/L^2t
	ratio of system parameter defined in equation (2-14)	none
b	mass of a chemical element	M
	coefficients in the polynomial defined in equation (2-29)	none
C	ratio of the fluid to matrix thermal conductivity	none
	molar concentration defined in equation (2-38)	$mole/L^3$
C_p	heat capacity of a pure component at constant pressure	L^2/t^2T
$\bar{C}_p$	heat capacity of a mixture at constant pressure	L^2/t^2T

Symbol	Description	Units
c	total number of atoms of a chemical element in the system defined by equation (3-41)	none
	coefficients in the polynomial defined in equation (2-35)	none
D	substantial derivative	none
	mass diffusivity	L^2/t
E	energy of activation	ML^2/t^2-mole
F	free energy	ML^2/t^2
F°	free energy at a standard state of 298°K and 1 atom	ML^2/t^2
f	free energy function defined in equations (3-31) and (3-33)	ML^2/t^2
	any mathematical function	none
G	augmented function of the quadratic approximation to the free energy function defined in equation (3-37)	ML^2/t^2
g	force of gravity	L/t^2
H	enthalpy	ML^2/t^2
H°	enthalpy at a standard state of 298°K and 1 atom	ML^2/t^2
h	heat transfer coefficient in equation (2-3)	M/t^3t
	numerical integration increment sizes	none

Symbol	Description	Units
J	molar flux	moles/tL^2
j	mass flux	M/tL^2
K	total number of gas species in the system	none
k	thermal conductivity	ML/t^3T
	reaction rate constant	*function of reaction order.
k°	frequency factor	
L	char thickness	L
M	mobility of a porous matrix defined in equation (2-84)	none
M_w	molecular weight	M/moles
m	total number of chemical reactions in the system	none
N	molar flux of species in the char zone	mole/tL^2
n	moles of species	moles
$\bar{n}$	mole fraction of species	none
P	pressure	M/Lt^2
p	stoichiometric coefficient of the products in a chemical reaction	none
p'	power on the concentration terms for products in a chemical reaction	none
Q	volumetric flow rate	L^3/t
	quadratic approximation of the free energy function (3-36)	ML^2/t^2
q'''	heat generation by chemical reaction	M/t^3

Symbol	Description	Units
q	number of gas plus solid (condensed) phases in the system	none
	energy transfer by conduction, convection or radiation	M/t^3
R	ideal gas constant	$\frac{ML^2/t^2T}{mole}$
	chemical reaction rate	$mole/tL^3$
$\bar{R}$	effective chemical reaction rate for gas and solid species defined in equation (3-21)	$mole/tL^3$
R_e	Reynold's number	none
R_o	dimensionless mole flux defined in equation (2-43)	none
r	chemical reaction rate of a chemical species	$mole/tL^3$
	stoichiometric coefficient of the reactants in a chemical reaction	none
	radius of a cylindrical graphite test section included in equation (2-83)	L
r'	power on the concentration terms for reactants in a chemical reaction	none
s	power on the temperature in the rate equation (3-52)	none
T	temperature	T
T'	temperature gradient	T/L
t	time	t
$\bar{u}$	ratio of the actual to estimated mole fraction in the free energy minimization calculation (3-42)	none
V	volume	L^3

Symbol	Description	Units
v	velocity	L/t
W	mass flux based on the superficial velocity	M/L^2t
W_p	mass flux based on the velocity in the pores spaces of chars and graphite	M/L^2t
x	mass fraction of the species	none
	distance in the axial direction (Chapter II)	L
y	distance in the radial direction (2-82)	L
	estimated moles of species in the free energy minimization calculation	none
$\bar{y}$	estimated mole fraction in the free energy minimization calculation	none
z	distance in the axial direction (Chapter II and III)	L
$\bar{z}$	compressibility factor	none
Greek		
α_o	ratio of the mass flux to the mass diffusivity used in equation (2-44)	M/L^4
α	viscous coefficient in the modified Darcy's law equation (2-82)	L^{-2}
β	inertial coefficient in the modified Darcy's law equation (2-82)	L^{-1}
γ	permeability of a porous medium	L^2
δ	Kronecher Delta	none
Δ	a difference between two parameters	none
∇	del operator	none

Symbol	Description	Units
ϵ	porosity of a porous medium	none
$\bar{\epsilon}$	emissivity of a porous medium	none
η	dimensionless char distance defined in equation (2-15)	none
θ	dimensionless temperatures defined in equations (2-11) and (2-12)	none
λ	parameter of a straight line (0-1)	none
μ	viscosity	M/Lt
π	3.1416	none
ρ	density	M/L^3
$\bar{\sigma}$	Stefan-Boltzmann constant	M/t^3T^4
σ	collision diameter	L
τ	shear stress	M/t^2L
ϕ	dimensionless parameters defined in equations (2-25), (2-26) and (2-27)	none
	parameter used to calculate the viscosity of a gas mixture in equation (3-57)	none
Ω	collision integral	none
Π	Lagrangian multipliers in equation (3-37)	none

Subscripts

c	convection or conduction
d	carbonaceous deposit
e	effective or overall value
f	fluid or gas phase

Symbol	Description
g	gas phase
L	front surface of a char
m	matrix or solid phase
o	initial or inlet condition
P	pressure
	pyrolysis
	pores
r	radiation
s	solid phase
T	temperature
	total
y	distance in the radial direction
z	distance measured from the char back surface
∞	free stream condition
1	inside surface of a cylindrical tube
2	outside surface of a cylindrical tube

Superscripts

*	a standard or reference condition
°	a standard or reference state
'	derivative

REFERENCES

1. Ely, Lawrence D., Return from Space, Charles C. Thomas, Publisher, Springfield, Illinois, 6-9 (1966).

2. Seifert, Howard S., and Kenneth Brown, Ballistic Missile and Space Vehicle Systems, John Wiley and Sons, Inc., New York, 448-9 (1961).

3. Ordway, Fredrick I., James P. Gardner, and Mitchell R. Sharpe, Jr., Basic Astronautics, Prentice-Hall, Inc., Englewood Cliffs, New Jersey, 346-9 (1962).

4. Duncan, Robert C., Dynamics of Atmospheric Entry, McGraw-Hill Book Co., Inc., New York, 117-9 (1962).

5. Martin, John J., Atmospheric Reentry, Prentice-Hall, Inc., Englewood Cliffs, New Jersey, 83-6 (1966).

6. Wingrove, Rodney C., "Flight Dynamics of Planetary Entry," Recent Developments in Space Flight Mechanics, 9, 225 (1966).

7. Steverding, Bernard, and Vernon A. Nieberlein, "Ablation for Heat Shielding," Chemical Engineering, 72 (15), 163 (July 19, 1965).

8. Kelley, J. B., and M. R. L'Ecuyer, "Transpiration Cooling - Its Theory and Application," Report No. TM-66-5, Jet Propulsion Center, Purdue University, Contract NsG 592, N66-30856 (June 1966).

9. Abraham, Lewis H., Structural Design of Missiles and Spacecraft, McGraw-Hill Book Co., Inc., New York, 247-65 (1962).

10. Fein, M. M., S. J. Tunkel and M. S. Cohen, "New Developments in Ablative Cooling," CEP Symposium Series, 60 (52), 99 (1964).

11. Matting, Fred W. and Dean R. Chapman, "Analysis of Surface Ablation of Noncharring Materials with Description of Associated Computing Program," NASA TN D-3758 (December 1966).

12. Kuehn, Donald M. and Daryl J. Monson, "Attached and Separated Boundary Layers on Highly Cooled, Ablating and Nonablating Models at M = 13.8," NASA TN D-4041 (June 1967).

13. Diaconis, N. S., W. R. Warren, Jr. and T. E. Shaw, "The Hypervelocity Heat Protection Problem," Propulsion and Reentry, XVIth. International Astronautical Congress, Athens (1965).

14. Schmidt, Donald L., Engineering Design for Plastics, Chapter 13, Reinhold Publishing Co., Inc., New York (1962).

15. Freedman, S. I., Developments in Heat Transfer, Chapter 5, M. I. T. Press, Cambridge, Massachusetts (1962).

16. Kratsch, K. M., L. F. Hearne and N. R. McChesney, "Thermal Performance of Heat Shield Composites During Planetary Entry," AIAA-NASA National Meeting, Palo Alto, California, 3 (September 30-October 1, 1963).

17. Kendall, Robert M, Eugene P. Bartlett, and Ronald A. Rindal, "A Multi-component Boundary Layer Chemically Coupled to an Ablating Surface," AIAA Journal, 5 (6), 1063 (June 1967).

18. Swann, Robert T., Claud M. Pittman and James C. Smith, "One Dimensional Numerical Analysis of the Transient Response of Thermal Protection Systems," NASA TN D-2976 (September 1965).

19. Koh, J. C. Y. and E. P. del Casal, "Heat and Mass Flow Through Porous Matrices for Transpiration Cooling," Paper 16, Proceedings of the 1965 Heat Transfer and Fluid Mechanics Institute, Stanford University Press, Los Angeles, California, 263-81 (June 21-23, 1965).

20. Koh, J. C. Y. and E. P. del Casal, "Heat and Mass Transfer with Chemical Reactions for Fluid Flow Through a Porous Matrix in Re-Entry Thermal Protection," A.I.A.A. Fourth Aerospace Sciences Meeting, Los Angeles, California (June 27-29, 1966).

21. Koh, J. C. Y., E. P. del Casal, R. W. Evans, and V. Deriugin, "Fluid Flow and Heat Transfer in High-Temperature Porous Matrices for Transpiration Cooling," Technical Report AFFDL-TR-66-70, The Boeing Company, 209 pages (May 1966).

22. Clark, Ronald K., "Flow of Hydrocarbon Gases in Porous Media at Elevated Temperatures," M.S. Thesis, University of Virginia, 108 pages (August 1968).

23. Weger, Eric, Jere Brew and Roger Schwind, "An Investigation of Carbon Deposition in Chars," Report BSD-TR-66-385, Washington University, St. Louis, Missouri, 84 pages (1966).

24. Weger, Eric, Jere Brew and Ronald Servais, "An Investigation of Carbon Deposition in Chars - II," Report SAMSO-TR-68-123, Washington University, St. Louis, Missouri 96 pages (January 1968).

25. Bird, R. B., W. E. Stewart, and E. N. Lightfoot, Transport Phenomena, John Wiley & Sons, Inc., New York, 328-30 (1960).

26. April, Gary C., "Evaluation of the Energy Transfer in the Char Zone During Ablation," Final Report on NASA Grant NGR 19-001-016, Louisiana State University, Baton Rouge, Louisiana, 568 pages (May 1, 1969).

27. del Valle, E. G., R. W. Pike and G. C. April, "Transport Phenomena in the Char Zone During Ablation. II: Equilibrium Composition of Degradation Products of Ablation," Paper 13e, 63rd National Meeting of the A.I.Ch.E., Salt Lake City, Utah (May 1967).

28. Zeleznik, F. J. and S. Gordon, "A General IBM 704 or 7090 Computer Program for Computation of Chemical Equilibrium Composition, Rocket Performance, and Chapman-Jouguet Detonation," NASA TN D-1454 (October 1962).

29. Schmidt, D., "Thermal Parameters of Re-Entry Ablative Plastics," WADD Technical Report 60-90, Wright-Patterson AFB, Ohio, Aeronautical Systems Division (1960).

30. Pike, R. W., "Evaluation of the Literature for Chemical Reactions and the Reaction Rates for the Decomposition Products from Charring Ablators," NASA LWP-181, Langley Research Center, Hampton, Virginia (January 1966).

31. Pike, R. W., Gary C. April and E. G. del Valle, "Non-Equilibrium Flow and the Kinetics of Chemical Reactions in the Char Zone," NASA CR-66455 (July 1967).

32. Nelson, James B., "Determination of Kinetic Parameters of Six Ablation Polymers by Thermogravimetric Analysis," NASA TN D-3919 (April 1967).

33. Sykes, George F., Jr., "Decomposition Characteristics of a Char-Forming Phenolic Polymer Used for Ablative Composites," NASA TN D-3810 (February 1967).

34. Scala, S. M. and L. M. Gilbert, "Thermal Degradation of a Char-Forming Plastic During Hypersonic Flight," ARS Journal, 32 (6), 917-24 (June 1962).

35. Kratsch, K. M., L. F. Hearne and H. R. McChesney, "Thermal Performance of Heat Shield Composites During Planetary Entry," AIAA-NASA National Meeting, Palo Alto, California, 3 (September 30-October 1, 1963).

36. Sykes, G. F., Private Communication to R. W. Pike (March 14, 1968).

37. Abramowitz, Milton and I. A. Stegun, editors, Handbook of Mathematical Functions with Formulas, Graphs, and Mathematical Tables, 3rd Printing, National Bureau of Standards Applied Mathematics Series 55, Washington, D.C., 886, 896-7 (1965).

38. Sax, N. Irving, Dangerous Properties of Industrial Materials, 2nd. Ed., Reinhold Publishing Corp., New York (1963).

39. Manufacturing Chemists' Association, "Properties and Essential Information for Safe Handling and Use of Acetylene," SD-7, Washington, D. C. (1957).

40. Manufacturing Chemists' Association, "Properties and Essential Information for Safe Handling and Use of Phenol," SD-4, Washington, D. C. (1964).

41. Manufacturing Chemists' Association, "Properties and Essential Information for Safe Handling and Use of Cresol," SD-48, Washington, D. C. (1952).

42. Kozlov, G. I.; and Knorre, V. G.: "Single Pulse Shock Tube Studies on the Kinetics of the Thermal Decomposition of Methane," Combustion and Flame, 6, 253-263 (Dec. 1962).

43. Hirt, T. J.; and Palmer, H. B.: "Kinetics of Deposition of Pyrolytic Carbon Films From Methane and Carbon Suboxide," Carbon, 1, 65-70 (1963).

44. Kozlov, G. I.; and Knorre, V. G.: "Kinetics of Thermal Decomposition of Methane by the Single-Pulse Shock Tube Method," Russian Jour. Phys. Chem., 37 (9), 1128-1130 (Sept. 1963).

45. Bradley, J. N.: Shock Waves in Chemistry and Physics, John Wiley, Inc., New York (1962).

46. Thon, N., ed.: Table of Chemical Kinetics Homogeneous Reactions, N.B.S. Circular 510 (Sept. 1958), Supplement 1 (Nov. 1956); N.B.S. Monograph 34, vol. 1 (Sept. 1961), vol. 2 (July 1954).

47. Palmer, H. B.; and Hirt, T. J.: "The Activation Energy For the Pyrolysis of Methane," Journal Phys. Chem., 67 (3), 709-711 (March 1963).

48. Bartlit, J. R.; and Bliss, H.: "Kinetics of Ethane Pyrolysis," A.I.Ch.E. Journal, 11 (3), 562-572 (May 1965).

49. Quinn, C. P.: "The Thermal Dissociation and Pyrolysis of Ethane," Proc. Roy. Soc., 275 1361 (Sept. 1963).

50. Cummings, G. A. McD.; Hall, A. R.; and Straker, R. A. M.: "Decomposition Flame of Acetylene and Methyl Acetylene," Eighth Int. Symp. on Combustion, Williams and Wilkins Co., Baltimore, 503-510 (1962).

51. Blair, J. D.; and Seschske, A.: "Graphite-Hydorgen Methane Kinetics Above 1600° K," A.E.C. Contract W-7405 ENG 36, LASL2896 (May 1962).

52. Hedden, K., Proceedings of the Fifth Conference on Carbon, Macmillan Co., New York, 125-31 (1962).

53. Gulbrasen, E. A.; Andrews, K. F.; and Brassert, F. A.: "The Reaction of Hydrogen With Graphite at 1200° to 1650°C," Jour. Electrochem. Soc., 112 (1), 49-52 (Jan. 1965).

54. King, A. B.; and Wise, H.: "Reaction Kinetics of Hydrogen Atoms With Carbon Films," Jour. Phys. Che., 67 (6), 1163-9 (June 1963).

55. Happel, John, and Kramer, Leonard, "Acetylene and Hydrogen from the Pyrolysis of Methane," Industrial and Engineering Chemistry, 59, 39-50 (Jan. 1967).

56. Breisacher, P., and Marx, P. C., "The Hydrogen-Graphite Reaction Between 360° and 800°," Jour. Am. Chem. Soc., 85, 3518-9 (Nov. 1963).

57. Carney, N. S., and R. B. Thomas, "Reactor of Carbon and Graphite Below 950° C.," British Report AERLE-C/R 2502 (June 1958).

58. King, Bruce A., and Henry Wise, "Reaction Kinetics of Hydrogen Atoms with Carbon Films," The Journal of Physical Chemistry, 67 (6), 1163-70 (June 1963).

59. Hou, K. C., and Palmer, H. B., "The Kinetics of Thermal Decomposition of Benzene in a Flow System," Jour. Phys. Chem., 69 (3), (March 1965).

60. Scott, G. S., "Mechanism of the Steam-Carbon Reaction," Industrial and Engineering Chemistry, 33, 1279-84 (1941).

61. Lewis, W. K., E. R. Gilliland, and Howard Hipkine, "Carbon-Steam Reaction at Low Temperatures," Industrial and Engineering Chemistry, 45, 1697-1703 (August 1953).

62. Thiele, E. W., and R. T. Haslam, "Mechanism of the Steam-Carbon Reactions," Industrial and Engineering Chemistry, 19, 882-7 (August 1927).

63. Mayers, Martin A., "The Rate of Oxidation of Graphite by Steam," Journal of the American Chemical Society, 56, 1879-1884 (September 1934).

64. Warner, B. R., "Mechanism of the Steam-Carbon Reaction," Journal of the American Chemical Society, 60, 1447 (Aug. 1943).

65. Walker, P. L., Jr., Chemistry and Physics of Carbon, Volume 1, Marcel-Dekker, Ind., New York, 203-64 (1965).

66. Walker, P. L., Jr., F. Rusinko, Jr., and L. G. Austin, Gas Reactions of Carbon, Advances in Catalysis, 11, Academic Press, Inc., New York (1959).

67. Johnstone, H. F., C. Y. Chen, and Donald S. Scott, "Kineitcs of the Steam-Carbon Reaction in Porous Graphite Tubes," Industrial and Engineering Chemistry, Volume 44, No. 7, 1564-69 (July 1952).

68. Binford, Jesse S., Jr., and Henry Eyring, "Kinetics of the Steam-Carbon Reaction," Journal of the American Chemical Society, 60, 486-491 (April 1956).

69. Austin, L. G., and P. L. Walker, Jr., "Effect of Carbon Monoxide in Causing Nonuniform Gasification of Graphite by Carbon Dioxide," A.I.Ch.E. Journal, 9 (3), 303-6 (May 1963).

70. Glovina, E. S., and G. P. Khaustovich, "The Interaction of Carbon with Carbon Dioxide and Oxygen at Temperatures Up to 3000°K", Eighth Int. Symp. on Combustion, Williams and Wilkins Co., Baltimore (1962).

71. Walker, P. L. Jr., Chemistry and Physics of Carbon, Volume 4, Marcel Dekker, Inc., New York, 287-383 (1965).

72. Berkman, Sophia, J. C. Morrell and Gustov Egloff, Catalysis: Inorganic and Organic, Reinhold Publishing Co., New York, 572 (1940).

73. del Valle, E. G., R. W. Pike and G. C. April, "Modeling for a Set of Complex Chemical Reactions at High Temperatures," Sixty-First Annual Meeting (A.I.Ch.E.), Preprint 8F, Los Angeles, Calif. (1968).